NANYANG TECHNOLOGICAL UNIVERSITY

Multifactorial heterogeneity of virus-specific T cells: Complex relationships during the progression of human chronic hepatitis B infection

Yang Cheng

鄭揚

SCHOOL OF BIOLOGICAL SCIENCE

Joint Doctoral program of Singapore Immunology Network,
A*STAR and Nanyang Technological University

August 2017

Multifactorial heterogeneity of virus-specific T cells: Complex relationships during the progression of human chronic hepatitis B infection

Yang Cheng

鄭揚

SCHOOL OF BIOLOGICAL SCIENCE

A thesis submitted to the Nanyang Technological University in partial fulfilment of the requirement for the degree of Doctor of Philosophy

August 2017

"My time is over and now is your time. Let's together make HBV the disease of past" – *Dr. Francis V. Chisari, the pioneer of HBV research.*

Retirement Speech in 2014 International HBV Meeting

UCLA, California, USA

2017 International HBV Meeting, Washington DC, USA

ACKNOWLEDGEMENTS

First and the foremost, my greatest gratitude goes to my parents who have supported me mentally and financially from the very beginning of my long journey in the field of science. I would not stand here without their unconditional support and love.

I sincerely thank my supervisor Prof. Evan Newell for giving me the opportunity to fulfil my PhD training with such exciting project that I had always looked for. I also appreciate all of his constant supports and guidances, especially for giving me much of freedom and funding resource throughout this complicated and difficult project. The enthusiastic discussions and challenges have been only driving me forwards with more passion in the research field of immunology. It has not only broaden my view, but also helped me to develop the necessary characteristic and profession for becoming a fully independent scientist in the foreseeable future.

I would thank my Thesis Advisory Committee members, Prof. Antonio Bertoletti, Prof. Katja Fink and Prof I-Hsin Su. Their consults have been invaluable and helpful for the past four years. I am also personally thankful for the SINGA scholarship from A*STAR and the productive environment in SIgN.

My heartfelt appreciation also goes to all the members in Newell's lab, for their professional works and enjoyable companies. I would like to thank Dr. Michael Wong for his always resourceful discussion and the broad knowledge in T cell biology. I also thank Karen Teng for helping me from general lab issues to the daily maintenances and the often trouble shooting of CyTOF. Many works would not be accomplished without Cheryl Loh, who have shared and eventually took over the duty on producing MHC protein and Streptavidin. I thank Dr. Michael Fehlings for his always being kind and optimistic, and the pleasure atmosphere he created in the lab. I am also deeply indebted to Dr. Etienne Becht for his remarkable helps in developing several analytical

approaches upon my frequent requests. I am very grateful to Dr. Harsimran Singh, for her indispensable contribution in the early work of liver tissue and her tolerance to my daily sarcasm. I would also like to thank Bavani Gunasegaran for her recent addition to the lab and contributing largely to one of my very demanding project. All in all, I truly appreciate every member in Newell's lab who has been contributing and working as a team.

This intense project would not be possible without the essential help from our collaborators. I sincerely thank to Prof. Seng Gee Lim for his unlimited support in the accessibility of precious patient samples. I also thank Juling Wang and Wah Wah Phyo for their enormous efforts on the sampling and coordination. I would like to mention Prof. Antonio Bertoletti again for providing samples of a rare patient cohort. Equally important, I am grateful to Dr. Yuan Zhu and Dr. Paola Florez De Sessions for their help on viral sequencing and their unmatched input from virology perspective. I would also like to thank Dr. Jinmiao Chen and Prof. Michael Poidinger for their early and continuous support on the bioinformatics for this project.

Last but not the least, I would not be where I am today without the previous experience and training from my former mentors. I thank deeply to Prof. Nan-Shih Liao in Academia Sinica, Taiwan, where I had the first glance of the research world in immunology. I am also sincerely grateful to Prof. Matthias von Herrath in La Jolla Institute for Allergy and Immunology, where I had the opportunity to work on two exciting fields of immunology, the type 1 diabetes and chronic LCMV model. My appreciation also goes to Prof. Mala Maini in University College London, who brought me into the research of HBV immunology and the chance to work closely with real world patients. Together with the experience I have gained under Prof. Evan Newell, the continuous accumulation of knowledge and confidence brings me where I stand today.

I am truly grateful to all the supports from everywhere and everyone during this long lasting journey. I also hope that our work can

one day contribute to the scientific world for the greatest benefit of mankind.

TABLE OF CONTENTS

ACKNOWLEDGEMENTS **3**

TABLE OF CONTENTS **6**

LIST OF FIGURES **8**

LIST OF TABLES **10**

ABBREVIATIONS **11**

ABSTRACT **14**

1. INTRODUCTION **15**

1.1. Hepatitis B virus (HBV) **15**

1.2. Virus-specific CD8+ T cells **19**

1.3. T cell exhaustion and memory **22**

1.4. Mass cytometry (Cytometry by Time-Of-Flight) **27**

1.5. High-dimensional cytometric data analysis **31**

1.5.1 Principal Component Analysis (PCA) 33

1.5.2 t-distributed Stochastic Neighbor Embedding (t-SNE) 33

1.5.3 One-dimensional Soli-Expression Nonlinear Stochastic Embedding (One-SENSE) 34

1.5.4 Diffusion map 35

2. AIMS **36**

3. MATERIALS AND METHODS **37**

3.1 Patient samples and PBMC isolation **37**

3.2 Amplification of HBV genome and library construction **38**

3.3 HBV epitope prediction and peptide synthesis **39**

3.4. Peptides sequence similarity and cluster assignment **39**

3.5. Antibody-metal conjugation **45**

3.6. Streptavidin (SAv) production and metal labeling **47**

3.7. Generation of HLA-A*11:01 monomer and 562-plex pMHC library **47**

3.8. 562-plex combinatorial (Quadruple/Triple SAv-metal coded) pMHC tetramers **48**

3.9. Highly multiplex pMHC tetramer, antibody staining and CD8 T cell enrichment **48**

3.10. Mass cytometry and data pre-processing **50**

3.11. Self-validated automatic deconvolution of antigen-specific T cells **50**

3.12. High-dimensional cytometric data visualization and trajectory **54**

3.13. Flow cytometry and cell sorting **55**

3.14. TCR high-throughput sequencing **55**

3.15. TCR repertoire spectratyping and motif analysis **56**

3.16. Enzyme-linked immunosorbent assay (ELISA) **56**

3.17. *In vitro* virus-specific CD8+ T cells expansion **57**

3.18. Statistical analysis **57**

4. RESULTS **58**

4.1. Comprehensive HBV epitope mapping **58**

4.2. Development of One-dimensional Soli-Expression by Nonlinear Stochastic Embedding (One-SENSE) **71**

4.3. Diverse interrelations of exhaustion and memory by One-SENSE **75**

4.4. Multifactorial exhaustion and memory atlas of HBV_{pol387}-specific $CD8^+$ T cells 81
4.5. Immunodominant $HBV_{core169}$-specific $CD8^+$ T cells are associated with viral clearance 86
4.6. Diffusion map projects the cellular dynamics between exhaustion and memory 88
4.7. HBV_{pol282}-specific $CD8^+$ T cells are pre-existing naïve precursor 91
4.8. Nonlinear correlation of functional capacity and inhibitory receptors on virus-specific $CD8^+$ T cells 94
4.9. Diverse epitope-specific T cell receptor (TCR) spectratype linked to HBV clinical stages in an epitope dependent manner 99
4.10. $HBV_{core169}$-specific public TCR clones and motif analysis linked to viral clearance 105
4.11. The presence of a HBV-specific conserved CDR3β motif is virus dependent 109

5. DISCUSSION 116
5.1. T cell response during the progression of HBV infection 116
5.2. T cell exhaustion or functional adaption? 119
5.3. Nonlinear T cell functionality and inhibitory receptors 124
5.4. Naïve-like virus-specific $CD8^+$ T cells 125
5.5. Immunodominant virus-specific $CD8^+$ T cells in viral control 127
5.6. Epitope-specific T cell receptor repertoire during viral infection 130

6. CONCLUSION 133

7. REFERENCES 134

LIST OF FIGURES

FIGURE 1. CLINICAL AND VIROLOGICAL COURSES DURING ACUTE VERSUS CHRONIC HEPATITIS B INFECTION 18
FIGURE 2. DISTINCT FEATURES OF HOST T CELL RESPONSES DURING ACUTE VERSUS CHRONIC VIRAL INFECTION 26
FIGURE 3. MASS CYTOMETRY EXPERIMENT WORKFLOW FOR INTERROGATING ANTIGEN-SPECIFIC T CELLS. 29
FIGURE 4. MACHINE LEARNING OF HIGH-DIMENSIONAL CYTOMETRIC DATA. 32
FIGURE 5. COMPREHENSIVE EPITOPE MAPPING STRATEGY AGAINST HEPATITIS B VIRUS (HBV). 52
FIGURE 6. DETECTION AND THE FREQUENCY OF FOUR DOMINANT ANTIGEN-SPECIFIC CD8+ T CELLS IN CHB. 60
FIGURE 7. VALIDATION OF HIGHLY MULTIPLEX COMBINATORIAL PMHC TETRAMER STRATEGY IN HLA-A*11:01 AND NON-HLA-A*11:01 DONORS. 61
FIGURE 8. REPRODUCIBILITY OF DETECTED HBV EPITOPES USING FLOW CYTOMETRY. 64
FIGURE 9. TOTAL ANTIGEN-SPECIFIC CD8+ T CELLS RESPONSE IN VARIOUS CLINICAL STAGES DURING HBV INFECTION 65
FIGURE 10. TOTAL ANTIGEN-SPECIFIC CD8+ T CELLS RESPONSE IN VARIOUS CLINICAL STAGES DURING HBV INFECTION. 66
FIGURE 11. HBV SEROLOGICAL STATUS AND THE RELATIONSHIP WITH HBV_{POL387}-SPECIFIC CD8+ T CELLS IN HEALTHY DONORS. 67
FIGURE 12. *IN VITRO* EXPANSION OF ANTIGEN-SPECIFIC CD8+ T CELLS UPON PEPTIDE STIMULATION. 70
FIGURE 13. *T*-SNE ILLUSTRATED THE PHENOTYPIC DIVERSITY OF SELECTED ANTIGEN-SPECIFIC CD8+ T CELLS ACROSS VARIOUS PATIENT GROUPS. 70
FIGURE 14. THE RATIONALE AND REPRESENTATION OF ONE-SENSE. 72
FIGURE 15. NEIGHBORHOOD PRESERVATION ANALYSIS OF *T*-SNE VS. PCA USED AT VARYING DEGREES OF DIMENSIONALITY REDUCTION 73
FIGURE 16. OVERVIEW OF THE EXPRESSIONS FOR NINE MAJOR INHIBITORY RECEPTORS. 76
FIGURE 17. EXPRESSION LEVELS OF NINE DIFFERENT INHIBITORY RECEPTORS ON ANTIGEN-SPECIFIC CD8+ T CELLS. 76
FIGURE 18. COMPARISON OF NINE INHIBITORY RECEPTORS ON FOUR DOMINANT VIRUS-SPECIFIC CD8+ T CELLS. 77
FIGURE 19. EXPRESSION LEVELS OF NINE INHIBITORY RECEPTORS USING *T*-SNE ANALYSIS. 78
FIGURE 20. CATEGORICAL ANALYSIS USING ONE-SENSE UNCOVERS THE RELATIONSHIPS BETWEEN EXHAUSTION- AND MEMORY-ASSOCIATED MARKERS OF VIRUS-SPECIFIC CD8+ T CELLS. 80
FIGURE 21. UNSUPERVISED HIGH-DIMENSIONAL AND CLUSTERING ANALYSIS SHOWED THE MULTIFACTORIAL IMMUNOME OF HBV_{POL387}-SPECIFIC CD8+ T CELLS ACROSS VARIOUS PATIENT GROUPS. 82
FIGURE 22. ONE-SENSE ANALYSIS OF HBV_{POL387}-SPECIFIC CD8+ T CELLS FOR FURTHER INVESTIGATION OF SELECTED *T*-SNE-DEFINED CELLULAR CLUSTERS. 84
FIGURE 23. SIGNIFICANT ELEVATION OF PMHC TETRAMER INTENSITY OF $HBV_{CORE169}$-SPECIFIC CD8+ T CELLS IN ACUTE RESOLVED PATIENTS. 86
FIGURE 24. DIFFERENTIAL PHENOTYPIC ANALYSIS OF $HBV_{CORE169}$-SPECIFIC CD8+ T CELLS IN VARIOUS PATIENT GROUPS. 87
FIGURE 25. PUTATIVE TRIFURCATION IN 3D CELLULAR TRAJECTORIES OF HBV_{POL387}- AND $HBV_{CORE169}$-SPECIFIC CD8+ T CELLS USING DIFFUSION MAP. 89
FIGURE 26. ASYNCHRONY AND OSCILLATING EXPRESSION OF EXHAUSTION- AND MEMORY-ASSOCIATED CELLULAR PROTEINS IN EACH ANTIGEN-SPECIFIC CD8+ T CELLS TRAJECTORY. 90
FIGURE 27. NAIVE-LIKE HBV_{POL282}-SPECIFIC CD8+ T CELLS IN ADULT AND CORD BLOOD. 93
FIGURE 28. NONLINEAR RELATIONSHIPS OF VIRUS-SPECIFIC CD8+ T CELLS MULTI-FUNCTIONALITY AND INHIBITORY RECEPTORS BY ONE-SENSE. 94
FIGURE 29. HIGHLY HETEROGENEOUS MULTI-FUNCTIONAL SUBSETS OF VIRUS-SPECIFIC CD8+ T CELLS AND THEIR EXHAUSTION AND DIFFERENTIATION STATUS AFTER TCR-VIRAL EPITOPE ENGAGEMENT. 97
FIGURE 30. MULTI-FUNCTIONALITY OF SELECTED HBV-SPECIFIC CD8+ T CELLS. 98
FIGURE 31. THE CLONALITY OF T CELL RECEPTOR (TCR) REPERTOIRE OF SELECTED HBV-SPECIFIC CD8+ T CELLS IN EPITOPE DEPENDANT MANNER 100
FIGURE 32. DISTINCT PAIRING OF Vβ AND Jβ GENE SEGMENT AND COVARIATION IN HBV EPITOPE-SPECIFIC TCR. 103

FIGURE 33. DISTINCT USAGE OF Jβ IN HBV EPITOPE-SPECIFIC TCR AND THE CDR3β CHARACTERISTICS OF TOTAL $CD8^+$ T CELLS. 104
FIGURE 34. EPITOPE-SPECIFIC TCR CHARACTERISTICS AND MOTIF ANALYSIS OF $HBV_{CORE}169$-SPECIFIC TCR REVEAL PUBLIC CLONOTYPES. 107
FIGURE 35. TCR MOTIF ANALYSIS OF $HBV_{POL}282$-SPECIFIC $CD8^+$ T CELLS. 111
FIGURE 36. TCR MOTIF ANALYSIS OF $HBV_{POL}387$-SPECIFIC $CD8^+$ T CELLS. 112
FIGURE 37. TCR MOTIF ANALYSIS OF $HBV_{CORE}195$-SPECIFIC $CD8^+$ T CELLS. 113
FIGURE 38. A VIRUS DEPENDENT HBV-SPECIFIC CONSERVED CDR3β MOTIF. 114

LIST OF TABLES

TABLE 1. LIST OF HLA-A*11:01-RESTRICTED PEPTIDES USED IN COMPREHENSIVE HBV EPITOPE MAPPING AND THE DETECTED FREQUENCY ACROSS VARIOUS PATIENT GROUPS. 41
TABLE 2. ANTIBODY STAINING PANEL FOR MASS CYTOMETRY AND PARAMETERS FOR HIGH-DIMENSIONAL CYTOMETRIC DATA ANALYSIS. 45
TABLE 3. COMPARISON OF A*11:01-RESTRICTED $HBV_{CORE169}$-SPECIFIC AND A*02:01-RESTRICTED $HBV_{CORE18-27}$-SPECIFIC $CD8^+$ T CELLS FROM LITERATURES. 129

ABBREVIATIONS

A

ALT: Alanine aminotransferase

APSAL: The Asian Pacific Association for the Study of the Liver

B

BTLA: B- and T-lymphocyte attenuator

C

CB: Healthy cord blood

CDR3: Complementarity-determining region 3

CHB: Chronic Hepatitis B

CMV: Cytomegalovirus

CTL: Cytotoxic T Lymphocytes

CTLA-4: Cytotoxic T-lymphocytes-associated protein 4

CyTOF: Cytometry by Time-Of-Flight

E

EASL: European Association for the Study of the Liver

EBV: Epstein-Barr virus

ELISA: Enzyme-linked immunosorbent assay

ELISPOT: Enzyme-Linked ImmunoSpot

F

FACS: Fluorescence-activated cell sorting

G

GM-CSF: Granulocyte macrophage colony-stimulating factor

H

HBV: Hepatitis B virus

HCC: Hepatocellular carcinoma

HCV: Hepatitis C virus

HD: Healthy donor

HIV: Human immunodeficiency virus

HLA: Human leukocyte antigen

HVEM: Herpesvirus entry mediator

I

IL-2: Interleukin 2

IA: Immune Active

IAV: Influenza A virus

ICS: Intracellular cytokine staining

IFN-α: Interferon alpha

IFN-γ: Interferon gamma

InA: Inactive carrier

IT: Immune Tolerant

L

LAG-3: Lymphocyte-activation gene 3

LCMV: Lymphocytic choriomeningitis virus

M

MHC: Major histocompatibility complex

MIP-1β: Macrophage inflammatory protein 1 beta

N

NTCP: sodium-taurocholate cotransporting polypeptide

O

One-SENSE: One-dimensional Soli-Expression by Nonlinear Stochastic Embedding

P

PBMC: Peripheral blood mononuclear cell

PCA: Principal Component Analysis

PD-1: Programmed death 1

R

R: acute resolved

RTE: recent thymic emigrants

S

SAv: Streptavidin

T

t -SNE: *t*-distributed Stochastic Neighbor Embedding

TCR: T cell receptor

T_{EX}: Exhausted T cells

TIGIT: T-cell immunoreceptor with Ig and ITIM domains precursor

TIM-3: T-cell immunoglobulin and mucin-domain containing-3

T_{MNP}: Memory T cell with a naïve phenotype

TNF-α: Tumor necrosis factor alpha

TNFR: Tumor necrosis factor superfamily receptor

Y

YFV: Yellow fever virus

ABSTRACT

Human chronic viral infection is associated with T cell dysfunction and persistent yet highly variable viral burden. How such viral antigen-driven disease persistently reshapes the state of antigen-specific T cells by sustaining expression of inhibitory receptors remains unclear. By coupling mass cytometry and a highly multiplexed combinatorial pMHC tetramer staining strategy, we simultaneously probed 484 unique HLA-A*1101-restricted T cell epitopes spanning the entire hepatitis B virus (HBV) genome on $CD8^+$ T cells from chronic hepatitis B patients across various clinical stages. We explored several novel epitope candidates and highlighted diverse cellular profiles on dominant epitopes. Together with the analysis of virus-specific TCR repertoires, various methods of high-dimensional phenotypic analysis of exhaustion and memory markers were explored in relation to HBV disease progression. We identified an immunodominant $HBV_{core169}$-specific $CD8^+$ T cell population, and their memory and multi-functional profiles were linked to viral clearance. Additionally, T cells dysfunctionality was not linearly correlated with the reciprocal accumulation of multiple inhibitory receptors. This report works toward unraveling the unprecedented degree of antigen-specific T cell heterogeneity and T cell exhaustion during natural viral infection.

1. INTRODUCTION

1.1. Hepatitis B virus (HBV)

Hepatitis B virus is a double stranded DNA (dsDNA) virus belongs to hepadnaviridae family. It is a non-cytopathic and highly hepatotropic virus during viral replication. The formation of episomal DNA (covalently closed circular DNA, or cccDNA) as its transcriptional template in the nucleus of infected hepatocytes is thought to be responsible for the chronicity of HBV infection, and therefore avoid from the elimination by nucleotide analogue (NUC) antiviral drug. To date, chronic hepatitis B (CHB) infection still holds a major health issue and leading causative agent of hepatocellular carcinoma (HCC) worldwide. Despite the effective prophylactic vaccine and antiviral drug, HBV-associated deaths have escalated from an estimated 0.89 to 1.45 million in recent years (1). The disease progression of HBV is driven by host immune response, while the HBV-induced immunopathology can eventually lead to liver cirrhosis and the development of HCC.

HBV can either be vertically transmitted via perinatal pathway, or horizontally, through sexual or blood transmission. Unlike the perinatal exposure of HBV where more than 90% of infected children develop CHB, 9095% of horizontally HBV infected adults can clear the virus spontaneously within months by host immunity and establish lifelong immunity. This is associated with robust innate and adaptive immune response and the appearance of antibodies against surface antigen HBsAg (anti-HBs). However, the remaining (5~10%) of infected adults does not resolve the virus and have prolonged infection. Compared to acute resolved HBV infected individuals who typically mount a vigorous multi-epitope-specific T cell response (2-4), chronic HBV infection is associated with an impaired antiviral T cell response (3, 5-10).

The end-stage liver disease (e.g. liver cirrhosis and HCC) jeopardizes the lives of more than 400 million people that are persistently infected by HBV worldwide, especially in Africa, East and

Southeast Asia, which has the highest prevalence of HBV infection. This is despite the availability of an effective prophylactic vaccine almost three decades ago and the various direct antiviral drugs that provide suppression of viral replication. In addition, these common antiviral drugs usually require lifelong administration to achieve viral control. Discontinuation of treatment may trigger viral re-activation and fatal flare of liver inflammation (11, 12). Current management of chronic HBV infection lacks therapeutics that are able to eradicate the virus and maintain immunological suppression over time (3, 13). Therefore, there is an urgent need for the development of an immune-based therapeutic that elicits a full immune response specifically targeting HBV.

During an acute HBV infection, HBV DNA can be detected within the first 4 weeks, followed by the appearance of HBeAg and HBsAg in the next 2 weeks **(Fig. 1)** (3). In the early stage of disease, the titre of anti-HBV core antigen (HBcAg) IgM start to elevate, then sequentially develop HBcAg-specific IgG, which exist lifelong after recovery. Such anti-HBc antibody can be found during chronic HBV infection. In the coming 3-4 months, the peak value of serum alanine aminotransferase (ALT) occurs implying an ongoing hepatic T cell-mediated liver damage. Patients who are able to acutely resolve (R) the infection further recuperate from clinical symptoms and establish specific antibodies against HBeAg and HBsAg, which is considered the signature of full recovery. On the contrary, patients who have chronic HBV infection develop a distinct serological pattern and fail to generate HBsAg-specific antibody, allowing the period of infection to persist from years to decades **(Fig. 1)**. The progression of disease during chronic HBV infection is characterized by different stages based on serological evidence. Conventionally (3, 14), young patients who are in Immune Tolerant (IT) are defined by the presence of HBeAg with high circulating HBV DNA (HBV DNA>2,000 IU/ml), but a normal serum ALT level (vary from EASL (15) to APASL (16) guidelines). This stage can last for decades without significant disease symptoms. Patients can further progress into an Immune Active (IA) phase, an aggressive stage that

can result severe liver failure without appropriate treatment. These patients have high but fluctuating HBV DNA (>2,000 IU/ml) and high ALT above upper limit level. Either by spontaneous or treatment-induced HBeAg-seroconversion, some patients can seroconvert by developing HBeAg-specific antibody (HBeAb) with the loss of HBeAg. By converting HBeAg, which is the indicator of active viral replication, these Inactive Carriers (InA) are considered in a stable state with lower viral replication, with low or undetectable HBV DNA (<200 IU/ml) and normal ALT level. It is noteworthy that patients can stay at this phase for life, but it is also common that patients can have recurrence of HBV and have acute flare due to various factors, such as sudden withdrawal of medication. The characterization of disease stages of HBV, including Immune Tolerant, Immune Active and Inactive Carrier, has been used to identify patient's status in both clinic and research as a well-accepted concept in referring disease progression and host immune response, until recently be challenged (17, 18), arguing such vague definitions without direct immunological evidence could impede early treatment opportunity. In this report, the terminology of Immune Tolerant (or non-inflammatory), Immune Active (or inflammatory) and Inactive Carrier are only used for the characterization of different CHB stages based on the objective serological evidences (HBeAg, viral load and ALT) instead of representing the actual immunological events occur within infected individual.

A

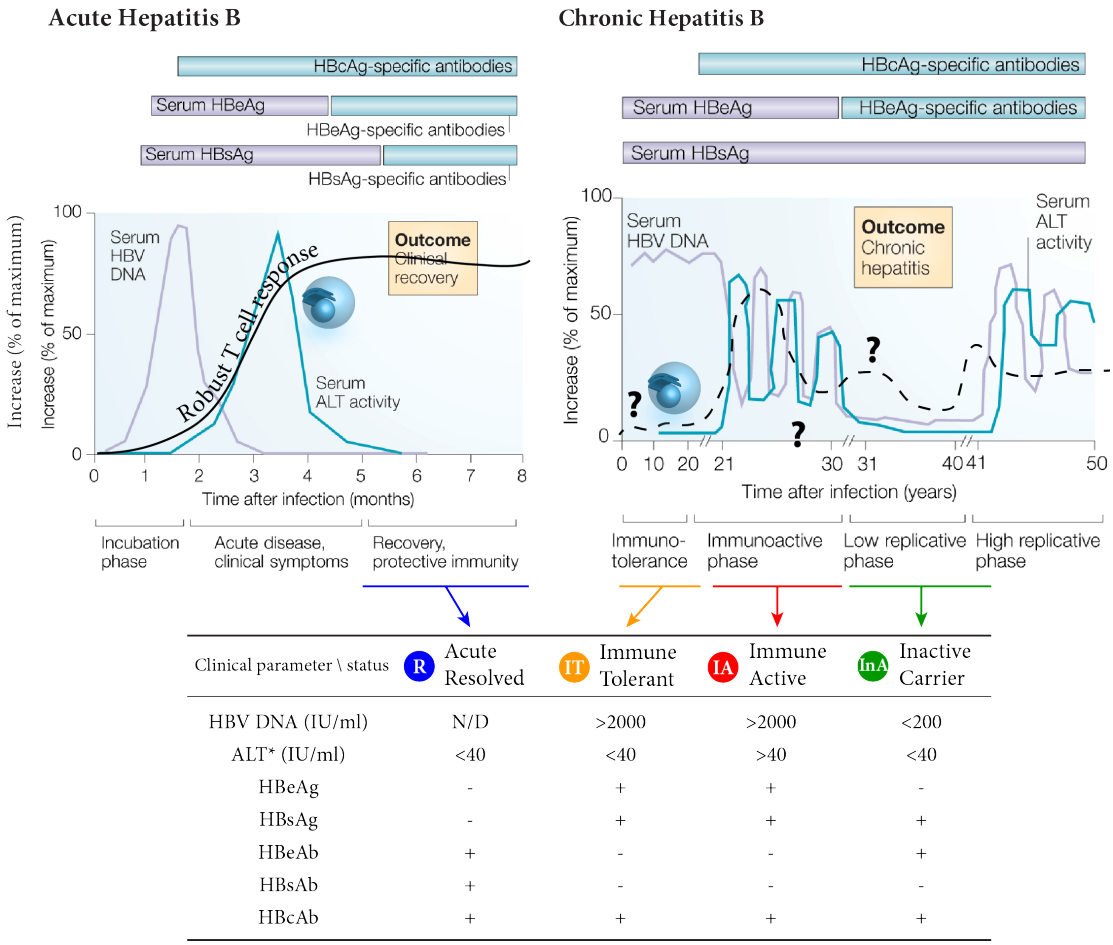

Clinical parameter \ status	R Acute Resolved	IT Immune Tolerant	IA Immune Active	InA Inactive Carrier
HBV DNA (IU/ml)	N/D	>2000	>2000	<200
ALT* (IU/ml)	<40	<40	>40	<40
HBeAg	-	+	+	-
HBsAg	-	+	+	+
HBeAb	+	-	-	+
HBsAb	+	-	-	-
HBcAb	+	+	+	+

Figure 1. Clinical and virological courses during acute versus chronic hepatitis B infection.

(A) HBV infection can lead to distinct clinical outcomes. Horizontal transmission in adult patients usually develop acute HBV infection (Left). Patients are able to spontaneously clear the virus, with the generation of strong virus-specific T cell responses and anti-HBsAg antibody, followed by clinical recovery within several months. Whereas chronic HBV infection that are often seen in vertical transmission (Right) can lead to lifelong infection. It features the presence of HBsAg, and the failure to develop anti-HBsAg antibody (HBsAb). This persistent HBV infection can last for decades and eventually leads to severe liver injury. Chronic hepatitis B infection can be traditionally characterized into different clinical stages based on serological evidence (serum ALT, serum HBV DNA and the appearance of HBeAg). Adapted and modified from Rehermann B & Nascimbeni M, 2005 Nat Rev Immunol. *ALT, alanine transaminase, as the indicator of liver inflammation, which could vary from gender and regional guidelines.

1.2. Virus-specific $CD8^+$ T cells

HBV is a hepatotropic virus that is capable of inducing T cell-mediated immunopathology during the course of immune response, leading to severe liver injury. As the foot soldiers of host immunity, $CD8^+$ T cells are critical in fighting against invading pathogens, especially viral infection. During the HBV infection, intrahepatic $CD8^+$ T cells control the virus at the site of infection through cytolytic or noncytolytic pathways (19). Virus-specific $CD8^+$ T cells targeting multiple epitopes and their antiviral cytokine responses are the key immunological events in eliminating HBV infection (20-24). Chisari and colleagues have shown the $CD8^+$ T cell is associated with viral clearance in HBV infected chimpanzees (19, 25). The depletion of $CD8^+$ T cells resulted prolonged infection and postponed the onset of viral clearance, while CD4-depleted animal was unaffected (19).

In contrast to the robust adaptive immune response induced in acute HBV infection, patients who develop chronic HBV infection have impaired T cell responses, including lower frequency of virus-specific T cells (2, 3, 20, 22), downregulation of antiviral cytokines (e.g. IFN-γ and TNF-α) (6, 26, 27), less T cell proliferation (27, 28), upregulation of inhibitory receptors (26, 27, 29, 30), increased T cell death (31) and altered T cell metabolism (32).

It is known that several viral epitopes contribute largely in triggering virus-specific $CD8^+$ T cells responses that could provide potential protection against HBV (20, 22, 24). Despite the difficulties associated with the study of HBV-specific $CD8^+$ T cells derived from human liver, several studies have successfully identified these cells. For instance, the frequency of intrahepatic $HBV_{core18-27}$-specific $CD8^+$ T cells has been shown to be inversely correlated with HBV DNA viral load and has been intensively studied (22, 24, 33). Interestingly, *in vitro* expansion showed a larger increase of circulating IFN-γ-producing HLA-A*02:01-restricted $HBV_{core18-27}$-specific $CD8^+$ T cells in acute resolved patients (20, 34), and less expansion in patients with moderate HBV

DNA viral load, and no expansion in patients with high HBV DNA viral load (24, 26). However, this viral replication-associated phenomenon was not observed in HBV env (envelop)- or pol (polymerase)-specific $CD8^+$ T cells.

Identifying the antigen-specific T cells and understanding their immune response in the host-virus interaction has been one of the major goals in the field of viral immunology. Until the invention of peptide-MHC (pMHC) tetrameric complex technology (35), traditional approaches in investigating the antigen-specific T cells differ greatly, including the adoptive transfer of antigen-specific T cells (e.g. murine LCMV model), CTL ^{51}Cr release assay, and peptide-induced Enzyme-Linked ImmunoSpot (ELISPOT) or peptide-stimulated intracellular cytokine staining (ICS) assay (36). These methods offer the first attempts for immunologists in spite of several drawbacks. For instance, although adoptive transfer of LCMV-specific T cells provides a well-defined model in the study of antigen-specific T cells dynamic and function, it does not always reflect the broad spectrum of antigen-specific T cells induced by a natural infection in human. CTL ^{51}Cr release assay is based on the calculation of "lytic unit", which is not quantitative and could be confounded. Indeed, ELISPOT provides single cell resolution and is able to detect rare virus-specific T cells, but the experiment procedure is time consuming and can be easily affected by contamination. Importantly, the peptide-induced cytokine release ELISPOT or ICS allows only the detection of antigen-specific T cells that can produce certain cytokine (usually IFN-γ), ignoring the possibility of multifunctional antigen-specific T cells, naïve T cell precursor or nonresponsive antigen-specific T cells. The latter have been described as T cell exhaustion and often seen in persistent viral infection, such as HBV (27, 29).

Through decades, mapping for potential virus-specific $CD8^+$ T cells against HBV has focused on HLA-A*02:01-restricted epitopes (20), covering the dominant HLA alleles in Europe and North America. Most of the studies have therefore mainly worked on this single allele (22, 24, 26, 27, 31, 33, 34, 37, 38). For instance, A*02:01-restricted $HBVc_{18-27}$-

specific $CD8^+$ T cells response has been linked to viral clearance, and variants of such epitope can lead to immune escape by hampering the TCR recognition and antiviral effect (20, 39). Intense studies on this immunodominant epitope have drawn many implications on T cell-based immunotherapy, including the blockade of overexpressed inhibitory receptor Programmed Death-1 (PD-1) to reinstate T cell function (26, 27, 29), adoptive transfer of engineering T cells (40), and TCR-like (TCR-L) antibody (41) to deliver interferon-α (IFN-α) directly onto infected hepatocytes. However, in Asia, where has one of the highest prevalence of HBV infection, the predominant allele is A*11:01, whose immunogenicity against HBV is poorly defined.

Presently, the major obstacles in studying HBV-specific $CD8^+$ T cells are, i) the extremely low frequency that can be detected in chronic HBV infected patients, ii) the limited amount of known HBV epitopes for HLA-A*02:01, HLA-A*11:01 or other HLA alleles. Recently, the revolutionary UV-cleavable MHC class I (MHCI) peptide (42) and multiplex combinatorial tetramer strategy (43, 44) have facilitated the discovery of novel antigen-specific T cells in a high-throughput manner. The combined power of mass cytometry (CyTOF, Cytometry by Time-Of-Flight) and bioinformatics provide the feasibility to simultaneously assess up to hundreds of antigen specificities in a single human sample with an objective computational validation, allowing the detection of rare population of antigen-specific T cells (44, 45).

Another excellent question of adaptive immune response in persistent viral infection is whether there is T-cell deletion induced by viral epitope recognition. This has not been adequately addressed in chronic HBV infection due to the accessibility of direct epitope mapping and the extremely low frequency of virus-specific T cells. Such low detectability could confound whether or not they are deleted in the patients. Future studies may be able to more adequately address this through the use of large blood volumes and higher sensitivity detection methods (46). In persistent lymphocytic choriomeningitis virus Clone 13 (LCMV C13) infection, GP_{33}-specific $CD8^+$ T cells maintained overtime,

while $CD8^+$ T cells specific for NP_{396} epitope, which has higher functional affinity than GP_{33}, were largely deleted (47, 48). It has been reported that the envelope-specific $CD8^+$ T cells may escape deletion by a state of partial tolerance in chronic HBV patients with high viral load (33). Nonetheless, how such repetitive presentation of high affinity viral epitopes drives the T cell deletion or exhaustion during chronic HBV infection remains elusive.

1.3. T cell exhaustion and memory

Fifteen years ago, Guidotti et al. reported that HBV cccDNA could be cleared without the destruction of hepatocytes in chimpanzees during acute HBV infection (25). This challenged the existed concept that HBV infection was exclusively cleared by cell-mediated cytopathic mechanisms, and suggested the involvement of non-cytopathic pathways, such as IFN-γ and TNF-α. On the other hand, chronic HBV infection is associated with T cell dysfunction resulting the failure of long-term immunity and persistent yet highly variable viral burden. Prolonged viral antigen exposure coincides with the upregulation of multiple inhibitory receptors/ligands on dysfunctional T cells.

Learning from murine chronic LCMV infection **(Fig. 2)**, sustained and elevated viral antigenic exposure coincides with the upregulation of multiple inhibitory receptors on virus-specific T cells has been addressed as a state of T cell exhaustion (49-52). It was firstly introduced by Rolf Zinkernagel (51, 53), and later well defined by Ahmed and Wherry (49, 52). The resemblance of exhausted T cells (T_{EX}) observed in human chronic viral infection not only provides an explanation for the functional failure of immune response, but also a valuable target to boost adaptive immunity. Such phenomenon has been widely described in HBV (26, 29, 31, 32), HCV (54-57) and HIV (58). In acute viral infection, a robust adaptive immune response is followed by memory T cell development after the contraction phase, which protects the host for future challenge. However, when the antigen persists, the cellular program governing effector and memory T cell development are

altered greatly by the continuous antigen stimulation, and dysfunctional or so called “exhausted” T cells are generated (49) (**Fig. 2)**. Various lines of evidence have suggested that such exhausted virus-specific T cells arise from the altered path of $CD127^{+}KLRG\text{-}1^{-}$ memory T cells compartment (59), along with several other defects, such as impaired effector functions (IFN-γ, TNF-α, IL-2 and CD107a) (50), incapable or limited self-renew and proliferation (49), upregulation of inhibitory receptors (or “exhaustion markers”, e.g. PD-1) (60), increased pro-apoptotic molecule (31), and epigenetic (61) and transcriptional reprogramming (57, 62, 63).

T cells undergoing the exhaustion program differ significantly from naïve and effector T cells not only in their functionality but also at the transcriptional level (52, 64). Typically, exhausted T cells have been characterized as $PD\text{-}1^{+}CD127^{lo}CD45RO^{+}$ T cells (58, 60, 65), with the recent addition of transcription factor Blimp-1 (66), and a reciprocal expression of EOMES and T-bet (57). Importantly, in the observation of LCMV and HCV, only $EOMES^{lo}$ $T\text{-}bet^{hi}$ $PD\text{-}1^{mid}$ T_{EX} cells were able to restore functional capacity by PD-1 blockade (57), while $EOMES^{hi}$ $T\text{-}bet^{lo}$ $PD\text{-}1^{hi}$ T_{EX} cells were nonresponsive or prone to deletion. Adding on this point, pro-apoptotic molecule BIM was shown to be significantly upregulated in virus-specific T_{EX} cells, and mediated T cell death in chronic but not acute HBV infection (31).

Ever since the discovery of PD-1-regulated immune suppression (67, 68), numerous inhibitory receptors have been suggested and used as alternative exhaustion markers, and contribute to the state of T cell exhaustion in the context of various persistent viral infection, including TIM-3 (29, 56, 69, 70), LAG-3 (18, 71, 72), CTLA-4 (27, 71), 2B4 (54, 69), CD160 (54, 73), BTLA (30, 74) and TIGIT (75, 76). Supported by the abovementioned cellular signatures of T cell exhaustion and inhibitory receptors blockade experiments (60), Wherry and colleagues have proposed a model of “Hierarchical T cell exhaustion”, where the progressive lost of multi-functionality correlates with the expression of

more inhibitory receptors over the course of chronic viral infection (49, 77).

In recent years, rescuing the exhausted T cells to its full or partial functionality is therefore a primary goal for many immunologists. Although the hierarchical functional loss has been implied to correlate inversely with the increase of multiple exhaustion markers on antigen-specific T cells during chronic viral infection (49), which is the logical foundation of therapeutics design involving dual inhibitory receptors blockades (27, 29, 56, 78-80), compelling evidence has shown controversy in the differential usage of exhaustion markers and its defined subsets (69, 73, 81-84), challenging the model of hierarchical T cell exhaustion. For instance, *in vitro* dual blockade of PD-1 and TIM-3 showed enhanced cytokine production and proliferation in chronic viral infection (29, 56, 83), whereas cytotoxicity against hepatocytes that expressed cognate HCV epitope was increased exclusively by TIM-3 blockade (56). The distinct expression of phenotypic pattern of TIM-3^+ and PD-1^+ T cells has also been reported (56, 82, 85). In addition, in patients with HBV-associated hepatocellular carcinoma (HCC), the expression of TIM-3 and PD-1 is minimally overlapping in tumor-specific intrahepatic T lymphocytes (IHL) with only TIM-3^+ T cells having reduced expression of CD28 (83).

The hallmark of inhibitory molecules is the ability to receive or transmit coinhibitory signals. However, accumulating data have suggested the potential dual functionality of these “inhibitory receptors”. For instance, TIM-3 was been shown to synergize with Toll-like receptors (TLR) to induce innate immunity and promote Th1 response (86). Adoptive transfer of TIM-3 KO TCR-transgenic $CD8^+$ T cells demonstrated that TIM-3 signaling directly enhances $CD8^+$ T cells response against acute *Listeria monocytogenes* infection (87). In chronic HCV infection, 2B4 delivers both inhibition and stimulation signaling to HCV-specific $CD8^+$ T cells in a SAP (SLAM-Associated Protein)-dependent manner (84). Recently, Flynn et al. also addressed the *trans* signaling of BTLA to HVEM-expressing $CD8^+$ T cells that

promote effector T cell survival that is crucial for memory T cell development during a vaccinia virus (VACV) infection (88).

The recent success of PD-1 and CTLA-4 blockade in anti-tumor immunity dramatically facilitates the possible regime of boosting T cell response against other diseases (89). Comparing to acute viral infection (e.g. FLU) or latent viral reactivation (e.g. CMV and EBV), the antigen persistency during chronic viral infection divert effector and memory T cells differentiation through the persistent recognition of antigen and T cell receptor (TCR) (65). Notably, data comparing acute LCMV Armstrong (Arm) infection and chronic LCMV Clone 13 (C13) infection have indicated that the upregulation of PD-1 on virus-specific T cells is the consequence of continuous antigen recognition spanning the course of antigen persistency (90, 91), suggesting PD-1 is rather antigen specific (89). Nevertheless, given the nature of continual antigen-TCR binding throughout the course of decades of human chronic viral infection, the direct relationships of overexpressed PD-1, viral epitopes and corresponding TCR repertoire have yet defined. How such antigen-driven chronic HBV infection persistently reshapes the exhaustion and memory state of virus-specific $CD8^+$ T cells during HBV disease progression by upregulating exhaustion markers remains unclear.

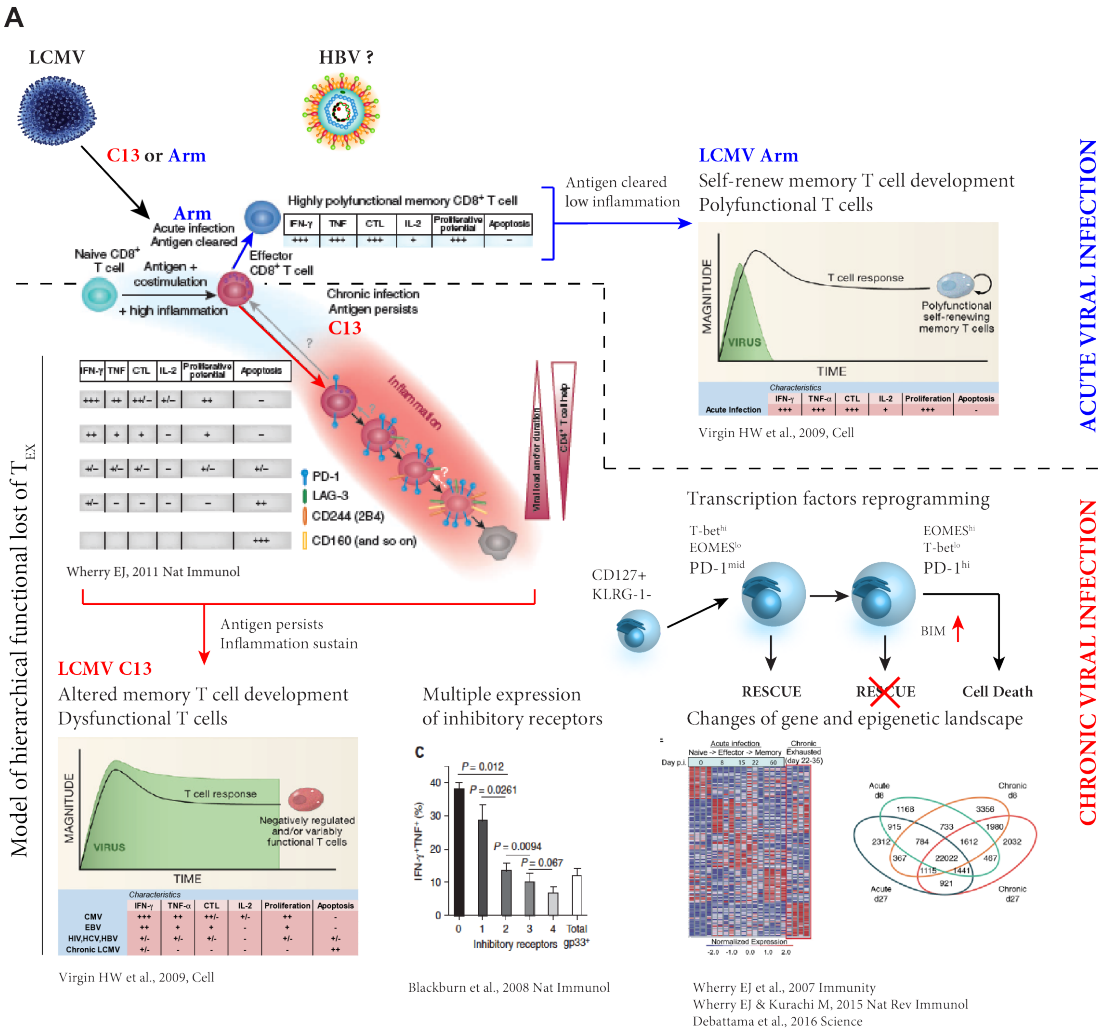

Figure 2. Distinct features of host T cell responses during acute versus chronic viral infection.

(A) When virus infection occurs, T cells response differently comparing acute versus chronic infection. In addition, some viruses can trigger both acute and chronic infection, such as HBV, HCV, and murine LCMV. Unlike acute viral infection that induces full adaptive immunity and clearance of virus, chronic viral infection features T cell dysfunction, or also termed T cell exhaustion. In chronic viral infection, sustained viral antigen recognition challenges the T_{EX} over time, resulting multiple signature markers that impair the functional immune response. The model of hierarchical T cell exhaustion suggests the progressive T cell functional lost is correlated to the over-expression multiple different inhibitory receptors on T_{EX}. Reciprocal expression of transcription factor T-bet and EOMES has been linked to dictate the date of T_{EX} and its implication on PD-1 blockade in both LCMV and HCV. In addition, the pro-apoptotic molecule BIM, has been shown to upregulated in virus-specific T_{EX} in chronic HBV infection. PD-1, Programmed cell Death-1. BIM, Bcl-2 Interacting Mediator. EOMES, Eomesodermin.

1.4. Mass cytometry (Cytometry by Time-Of-Flight)

Continuous improvements in single-cell analysis methods are allowing for exploration of cellular diversity at unprecedented depth and throughput. The development of fluorescence-based flow cytometry (92) and the ability to probe single-cell protein expression with high throughput has been instrumentally laid the foundations of modern cellular immunology (93). It offers the characterization of cell frequency, cell subsets, protein expression, and functional or proliferative assessment. More recently, high-dimensional poly-chromatic flow cytometry (94) and mass cytometry (95-97) allow for identification of numerous cellular subpopulations and the ability to probe relationships between expression levels of large numbers of proteins simultaneously.

Mass cytometry is a next-generation of flow cytometry based on atomic mass spectrometry (98, 99) that uses metal isotope tagged antibodies to probe cells for expression of protein antigens that are quantified on individual cells using time-of-flight mass spectrometry. These metal isotopes are purified mainly from lanthanide family (with atomic numbers from 57 to 71 on periodic table) that are rarely seen in biological system (95) making them ideal as exogenous tags to probe mammalian cells. Because of the limited fluorophores and the difficulties associated with spectral compensation in flow cytometry experiments, most laboratories measure cells with no more than 10~12 parameters at a time. However, with the development of novel dyes and improved flow cytometry instrumentation, this number will continue to rise (93). In contrast, the mass window (analog to fluorescent channel) of mass cytometry is >100 atomic mass channels with limited-to-no crosstalk. The measurements depend on the availability and quality of purified metal isotopes and the availability of appropriate chemistries for labeling probes (99). Current practice of mass cytometry allows simultaneously measuring more than 40 different antibody parameters, permitting in-depth analysis of multiple aspects of cellular diversity of immune cells, exemplified particularly in T cell biology.

Mass cytometry is composed of cell introduction system, inductively coupled plasma mass spectrometry (ICP-MS) (100), Time-Of-Flight (TOF) and computer that collects and processes data (95). The detailed methodology of mass cytometry has been described in detail elsewhere (93, 99, 101). Briefly, the cells labeled with metal-tag antibodies are pushed into machine by argon gas and nebulizer to form single-cell aerosol. Together with the inductive coil and flowing argon stream, they generate high-temperature (7,000°K at surface and 5,500°K in the core) plasma that construct the central component, ICP. Single cell is introduced into this toroidal plasma along the axis in a spray chamber heated to 200°C. The plasma further vaporizes the cells, breaking all molecular bonds to ionize each atom that have ionization capacity. Subsequently, this ionized cloud moves into the quadrupole that allows only heavier ions (>100 Da) to filter through, leaving the biological abundant atoms from cell (e.g. carbon, sulfur, hydrogen and nitrogen) behind. Filtered ions then enter into Time-Of-Flight and detector that configures the dual count of each metal signal, and finally processed by computer to produce data file. We have described a thorough mass cytometry experimental workflow and methodology (102), including antibody conjugation, cell staining, DNA and cellular barcoding, cell acquisition, data processing, and the rationale of panel design for probing T cells. All experiments in this report were done in this manner, which summarize here in **(Fig. 3)** and in section of **Materials and Methods**.

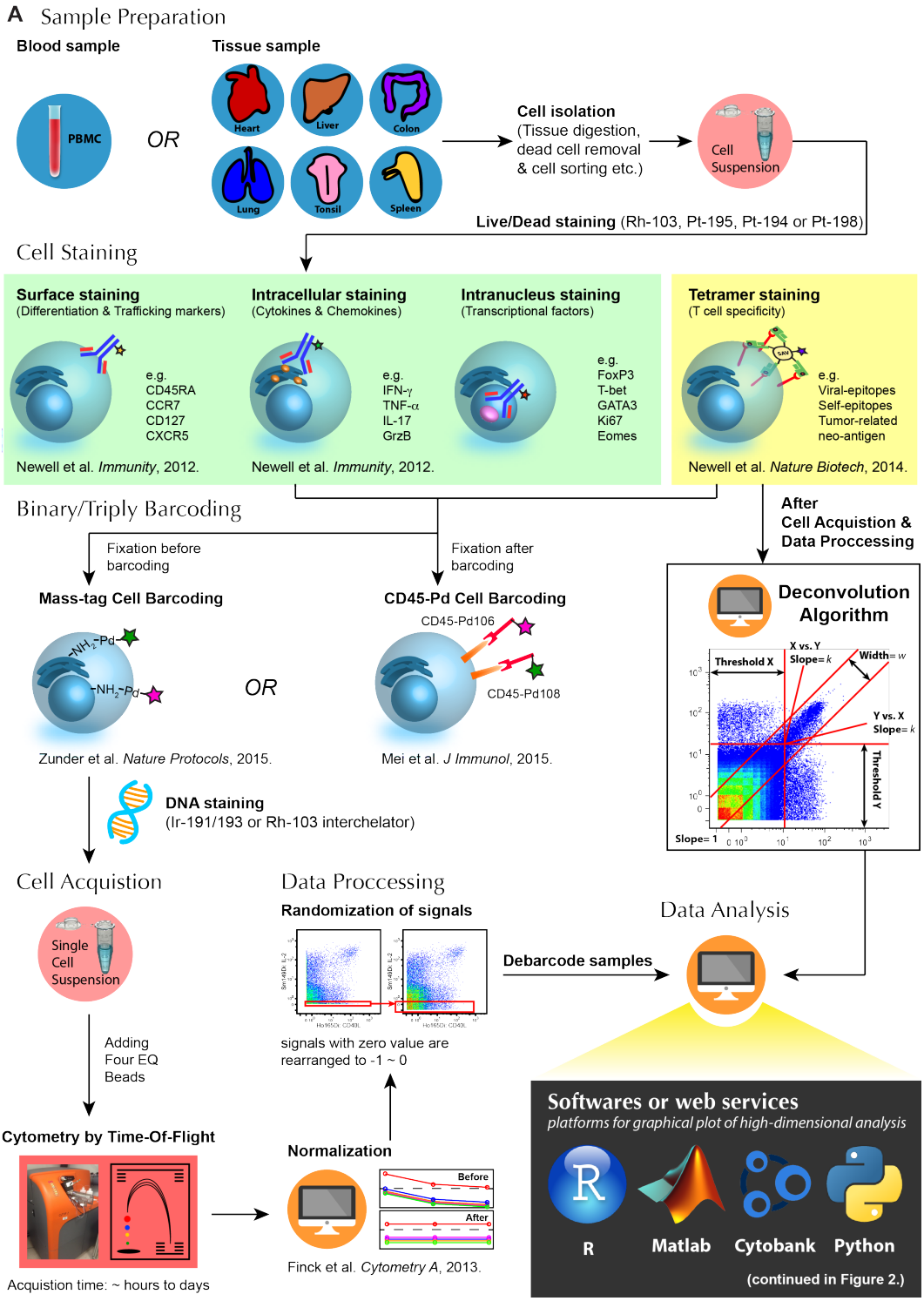

Figure 3. Mass cytometry experiment workflow for interrogating antigen-specific T cells.

(A) The experimental procedure for study of T cell using mass cytometry can be separated into multiple steps, including i) sample preparation, ii) cell staining, iii) cell barcoding, iv) acquisition of CyTOF, v) data processing (normalization, randomization and cell de-barcoding), and vi) high-dimensional data analysis. Briefly, cells are isolated from PBMC

(peripheral blood mononuclear cells) or tissue samples. After the optional enrichment step, cell suspension is stained with Cisplatin for distinguish dead cells. Principally, cells were probed with surface, intracellular, or intranuclear markers after tetramer staining (if applicable). Cells can be further barcoded by Mass-tag cell barcoding (after cell fixation), or CD45-Pd cell barcoding (before cell fixation) system. Fixed cells are stained with Iridium or Rhodium DNA-interchelator and re-suspended in deionized water for subsequent acquisition on CyTOF. Collected data are converted into FCS file and metal signals are normalized. De-barcoded samples are loaded onto a bioinformative platform (usually in a MATLAB or R environment, or online server such as Cytobank.org) of choice for high-dimensional cytometric analysis (Adapted from Cheng and Newell, 2016 *Adv Immunol*).

1.5. High-dimensional cytometric data analysis

The simple visualization using hierarchical sub-gating schemes based on the marker expression on biaxial dotplots has provided a straightforward approach to analyze flow cytometry data. However, subjective manual gating is based on expert training and expectation, which could vary between researchers and laboratories. The characterization of subsets could be therefore biased. The FlowCAP (Flow Cytometry: Critical Assessment of Population Identification Methods) consortium and several groups have established various computational methods to improve the precision and accuracy of flow cytometry analysis (103). These automated methods include density-, model-, or nonparametric clustering-based methods, which have open access and are easily available using R or MATLAB source code.

Given the complexity and high-dimensionality of mass cytometry data, limitations in the utility of biaxial gating approaches are immediately apparent and this has forced the adaptation and development of many high-dimensional data analysis methods (93, 104). Beyond this though, current platforms for high-dimensional (>10 dimensions) cytometric data analysis are mostly based on “Clustering” approaches, “Dimensionality Reduction” methods, or combinations thereof **(Fig. 4)**. We have reviewed several machine learning algorithms (102) currently used for analysis of mass cytometry data and discussed their benefits and limitations (105). In this section, we only emphasize the analytical approach we used for this report. All of the following methods belong to dimensionality reduction approach, whose main function is to reduce the number of random variables under different purpose-driven considerations by feature extraction.

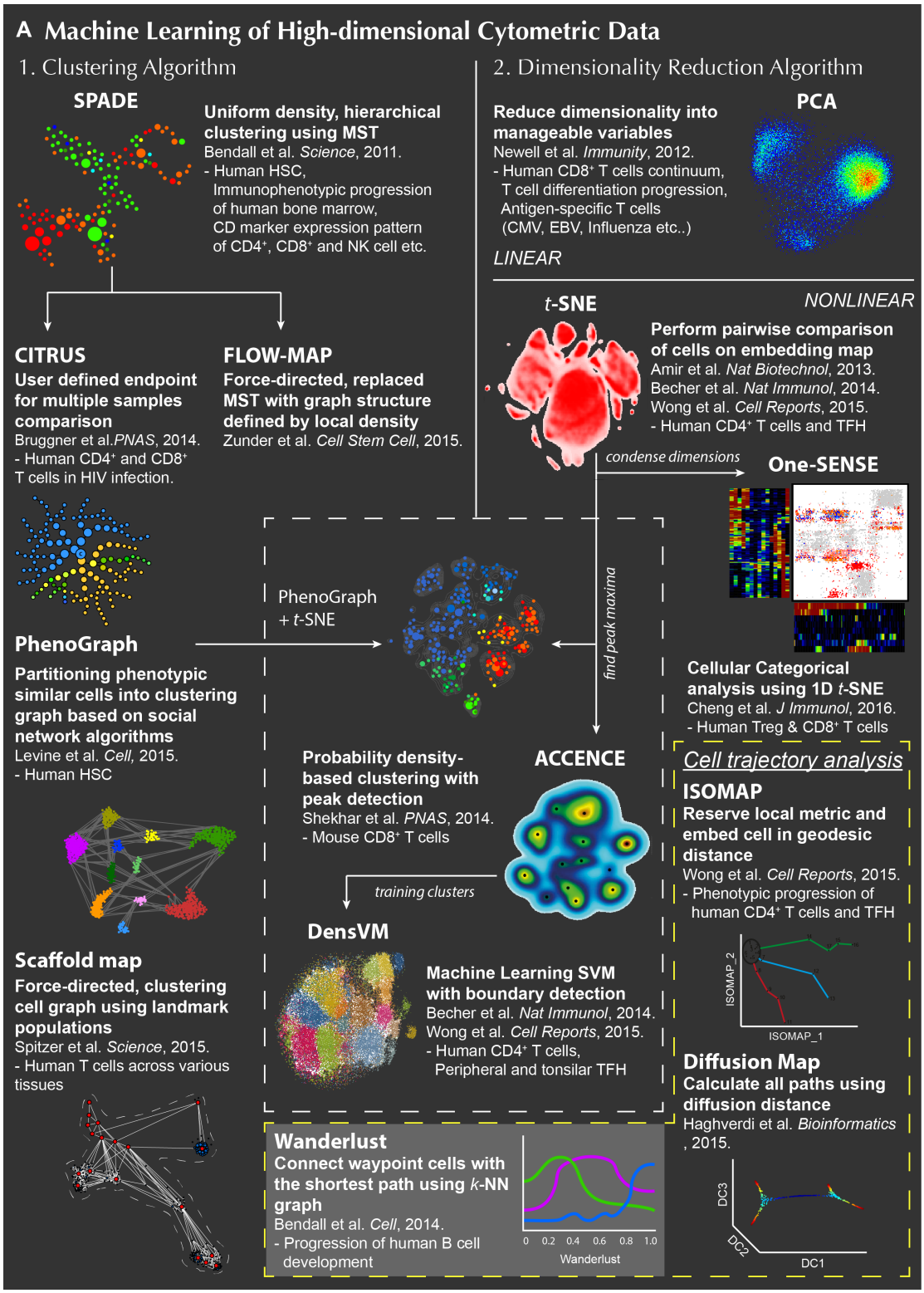

Figure 4. Machine learning of high-dimensional cytometric data.

(A) Comparing to traditional visualization of cellular marker on bivariate dotplots, high-dimensional cytometric analysis approaches can be separated into two categories based on their algorithms. Clustering algorithm: SPADE (Spanning Tree Progression of Density Normalized Events), a hierarchical clustering algorithm using MST (Minimum

spanning tree), and its derived forms including Citrus and FLOW-MAP. PhenoGraph and Scaffold map are the other two types of clustering analysis based on different rationales and algorithms. Dimensionality Reduction algorithm: PCA (Principal component analysis) reduces dimensionality in a linear manner. Alternatively, nonlinear dimensionality reduction algorithms that are useful for high-dimensional cytometric data are *t*-SNE (t-distributed stochastic nonlinear embedding), and its modified algorithms ACCENSE and DensVM with the clustering ability using density-based approach. Categorical dimensions of One-SENSE (One-dimensional Soli-Expression by Nonlinear Stochastic Embedding) are condensed from t-SNE along with the heatplots of markers expression. *t*-SNE can also be combined with PhenoGraph to better identify cell clusters. Other nonlinear dimensionality reduction algorithms used for cell phenotypic progression or trajectory analysis are ISOMAP (Isometric feature mapping), Wanderlust, and a recent proposed Diffusion map that simulates cell differentiation with branched continuums (Adapted from Cheng and Newell, 2016 *Adv Immunol*).

1.5.1 Principal Component Analysis (PCA)

It has been widely used in many biological datasets and is the first of its type proposed for such purpose. PCA (106) digests the high-dimensional cellular data into manageable surrogate variables (principal components) in a linear fashion in such a way that the first and second principal components contain the largest possible variance, and segregated major populations that resemble their relatedness. Several groups have applied PCA in analyzing human peripheral $CD8^+$ T cells (44, 97, 107-109) and shown a great magnitude of T cell heterogeneity within a continuum of cell differentiation and poly-functionality. Besides delineating the T cells in global population, the definite phenotypes between different antigen-specific T cells can be conveniently distinguished and visualized under the utilization of PCA, such as FLU, CMV, EBV-specific $CD8^+$ T cells (97, 109) located in regions of central memory (T_{CM}), effector memory (T_{EM}), to late-stage effector cells on PCA visualization, respectively.

1.5.2 t-distributed Stochastic Neighbor Embedding (t-SNE)

Building on nonlinear transformation, *t*-SNE (110) calculates the probability distribution of pairwise distances of points (cells) in high-

dimensional metric space, giving similar points high probability and dissimilar points infinitesimal probability of being chosen, and projects the points with respect to the distances on a two-dimensional (or three) map. It has been used to visually determine immune cell subsets (111) and worked exceptionally well in identification of rare population (112). The impressive utility of *t*-SNE analysis has been proved in uncovering high-dimensional cytometric data of $CD4^+$ T helper cells (113), regulatory T cell (Treg) (114) and $CD8^+$ T cells (115, 116).

1.5.3 One-dimensional Soli-Expression Nonlinear Stochastic Embedding (One-SENSE)

An effective reference map should enable unsupervised identification of cell with a data-driven organization that is flexible enough to accommodate different types of measurements. For instance, to directly assess the relationship of T cell exhaustion versus memory immunome profiles on antigen-specific T cells. We have recently developed One-SENSE (116), to orchestrate the cell using *t*-SNE with purpose-driven categorical analysis of cellular marker expression. It projects the cells using one-dimensional *t*-SNE analysis based on the pre-defined cellular category. Cells embedding are binned and defined by their categorical expression on One-SENSE map. This framework recalls the marker expressions that immerse in other high-dimensional cytometric analysis without the necessity of excessive marker annotation. Importantly, this improvement provides the opportunity to unbiasedly depict all possible combinations of proteins co-expression examined in the experiment. We have used this unique approach to decipher functional $CD8^+$ T cells, Treg heterogeneity and resident memory T cells (T_{RM}) trafficking profiles (116, 117) by direct comparison of different categories of T cell immunome, such as differentiation versus trafficking. Detailed rationale and methodology can also be found (116).

1.5.4 Diffusion map

One of the major goals in single-cell measurement is to understand the progression of cellular state (e.g. differentiation and function). Therefore, it is a great interest to model cell trajectory to resolve potential T cell heterogeneity during immune response. Diffusion map (118, 119), a dimension reduction algorithm using diffusion distance to preserve the data structure as a branched continuum. Haghverdi et al. refined the transition probability matrix to determine the diffusion distance between pair cells through all possible paths. It simulates the dynamics of cell differentiation while resisting to noise and sampling density heterogeneities. A recent report has shown the unique usage of Diffusion map in cellular trajectory to trace the development of human dendritic cells (DC) lineage (120).

2. AIMS

2.1. To comprehensively probe HLA-A*11:01-restricted T cell epitopes against HBV with simultaneous cellular phenotyping during the progression of chronic HBV infection using a highly multiplexed combinatorial pMHC tetramer staining strategy and mass cytometry.

2.2. To address virus-specific T cell exhaustion in human chronic HBV infection across the events of disease progression and to test the model of “Hierarchical T cell exhaustion” by investigating the relationships between nine major inhibitory receptors and other memory- or functional-associated markers.

2.3. To objectively and directly assess virus-specific T cell heterogeneity across human chronic HBV infection using various unsupervised high-dimensional analyses.

3. MATERIALS AND METHODS

3.1 Patient samples and PBMC isolation

Patients with HBV infection were recruited with fully informed written consent from Division of Gastroenterology and Hepatology at National University Health System, Singapore. The respective local ethical institutional review boards approved the study, and the recruitment and sampling of suitable patients was completed at hospital. Up to 60 ml of blood was taken, peripheral blood mononucleated cells (PBMC) were further isolated by using Ficoll-separation (Ficoll-Paque PLUS, GE Healthcare). Blood from anonymous healthy donors were also recruited under Singapore Immunology Network (SIgN) institutional review board. All patients had clinical, serological and virological evidences of chronic hepatitis B infection with detection of HBsAg and HBV DNA, and no positive result for the presence of HIV-1 and -2, and HCV. Three CHB patient groups, Immune Tolerant (IT, HBV DNA>2000 IU/ml, ALT<40 IU/ml, HBeAg+), Immune Active (IA, HBV DNA>2000 IU/ml, ALT>40 IU/ml, HBeAg+), Inactive Carrier (InA, HBV DNA<100 IU/ml or undetectable, ALT<40 IU/ml, HBeAg-) and one group of acutely resolved patients (R, HBsAg- and anti-HBc antibody+) were enrolled in this study. Each patient in three CHB groups had at least three adjacent time points indicating consistent virological and serological evidences for the referring clinical stages. All patients were treatment free from any antiviral drug or clinical intervention at the time of blood draw. Serological and virological scores (serum HBV DNA, HBeAg and HBsAg) and liver function test (ALT, AST, AFP, ALP, LDH, Albumin and Bilirubin) were determined by clinical laboratory at hospital or ELISA. Healthy cord blood samples were purchased from Singapore Cord Blood Bank under the institutional review board, without detection of HIV-1 and -2, HTLV-I and II, HCV, CMV, HBsAg and anti-HBc antibody. HLA-A was confirmed by HLA typing service from BGI Genomics.

3.2 Amplification of HBV genome and library construction

Seven HBeAg non-seroconverters and eight HBeAg seroconverters of patients chronically infected by HBV (including genotype B and C) were recruited in National University Health System, Singapore. Multiple longitudinal serum samples (5 to 15 time points per patient) from each patient were taken across the event of HBeAg seroconversion. Deep sequencing analysis was performed in all serums samples by sequencing the whole HBV viral genome. Briefly, Primers (*5'-GCTCTTCTTTTTCACCTCTGCCTAATCA-3'* and *5'-GCTCTTCAAAAAGTTGCATGGTGCTGG-3*') were used to generate full-length amplicons of the HBV genome. Polymerase chain reaction (PCR) was performed using the PfuUltra™ II Fusion HS DNA Polymerase (Stratagene, La Jolla, California, USA) according to the manufacturer's instructions. The 3.1 kb fragment was extracted from 1% agarose gel prepared in 1 x TBE buffer, using the QIAquick Gel Extraction Kit (Qiagen, Valencia, CA, USA) and the concentration of the extracted product was measured using the NanoDrop ND 1000 Spectrophotometer (Thermo Fisher Scientific, Waltham, MA, USA). Each sample was fragmented into 100-300 bp using the Covaris S2 (Covaris, Woburn, MA, USA). (Shearing conditions - Duty cycle: 20%; Intensity: 5; Cycles per burst: 200; Time: 110 seconds). After fragmentation, the samples were purified using the QIAquick PCR purification kit (Qiagen, Valencia, CA, USA). The DNA 1000 Chip was used with the 2100 Bioanalyzer (Agilent Technologies, Santa Clara, CA, USA) to check the size and quality of the fragmented products. For library construction, the KAPA Library Preparation Kit (KAPA Biosystems) was used according to the manufacturer's instructions. The library construction includes end repair, A-tailing, ligation of adapters and a final PCR step that incorporates the indexes into the samples. Illumina TrueSeq adapters and indexes were used (Illumina**,** San Diego, CA, USA). PfuUltra™ II Fusion HS DNA Polymerase was used for this final PCR step according to the manufacturer's instructions. The samples were then cleaned up using the Agentcourt AMPure XP

(Beckman Coulter) on a 1:1 ratio of beads to sample. To check on the size and concentration of the ligated products, the 2100 Bioanalyzer with DNA 1000 Chip was used. The quality and quantity of the products were determined by running a quantitative PCR. The reactions were prepared using the KAPA Library Quantification kit (KAPA Biosystems) and the run was done on the LightCycler 480 II real time thermal cycler (Roche Applied Science, Indianapolis, IN, USA) according to the manufacturer's instructions. Samples were sequenced in the Genome Institute of Singapore on the Illumina HiSeq 2500 to obtain multiplexed 101 bp paired-end reads.

3.3 HBV epitope prediction and peptide synthesis

The consensus sequences of HBV from each patient were further determined and translated into amino acid sequence for each open reading frame. The predicted binders (peptides) restricted to HLA-A*1101 were then generated by NetMHC software v3.4 server, http://www.cbs.dtu.dk/services/NetMHC/) based on the consensus sequences derived from HBV proteins (core, polymerase, x and envelope), including all possible binding variants for 8-, 9-, 10-, and 11-mer peptides that above the binding threshold (for score > 0.4 predicting weak binding and score > 0.6 predicting strong binding). The prediction scheme produced 484 unique HLA-A*1101-restricted HBV epitopes, together with 78 known HLA-A*1101-restricted epitopes derived from other pathogens or self-proteins, a total of 562 different pMHC tetramers **(Table 1)** were therefore made from these peptides for subsequent highly multiplex combinatorial pMHC tetramer mapping. Immune Epitope Database (IEDB) was used to report novel epitope sequences. All peptides were synthesized by Mimotopes (Australia) with purity > 85%.

3.4. Peptides sequence similarity and cluster assignment

To avoid the incorrect interpretation from cross-reactive T cell epitopes

in this inclusive 562-plex library that comprised of all viral proteins and variants, sequences of this library were pooled and loaded onto a Biostrings-based R-written environment. Similar to BLAST (Basic Local Alignment Search Tool), the biological sequence and matching algorithm performed pairwise alignment to calculate the peptide binding score based on their sequence similarity and HLA anchor point. Total of 284 peptide clusters (specificity) were assigned **(Table 1)**, and the peptides in each cluster are listed **(Table 1)**. Peptides within the same cluster were then given the same quadruple SAv-metal coding for highly multiplex combinatorial pMHC tetramer strategy.

Table 1. List of HLA A*11:01 restricted peptides used in comprehensive HBV epitope mapping and the detected frequency across various patient groups

Antigen Source	Cluster	Source Protein	Peptide Sequence	Peptides in Cluster					Hits (Freq>0.002%)				Average of hits (%)			
									IT	IA	InA	R	IT	IA	InA	R
Hepatitis B virus	1	HBV-S-27	HQLDPAFK													
	2	HBV-S-94	ASTNRQSGRK													
	3	HBV-S-95*	STNRQSGRK*	STNRQSGRK	STNRQSGR				5/8	7/12	4/13	1/10	0.003228	0.004132	0.004173	0.005883
	4	HBV-S-124*	STFHQALLDPR*	STFHQALLDPR	TTFHQALLDPR	TTFHQTLQDPR				1/12				0.008353		
	5	HBV-S-129*	TLQDPRVRALY*	TLQDPRVRALY	ALLDPRVRGLY											
	6	HBV-S-156*	TVSAISSILSK*	TVSAISSILSK	TVSTISSILSK	TASPISSIFSK	TASPISSIFSR		1/8	2/12		1/10	0.00508	0.002307		0.005196
	7	HBV-S-157*	VSAISSILSK*	VSAISSILSK	ASPISSIFSK	VSTISSILSK	ASPISSIFSR			1/12				0.005228		
	8	HBV-S-158*	STISSILSK*	STISSILSK	SAISSILSK	SPISSILSK	SPISSIFSR			1/12	1/13			0.003020	0.015373	
	9	HBV-S-159*	TISSILSK*	TISSILSK	AISSILSK	PISSIFSK										
	10	HBV-S-187*	VLQAGFFLLTK*	VLQAGFFLLTK	VLQAGFFSLTK	VLQAGFFLLTR										
	11	HBV-S-188*	LQAGFFLLTK*	LQAGFFLLTK	LQAGFFSLTK	LQAGFFLLTR				1/12				0.002898		
	12	HBV-S-189*	QAGFFLLTK*	QAGFFLLTK	QAGFFSLTK											
	13	HBV-S-190*	AGFFLLTK*	AGFFLLTK	AGFFSLTK						1/13				0.002499	
	14	HBV-S-210	TSLNFLGGAPK													
	15	HBV-S-211	SLNFLGGAPK													
	16	HBV-S-236	TSCPPICPGYR													
	17	HBV-S-264	LHFLIVLEDY													
	18	HBV-S-285*	GTSTTSTGPCK*	GTSTTSTGPCK	GSSTTSTGPCK											
	19	HBV-S-286*	SSTTSTGPCK*	SSTTSTGPCK	TSTTSTGPCK											
	20	HBV-S-287	STTSTGPCK													
	21	HBV-S-288	TTSTGPCK							1/12		1/10		0.002665		0.006913
	22	HBV-S-304	TSMFPSCCCTK						1/8	2/12	1/13		0.013587	0.003647	0.004037	
	23	HBV-S-305*	SMFPSCCCTK*	SMFPSCCCTK	SMYPSCCCTK											
	24	HBV-S-323	IPIPSSWAFAK													
	25	HBV-S-324	PIPSSWAFAK													
	26	HBV-S-325	IPSSWAFAK													
	27	HBV-S-326	PSSWAFAK													
	28	HBV-S-327	SSWAFAKY													
	29	HBV-S-366*	SVIWMMWY*	SVIWMMWY	SVIWMMWFW	SVIWMMWYW										
	30	HBV-S-369*	WMMWFWGPSIY*	WMMWFWGPSIY	WMMWYWGPSIY											
	31	HBV-S-370	MMWFWGPSIY													
	32	HBV-P-0*	MPLSYLHFRK*	MPLSYLHFRK	MPLSYQHFRK											
	33	HBV-P-1*	PLSYLHFRK*	PLSYLHFRK	PLSYQHFRK											
	34	HBV-P-2*	LSYLHFRK*	LSYLHFRK	LSYQHFRK				3/8	4/12	1/13	2/10	0.004069	0.005406	0.005959	0.008759
	35	HBV-P-44	NLNVSIPWTHK													
	36	HBV-P-46	NVSIPWTHK						4/8	8/12	3/13	1/10	0.004481	0.003864	0.007687	0.003309
	37	HBV-P-47	VSIPWTHK													
	38	HBV-P-54	KVGNFTGLY													
	39	HBV-P-62	YSSTVPCFNPK													
	40	HBV-P-63	SSTVPCFNPK													
	41	HBV-P-64	STVPCFNPK									1/10				0.002033
	42	HBV-P-65	TVPCFNPK								1/13				0.013511	
	43	HBV-P-74	QTPSPHHHLK													
	44	HBV-P-75	TPSPHHHLK													
	45	HBV-P-76	PSPHHHLK						1/8			1/10	0.00927			0.002264
	46	HBV-P-77	SPHHHLK													
	47	HBV-P-94	YVGPLTVNEK													
	48	HBV-P-98*	LTINENRRLK*	LTINENRRLK	LTVNETRRLK	LTVNENRRLK	LTVNEKRRLK			1/12				0.003304		
	49	HBV-P-99*	TVNETRRLK*	TVNETRRLK	TVNENRRLK	TVNEKRRLK	TINENRRLK		1/8	2/12	2/13		0.003505	0.004665	0.007724	
	50	HBV-P-107	KLIMPARFY													
	51	HBV-P-108	LVMPARFY													
	52	HBV-P-113*	RFYPNLTK*	RFYPNLTK	RFYPNVTK											
	53	HBV-P-117	NVTKYLPLDK													
	54	HBV-P-118*	VTKYLPLDK*	VTKYLPLDK	LTKYLPLDK				1/8		3/13	2/10	0.004096		0.019158	0.003800
	55	HBV-P-135*	HTVNHYFK*	HTVNHYFK	HTVNHYFQTR	HVVDHYFQTR	HVVNHYFQTR									
	56	HBV-P-136*	TVNHYFQTR*	TVNHYFQTR	VVNHYFQTR	TVNHYFKTR	IVNHYFQTR	TVNHYFQTRHY	5/8	4/12	5/13		0.003132	0.003651	0.003352	
				TVNHYFKTRHY	VVHHYFQTR	VVDHYFQTR	VVNHYFQTRHY									
	57	HBV-P-142*	KTRHYLHTIWK*	KTRHYLHTIWK	QTRHYLHTIWK											
	58	HBV-P-144	RHYLHTIWK													
	59	HBV-P-148*	HTLWKAGILYK*	HTLWKAGILYK	HTLWEAGILYK	HTLWKAGILY	HTLWEAGILY		1/8	4/12	1/13	2/10	0.005276	0.003741	0.006728	0.037610
	60	HBV-P-149*	TLWEAGILYK*	TLWEAGILYK	TLWKAGILYK											
	61	HBV-P-161	STRSASFY													
	62	HBV-P-163*	RSASFYGSPY*	RSASFYGSPY	RSASFCGSPY											
	63	HBV-P-164*	SASFYGSPY*	SASFYGSPY	SASFCGSPY											
	64	HBV-P-165*	ASFYGSPY*	ASFYGSPY	ASFCGSPY											
	65	HBV-P-182	RIVFQTSK													
	66	HBV-P-183*	IVFQTSER*	IVFQTSER	IVFQTSTR	IVFQTSKR					1/13	1/10			0.003668	0.002847
	67	HBV-P-186*	QTSERHGDK*	QTSERHGDK	QTSKRHGDK						1/13	1/10			0.015373	0.002615
	68	HBV-P-187*	TSERHGDK*	TSERHGDK	TSKRHGDK											
	69	HBV-P-197	CSQSSGILSR													
	70	HBV-P-198	SQSSGILSR													
	71	HBV-P-199	QSSGILSR									1/10				0.003660
	72	HBV-P-202	GILPRSSVGPR							1/12	3/13			0.002828	0.072039	
	73	HBV-P-208	SVGSCIQSQLR*	SVGSCIQSQLR	SVGPRIQSQLR	SVGPCIQSQLR										
	74	HBV-P-210*	GSCIQSQLRK*	GSCIQSQLRK	GSCIQSQLR				1/8				0.002406			
	75	HBV-P-211	SCIQSQLRK													
	76	HBV-P-212*	RIQSQLRK*	RIQSQLRK	GIQSQLRK	CIQSQLRK										
	77	HBV-P-214	RSQFKQSR													
	78	HBV-P-215	SQLRKSRLGPK													
	79	HBV-P-227	QQGSMASGK													
	80	HBV-P-229*	RSMASGKPGR*	RSMASGKPGR	GSMASGKPGR	GSMARGKSGR					1/13				0.004808	
	81	HBV-P-241	SIRARVIHPTSR													
	82	HBV-P-245*	RVHSSPWR*	RVHSSPWR	RVHPTSRR											
	83	HBV-P-267*	SASSASSCIY*	SASSASSCIY	STSSASYCIH											
	84	HBV-P-268	ASSASSCIY													
	85	HBV-P-269	SSASSCIY													
	86	HBV-P-271*	ASYCIHQSAVR*	ASYCIHQSAVR	SSSCIHQPAVR	SSSCIHQSAVR	ASSCIHQSAVR	ASSCIYQSAVR								
	87	HBV-P-272*	SSCIHQPAVRK*	SSCIHQPAVRK	SSCIYQSAVRK	SSCIHQSAVRK	SSCIYQSAVR	SSCIHQPAVR				1/10				0.009064
				SSCIHQSAVR	SYCLHQSAVRK											
	88	HBV-P-274*	CIYQSAVRK*	CIYQSAVRK	CIYQSAVRKK	CIHQPAVRK	CLHQSAVRK									
	89	HBV-P-276	YQSAVRKK													
	90	HBV-P-282*	KTAYSHLSTSK*	KTAYSHLSTSK	KTAYSLISTSK	KAAYSLISTSK	KAAYSLNSTSK		8/8	12/12	11/13	7/10	0.025309	0.021343	0.020005	0.014202
	91	HBV-P-283*	KAYSHLSSSK*	KAYSHLSSSK	TAYSHLSTSK	TAYSLISTSK	AAYSLISTSK	AAYSLNSTSK								
				TAYSHLSTSKR	TAYSLISTSKR	KAYSHLSSSKR										
	92	HBV-P-284*	AYSHLSSSK*	AYSHLSSSK	AYSHLSTSK	AYSLISTSK	AYSLNSTSK									
	93	HBV-P-285*	YSLNSTSK*	YSLNSTSK	YSLISTSK	YSHLSSSK	YSHLSTSK									

Table 1. List of HLA-A*11:01-restricted peptides used in comprehensive HBV epitope mapping and the detected frequency across various patient groups.

List of peptides included in the epitope. Peptides were named based on the peptide cluster number, name of pathogen, source protein and initial positions. Each cluster contains one or more peptide using the Biostrings-based peptide sequence similarity algorithm. The fractions indicate the numbers of patients in each group who had the given detected epitope. Subsequent numbers showed the average frequency in different patient groups who had valid detection for each epitope. Bald faces are previously unpublished peptide sequences. Orange and red showed the frequency that were >0.005 and >0.01, respectively. Blue

shaded are the preferential selected epitopes.

94	HBV-P-286	SLISTSKR														
95	HBV-P-289*	STSKGHSSSR*	STSKGHSSSR	STSKGHSSSGR												
96	HBV-P-290	TSKGHSSSR														
97	HBV-P-295	SSSRHAVELR														
98	HBV-P-304	RQFPPNTSR														
99	HBV-P-309	SSARSQSER										1/13			0.002307	
100	HBV-P-318*	SVLSCWWLQFR*	SVLSCWWLQFR	SVLSCWWLQ	PVLSCWWLQFR											
101	HBV-P-319*	VLSCWWLQFR*	VLSCWWLQFR	ILSCWWLQFR												
102	HBV-P-320*	LSCWWLQFR*	LSCWWLQFR	PSCWWLQFR												
103	HBV-P-324	WLQFRNSK														
104	HBV-P-367*	RVTGGVFLVDK*	RVTGGVFLVDK	RITGGVFLVDK							1/12			0.002254		
105	HBV-P-368*	VTGGVFLVDK*	VTGGVFLVDK	ITGGVFLVDK							1/12			0.002254		
106	HBV-P-387	LVVDFSQFSR								5/8	9/12	9/13	9/10	0.0612	0.086237	0.055185	0.066603
107	HBV-P-388	VVDFSQFSR														
108	HBV-P-392*	SQFSRGSTR*	SQFSRGSTR	SQFSRGNTR												
109	HBV-P-396*	RGNTRVSWPK*	RGNTRVSWPK	RGSTHVSWPK	RGSTRVSWPK					1/8	2/12	1/13	1/10	0.03817	0.029153	0.005767	0.010167
110	HBV-P-397*	GSTHVSWPK*	GSTHVSWPK	GSTRVSWPK	GSTQVSWPK					1/8	1/12			0.00763	0.002506		
111	HBV-P-398*	STQVSWPK*	STQVSWPK	STHVSWPK	STRVSWPK	NTRVSWPK				2/8			1/10	0.004475			0.004529
112	HBV-P-431	AAFYHLPLH														
113	HBV-P-447*	LVGSSGLPR*	LVGSSGLPR	LVGSSGLSR												
114	HBV-P-449*	GSSGLSRYVAR*	GSSGLSRYVAR	GSSGLPRYVAR												
115	HBV-P-450*	SSGLSRYVAR*	SSGLSRYVAR	SSGLPRYVAR												
116	HBV-P-456*	YVARLSSTSR*	YVARLSSTSR	YVARLSSNSR												
117	HBV-P-461	SSTSRNINY														
118	HBV-P-462*	STSRIINNQHR*	STSRIINNQHR	STSRNINY	STSRIINDQHR											
119	HBV-P-465	RIINNQHR									1/12		1/10		0.008372		0.012989
120	HBV-P-473*	TMQNLHSSCSR*	TMQNLHSSCSR AMQDLHDSCSR	TMQDLHNSCSR	TMQNLHNSCSR	TMQDLHDSCSR	TMQNLHDSCSR									
121	HBV-P-474	MQNLHSSCSR														
122	HBV-P-479	SSCSRNIY														
123	HBV-P-484*	NIYVSLMLIYK*	NIYVSLMLIYK	NIYVSLLLIYK	NIYVSLMLIY	NIYVSLLLIY										
124	HBV-P-485*	LYVSLMLIYK*	LYVSLMLIYK	LYVSLLLIYK												
125	HBV-P-486*	YVSLLLIYK*	YVSLLLIYK	YVSLMLIYK	YVSLMLIY	YVSLLLIY				2/8	2/12	3/13	1/10	0.006757	0.003553	0.010339	0.009762
126	HBV-P-487*	VSLMLIYK*	VSLMLIYK	VSLLLIYK									1/10				0.002615
127	HBV-P-488*	SLMLIYKTYGR*	SLMLIYKTYGR	SLLLIYKTFGR													
128	HBV-P-489*	LMLIYKTYGRK*	LMLIYKTYGRK	LLLIYKTFGRK													
129	HBV-P-490*	MLIYKTYGRK*	MLIYKTYGRK	LLIYKTFGRK	MLIYKTYGR							1/13				0.002855	
130	HBV-P-491*	LIYKTFGRK*	LIYKTFGRK	LIYKTYGRK	LIYKTFGR					4/8	5/12	5/13	1/10	0.003013	0.004777	0.009704	0.025620
131	HBV-P-494*	KTYGRKLHLY*	KTYGRKLHLY	KTFGRKLHLY						1/8				0.002007			
132	HBV-P-503	YSHPIILGFRK														
133	HBV-P-506	PIILGFRK														
134	HBV-P-528	FTSAICSVVRR														
135	HBV-P-529*	TSAICSVVRR*	TSAICSVVRR	TSAICSVVR													
136	HBV-P-530*	SAICSVVRR*	SAICSVVRR	SAICSVVR													
137	HBV-P-531	AICSVVRR														
138	HBV-P-534	SVVRRAFPH								1/8	3/12	2/13		0.041982	0.003832	0.005224	
139	HBV-P-538	RAFPHCLAFSY															
140	HBV-P-547	SYMDDVVLGAK															
141	HBV-P-548	YMDDVVLGAK															
142	HBV-P-558*	SVQHLESIY*	SVQHLESIY	SVQHLESVY													
143	HBV-P-564	SVYAAVTNFLL															
144	HBV-P-574*	LSLGIHLNPNK*	LSLGIHLNPNK	LSLGIHLNPHK							3/12	1/13			0.004279	0.002691	
145	HBV-P-575*	SLGIHLNPNK*	SLGIHLNPNK	SLGIHLNPHK													
146	HBV-P-577*	GIHLNPNK*	GIHLNPNK	GIHLNPHK	GIHLNPHKTK	GIHLNPNKTK											
147	HBV-P-590	YSLNFMGY															
148	HBV-P-603*	GTLPQEHIVLK*	GTLPQEHIVLK	GTLPQEHIVQK									1/10				0.004185
149	HBV-P-604*	TLPQEHIVLK*	TLPQEHIVLK	TLPQEHIVQK													
150	HBV-P-609	HIVQKIKMCFK															
151	HBV-P-610*	IVQKIKMCFRK*	IVQKIKMCFRK IVQKIKQCFRK	IVQKIKMCFK IVQKIKMCFR	IVQKIKLCFRK IVQKIKLCFR	IVQKIKMCFKK IVLKIKQCFR	IVLKLKQCFRK IVQKIKQCFR			1/8	1/12		2/10	0.002278	0.009584		0.004296
152	HBV-P-611*	VQKIKMCFK*	VQKIKMCFK VQKIKQCFRK	VQKIKMCFRK	VQKIKLCFRK	VQKIKMCFKK	VLKLKQCFRK										
153	HBV-P-613*	KIKMCFRK*	KIKMCFRK	KIKMCFKK	KIKLCFRK	KIKQCFRK	KLKQCFRK			2/8			1/10	0.00505			0.005196
154	HBV-P-615*	KMCFRKLPVNR*	KMCFRKLPVNR	KQCFRKLPINR	KMCFKKLPVNR	KQCFRKLPVNR	KLCFRKLPVNR										
155	HBV-P-622	PVNRPIDWK								1/8	3/12			0.005276			0.000000
156	HBV-P-655*	PLYACIQAK*	PLYACIQAK	PLYACIQTK													
157	HBV-P-663*	KQAFTFSPTYK*	KQAITFSPTYK	KQAFTFSPTY													
158	HBV-P-664*	QAFTFSPTYK*	QAFTFSPTYK	QAFTFSPTY							2/12	2/13	1/10		0.010664	0.005043	0.002264
159	HBV-P-665	AFTFSPTYK															
160	HBV-P-666	FTFSPTYK															
161	HBV-P-668*	FSPTYKAFLSK*	FSPTYKAFLSK	FSPTYKAFLCK													
162	HBV-P-669*	SPTYKAFLCK*	SPTYKAFLCK	SPTYKAFLSK													
163	HBV-P-670*	PTYKAFLSK*	PTYKAFLSK	PTYKAFLCK						1/8	2/12	2/13	1/10	0.00791	0.003032	0.003198	0.002264
164	HBV-P-671*	TYKAFLSK*	TYKAFLSK	TYKAFLCK													
165	HBV-P-678*	KQYLHLYPVAR*	KQYLHLYPVAR	KQYLNLYPVAR													
166	HBV-P-731	AACFARSR															
167	HBV-P-745*	GTDNSVVLSRK*	GTDNSVVLSRK	GTDNSVVLSR													
168	HBV-P-748	NSVVLSRK															
169	HBV-P-765	CAANWILR															
170	HBV-P-781	SALNPADDPSR															
171	HBV-P-795*	GIYRPLLR*	GIYRPLLR	GIYRPLLRLIY	GIYRPLLRIVY												
172	HBV-P-803	LVYRPTTGR									1/12	1/13			0.002566	0.002594	
173	HBV-P-808	TTGRTSIY															
174	HBV-P-870*	SVPSHLPVR*	SVPSHLPVR	SVPHLPDR	SVPSHLPDR	SVPSHPPDR											
175	HBV-P-831	FASPLHVAWK															
176	HBV-P-832	ASPLHVAWK															
177	HBV-P-833	SPLHVAWK															
178	HBV-C-169*	STLPETAVVRR*	STLPETAVVRR STLPETTVVGR	STLPETAVVR STIPETTVVRR	STLPETTVVRR	STLPETTVIRR	STPPETTVVRR				4/12	7/13	7/10		0.098664	0.010236	0.026518
179	HBV-C-175*	AVVRRRCRSPR*	AVVRRRCRSPR	TVVRRRGRSPR	TVIRRRGRSPR	TVVGRRGRSPR				3/8	6/12	2/13	1/10	0.00546	0.004748	0.005453	0.004136
180	HBV X 3	RVCCQLDPAR															
181	HBV-X-63*	SSAGPCALR*	SSAGPCALR	SSTGPCALR								2/13				0.015895	
182	HBV X 64	STGPCALR															
183	HBV-X-80*	TTVNAHWNLPK*	TTVNAHWNLPK TTVNAHRNLPK	TTVNALGNLPK TTVNARQVLPK	TTVNAHGNLPK	TTVNAPGNLPK	TTVNAHQVLPK			1/8	3/12	2/13	1/10	0.002316	0.004083	0.004750	0.007793
184	HBV-X-81*	TVNAHQVLPK*	TVNAHQVLPK TVNAPGNLPK	TVNAHRNLPK TVNARQVLPK	TVNAHWNLPK	TVNAHGNLPK	TVNALGNLPK				1/12	3/13	2/10		0.005656	0.003399	0.002743
185	HBV-X-82	VNAHWNLPK															
186	HBV-X-83*	NAHWNLPK*	NAHWNLPK	NALGNLPK	NAHQVLPK	NAHGNLPK	NAHRNLPK										
187	HBV-X-84	ALGNLPKVLHK															
188	HBV-X-85*	RQVLPKVLHK*	RQVLPKVLHK	HQVLPKVLHK													

Table 1. List of HLA-A*11:01-restricted peptides used in comprehensive HBV epitope mapping and the detected frequency across various patient groups (continued).

	189 HBV-X-86*	QVLPKVLHK*	QVLPKVLHK	QVLPKVLHKR					1/12			0.002715			
	190 HBV-X-87	VLPKVLHK													
	191 HBV-X-100*	SVMSMTDLEAY*	SVMSMTDLEAY	SVMSTTDLEAY	SAMSTTDLEAY	SAMSATDLEAY									
	192 HBV-X-102*	MSMTDLEAYFK*	MSMTDLEAYFK	MSATDLEAYFK	MSTTDLEAYFK	MSMTDLEAY			1/12		1/10	0.003997		0.002033	
	193 HBV-X-103*	STTDLEAYFK*	STTDLEAYFK	SMTDLEAYFK	SATDLEAYFK	STTDLEAY									
	194 HBV-X-104*	TTDLEAYFK*	TTDLEAYFK	MTDLEAYFK	ATDLEAYFK				1/12	3/13	1/10	0.002297	0.003752	0.005196	
	195 HBV-X-108	EAYFKDCVFK													
	196 HBV-X-109	AYFKDCVFK													
	197 HBV-X-127	RLMIIFVLGGCR													
	198 HBV-X-129*	KVFVLGGCRHK*	KVFVLGGCRHK MIFVLGGCR	MIFVLGGCRHK	KIYVLGGCRHK	KVFVLGGCR	KIYVLGGCR		1/8	1/12	2/10	0.005276	0.007552		0.004401
	199 HBV-X-131	YVLGGCRHK													
	202 HBV-C-88*	YVNVNMGLK*	YVNVNMGLK YANVNMGIK	YVNTNMGLK YVNVNMRLK	YVNVNMGPK YVNVIMGLK	YVNVNTGLK	YVNVNMGIK			1/12	1/10	0.002576		0.003396	
	265 HBV-C-11*	CSCPTVQASK*	CSCPTVQASK	CSCSTVQASK	CSCPTVQTSK	CTCPTVQASK	CSCPTVQVSK			2/13			0.171478		
	266 HBV-C-13	CSTVQASK													
	267 HBV-C-15	TVQASKILCLGR													
	268 HBV-C-15v1	TVQASKIY													
	269 HBV-C-25	RIWGMDIDPYK													
	270 HBV-C-28*	GMDIDPYK*	GMDIDPYK	GMNIDPYK	GMDIDAYK	GMDIDTYK									
	271 HBV-C-113	VVSYVNVNMR													
	272 HBV-C-114*	VSYVNVNMGLK*	VSYVNVNMGLK VSYVNVNMRLK	VSYVNVNMGPK VSYVNVIMGLK	VSYVNVNTGLK	VSYVNVNMGIK	VSYANVNMGIK				1/10				0.002033
	273 HBV-C-114v6	VSYVNVNMR													
	274 HBV-C-115*	SYVNVNMGLK*	SYVNVNMGLK SYVNVIMGLK	SYVNVNMGPK	SYVNVNTGLK	GYVNVNMGLK	SYVNVNMRLK								
	275 HBV-C-126	RQLIWFHISCR													
	276 HBV-C-132	HISCLTFGR													
	277 HBV-C-136*	LTFGRETVLEY*	LTFGRETVLEY	RTFGRETVLEY	LTFGRQTVLEY						1/13 1/10		0.003706	0.003809	
	278 HBV-C-151*	GVWIRTPPAYR*	GVWIRTPPAYR GVWIRAPPAYR	GVWIRTPPAFR	GVWIRTPTAYR	GVWIRTPSAYR	GVWIRTPLAYR				1/13		0.010397		
	279 HBV-C-169v3*	STLPETTVVR*	STLPETTVVR	STLPETTVIR	STIPETTVVR						1/13 1/10		0.010508	0.004473	
	280 HBV-C-175v3	TVIRRRGR													
	281 HBV-C-195	RTQSPRRR													
	282 HBV-C-195v1	RTQSPRRRR							1/8	6/12	5/13 2/10	0.002316	0.006087	0.008052	0.005029
	283 HBV-C-195v2	RSQSPRRRRSK							8/8	12/12	6/13 6/10	0.010887	0.026361	0.007769	0.007808
	284 HBV-C-196	SQSPRRRRSK													
Control antigens	200 CMV-pp65_1	ATVQGQNLK							3/8	2/12	9/13 4/10	0.004221	0.004034	0.145515	0.014064
	201 HCV-GPP-2	STNPKPQK													
	203 Survivin-53	DLAQCFFCFK													
	204 EBV-EBNA3B	AVFDRKSDAK							2/8	5/12	4/13 1/10	0.121349	0.211809	0.209514	0.172746
	205 EBV-EBNA3B-416	IVTDFSVIK									1/10				0.003396
	206 HIV-Nef-85	AVDLSHFLK													
	207 HPV33-E6-86	NTLEQTVKK													
	208 DENV1-1-PP*	GTSGSPIVNR*	GTSGSPIVNR GTSGSPIINR	GTSGSPIIDK GTSGSPIIDK	GTSGSPIVDR	GTSGSPIVDK	GTSGSPIADK		5/8	4/12	4/13 4/10	0.013932	0.006662	0.016159	0.046505
	209 CMV-pp65_2	SVLGPISGHVLK									2/13			0.005887	
	210 CMV-2	TVRAFSRAYHHRINR									1/10				0.004067
	211 MTB-EsxR	QIMYNYPAM													
	212 MTB-EsxH	ANTMAMMAR													
	213 TG-MS*	KSFKDILPK*	KSFKDILPK	RSFKDLLKK											
	214 TG-DG_1	AMITAFFLR													
	215 TG-SAG_1	STFWPCLLR													
	216 TG-SAG_2	SSAYVFSVK													
	217 TG-DG_2	AVVSLLRLLK													
	218 IAV-MP1_1	ASCMGLIYNR							1/8		1/13 1/10	0.00247		0.003668	0.018185
	219 IAV-MP2	RLFFKCIYRR													
	220 IAV-NPv1	SVQPTFSVQR							2/8	3/12	4/13 1/10	0.01239	0.005795	0.009134	0.016267
	221 IAV-NPv2	SVQRNLPFER							4/8	4/12	6/13 3/10	0.004536	0.005311	0.044947	0.014219
	222 IAV-PA_1	KFLPDIYDYK													
	223 IAV-PCS_1	KLVGINMSKK									1/13			0.003386	
	224 IAV-PCS_2	GTFEFTSFFY													
	225 IAV-PB2_1	SFSFGGFTFK								2/12	2/13 1/10		0.003073	0.056170	0.008540
	226 IAV-PB2_2	VLRGFLILGK													
	227 DENV2-5-PP	SQIGAGVYK							1/8	3/12	2/13 1/10	0.002625	0.003189	0.002960	0.002847
	228 DENV2-7-PP	KTFDSEYVK									1/10				0.026576
	229 DENV2-8-PP	RIYSDPLALK													
	230 DENV2-9-PP	ATVLMGLGK							1/8	1/12	1/13	0.00791	0.002360	0.002428	
	231 DENV2-10-PP*	STYGWNLVR*	STYGWNLVR	ATYGWNLVK	STYGWNIVK				5/8	7/12	4/13 3/10	0.002984	0.004907	0.003946	0.006023
	232 DENV1-2-PP	TVMDIISRR							2/8			0.00698			
	233 DENV2-11-PP	RTTWSIHAK							2/8	5/12	3/13 3/10	0.003493	0.003315	0.003655	0.003184
	234 DENV2-12-PP	RQMEGEGVFK													
	235 IAV-MP2-70	KSMREEYRK													
	236 IAV-MP1-178	RMVLASTTAK													
	237 IAV-MP1-13	SIIPSGPLK													
	238 EBV-LMP2-340*	SSCSSCPLSK*	SSCSSCPLSK	SSCSSCPLSK					6/8	12/12	11/13 8/10	0.01116	0.031328	0.061079	0.024404
	239 DENV2-PP	AVQTKPGLFK													
	240 DENV3-PP	GAMLFLISGK													
	241 DENV4-PP	KSGAIKVLK									1/13			0.002257	
	242 DENV5-PP	KTFVDLMRR								1/12			0.003485		
	243 DENV6-PP	MANEMGFLEK													
	244 DENV7-PP*	MATYGWNLVK*	MATYGWNLVK	MSTYGWNIVK						1/12	1/13		0.002438	0.011825	
	245 DENV9-PP	MSYTMCSGK													
	246 DENV10-PP	MVSRLLLNR								1/12			0.004186		
	247 DENV11-PP	RQLANAIFK													
	248 DENV12-PP*	RVIDPRRCLK*	RVIDPRRCLK	RVIDPRRCMK					1/8			0.002803			
	249 DENV13-PP	TSGSPIIDK							1/8			0.00528			
	250 DENV16-PP	TTKRDLGMSK							1/8	2/12		0.003551	0.014267		
	251 DENV17-PP	VTRGAVLMHK													
	252 DENV18-PP	YVSAIAQTFK													
	253 DENV19-PP	SPGTSGSPIIDKKGK													
	254 EBV-BRLF1	ATIGTAMYK							1/8	3/12	3/13 2/10	0.004156	0.018045	0.078450	0.011428
	255 CMV-pp65_3	GPISGHVLK													
	256 IAV-MP1_2	AYQKRMGVQM													
	257 IAV-PA_2	LYASPQLEGF													
	258 LMAV-GP	LVTFLLLCGR													
	258 LCMV-GP_1	LVSFLLLAGR													
	259 LCMV-GP_2	FTNDSIISH													
	260 LCMV-RING-Z	TTYLGPLSCK													
	261 Mus musculus-GP	AINSEMFLR													
	262 Mus musculus-Insulin-1	LALEVARQKR	LALEVARQKR	TLALEVARQK											
	263 Mus musculus-Insulin-2	TLALEVAQQK													
	264 MTB-Ag85B	AMGDAGGYK									1/13			0.002307	

Table 1. List of HLA-A*11:01-restricted peptides used in comprehensive HBV epitope mapping and the detected frequency across various patient groups (continued).

3.5. Antibody-metal conjugation

Purified antibodies without carrier proteins were purchased as listed **(Table 2)**. 50 or 100 μg of antibody was conjugated with metal-attached maleimide-coupled DN3 MAXPAR (Fluidigm DVS) chelating polymer according to manufacturer's instruction (Fluidigm DVS) as previously described. All metal isotopes were purchased from Fluidigm DVS or TRACE Sciences International Inc. as listed **(Table 2).**

Table 2: Antibody staining panel for mass cytometry and high-dimensional cytometric data analysis

	PBMC *ex vivo* panel 1, 14(SAv)-choose-4				**PBMC *ex vivo* panel 2, , 9(SAv)-choose-3**			
Metal-Isotope	*Antibody (or label)*	*Clone*	*Company*	*t-SNE & Diffusion map*	*Antibody (or label)*	*Clone*	*Company*	*t-SNE & Diffusion map*
Y-89	CD45	HI30	Fluidigm (DVS)		CD45	HI30	Fluidigm (DVS)	
Pd-102	Cell barcode				Cell barcode			
Rh-103	DNA Intercalator		Fluidigm (DVS)		Live/Dead			
Pd-104	Cell barcode				Cell barcode			
Pd-105	Cell barcode				Cell barcode			
Pd-106	Cell barcode				Cell barcode			
Pd-108	Cell barcode				Cell barcode			
Pd-110	Cell barcode				Cell barcode			
Cd-112/114	Qdt800-CD14	TuK4	Molecular Probes		Qdt800-CD14	TuK4	Molecular Probes	
In-113								
In-115	CD57	HCD57	Biolegend	✔	CD57	HCD57	Biolegend	✔
La-139	Va7.2	3C10	Biolegend	✔	Va7.2	3C10	Biolegend	✔
Ce-140	CD3	UCHT1	BioXcell		CD3	UCHT1	BioXcell	
Pr-141	HLA-DR	L243	Biolegend	✔	HLA-DR	L243	Biolegend	✔
Nd-142	CD45RO	UCHL1	Biolegend	✔	CD27	LG.7F9	eBioscience	✔
Nd-143	CD38	HIT2	Biolegend	✔	CD38	HIT2	Biolegend	✔
Nd-144	CCR7	150503	R&D Systems	✔	CCR4	205410	R&D Systems	✔
Nd-145	CD27	LG.7F9	eBioscience	✔	CD45RA	HI100	BD Bioscience	✔
Nd-146	CD8α	SK1	Biolegend		CCR6	G034E3	Biolegend	✔
Sm-147	CD28	CD28.2	Biolegend	✔	CD45RO	UCHL1	Biolegend	✔
Nd-148	**SAv-Nd-148**		in-house		CTLA-4	BNI3	BD Bioscience	✔
Sm-149	CXCR3	1C6	BD Bioscience	✔	CXCR3	1C6	BD Bioscience	✔
Nd-150	KLRG-1	13F12F2	eBioscience	✔	KLRG-1	13F12F2	eBioscience	✔
Eu-151	**SAv-Eu-151**		in-house		CCR7	150503	R&D Systems	✔
Sm-152	CXCR5	RF8B2	BD Bioscience	✔	CXCR5	RF8B2	BD Bioscience	✔
Eu-153	**SAv-Eu-153**		in-house		**SAv-Eu-153**		in-house	
Sm-154	HVEM	94801	R&D Systems	✔	HVEM	94801	R&D Systems	✔
Gd-155	CTLA-4	BNI3	BD Bioscience	✔	**SAv-Gd-155**		in-house	
Gd-156	CD39	A1	Biolegend	✔	CD39	A1	Biolegend	✔
Gd-157	**SAv-Gd-157**		in-house		OX40	443318	R&D Systems	✔
Gd-158	CD45RA	HI100	BD Bioscience	✔	TIGIT	MBSA43	eBioscience	✔
Tb-159	**SAv-Tb-159**		in-house		GITR	110416	R&D Systems	✔
Gd-160	PD-1	eBioJ105	eBioscience	✔	PD-1	eBioJ105	eBioscience	✔
Dy-161	**SAv-Dy-161**		in-house		CCR5	HEK/1/85a	Abcam	✔
Dy-162	CD4	SK3	Biolegend		CD161	HP-3G10	Biolegend	✔
Dy-162	CD19	HIB19	Biolegend					
Dy-162	CD56	NCAM16.2	BD Bioscience					
Dy-163	**SAv-Dy-163**		in-house		BTLA	MIH26	Fluidigm (DVS)	✔
Dy-164	LAG-3	874501	R&D Systems	✔	LAG-3	874501	R&D Systems	✔
Ho-165	**SAv-Ho-165**		in-house		**SAv-Ho-165**		in-house	
Er-166	**SAv-Er-166**		in-house		**SAv-Er-166**		in-house	
Er-167	TIM-3	344823	R&D Systems	✔	TIM-3	874501	R&D Systems	✔
Er-168	**SAv-Er-168**		in-house		**SAv-Er-168**		in-house	
Tm-169	**SAv-Tm-169**		in-house		**SAv-Tm-169**		in-house	
Er-170	2B4	C1.7	Biolegend	✔	2B4	C1.7	Biolegend	✔
Yb-171	**SAv-Yb-171**		in-house		**SAv-Yb-171**		in-house	
Yb-172	BTLA	MIH26	eBioscience	✔	4-1BB	4B4-1	Biolegend	✔
Yb-173	**SAv-Yb-173**		in-house		**SAv-Yb-173**		in-house	
Yb-174	CD160	688327	R&D Systems	✔	CD160	688327	R&D Systems	✔
Lu-175	**SAv-Yb-175**		in-house		**SAv-Yb-175**		in-house	
Yb-176	CD127	A019D5	Biolegend	✔	CD127	A019D5	Biolegend	✔
Ir-191/193	CD161	HP-3G10	Biolegend	✔	DNA Intercalator		Fluidigm (DVS)	
Pt-194					CD8α	SK1	Biolegend	
Pt-195	Live/Dead							
Pt-198					CD4	SK3	Biolegend	
Pt-198					CD19	HIB19	Biolegend	
Pt-198					CD56	NCAM16.2	BD Bioscience	
Bi-209					CD16	3G8	Fluidigm (DVS)	

Table 2. Antibody staining panel for mass cytometry and parameters for high-dimensional cytometric data analysis.

Table 2: Continued

	PBMC *in vitro* panel, 8(SAv)-choose-3				IHL ex vivo panel, 12(SAv)-choose-3			
Metal-Isotope	*Antibody (or label)*	*Clone*	*Company*	*t-SNE & Diffusion map*	*Antibody (or label)*	*Clone*	*Company*	*t-SNE & Diffusion map*
Y-89	CD45	HI30	Fluidigm (DVS)		CD45	HI30	Fluidigm (DVS)	
Pd-102	Cell barcode				Cell barcode			
Rh-103	Live/Dead				Live/Dead			
Pd-104	Cell barcode				Cell barcode			
Pd-105	Cell barcode				Cell barcode			
Pd-106	Cell barcode				Cell barcode			
Pd-108	Cell barcode				Cell barcode			
Pd-110	Cell barcode				Cell barcode			
Cd-112/114	Qdt800-CD14	TuK4	Molecular Probes		Qdt800-CD14	TuK4	Molecular Probes	
Cd-112/114	Qdt800-CD19	HIB19	Molecular Probes					
In-113								
In-115	CD57	HCD57	Biolegend	✔	CD57	HCD57	Biolegend	✔
La-139	IL-15Ra		R&D Systems		Va7.2	3C10	Biolegend	✔
Ce-140	CD3	UCHT1	BioXcell		CD3	UCHT1	BioXcell	
Pr-141	IFN-γ	4S.B3	eBioscience	✔	CCR5	HEK/1/85a	Abcam	✔
Nd-142	CD27	LG.7F9	eBioscience	✔	CD27	LG.7F9	eBioscience	✔
Nd-143	Granzyme B	CLB-GB11	Abcam	✔	CCR2	K036C2	Biolegend	✔
Nd-144	CD107a	H4A3	BD Bioscience	✔	CD69	FN50	Biolegend	✔
Nd-145	CD45RA	HI100	BD Bioscience	✔	CD45RA	HI100	BD Bioscience	✔
Nd-146	MIP1-β	D21-1351	BD Bioscience	✔	CCR6	G034E3	Biolegend	✔
Sm-147	IL-2	MQ1-17H12	eBioscience	✔	CD103	B-Ly7	eBioscience	✔
Nd-148	CTLA-4	BNI3	BD Bioscience	✔	CTLA-4	BNI3	BD Bioscience	✔
Sm-149	TNF-α	Mab11	eBioscience	✔	CXCR3	1C6	BD Bioscience	✔
Nd-150	KLRG-1	13F12F2	eBioscience	✔	KLRG-1	13F12F2	eBioscience	✔
Eu-151	CCR7	150503	R&D Systems	✔	CCR7	150503	R&D Systems	✔
Sm-152	Perforin	B-D48	Abcam	✔	CXCR5	RF8B2	BD Bioscience	✔
Eu-153	GM-CSF	BVD2-21C11	Biolegend	✔	**SAv-Eu-153**		in-house	
Sm-154	HVEM	94801	R&D Systems	✔	HVEM	94801	R&D Systems	✔
Gd-155	**SAv-Gd-155**		in-house		**SAv-Gd-155**		in-house	
Gd-156	CD39	A1	Biolegend	✔	CD39	A1	Biolegend	✔
Gd-157	OX40	443318	R&D Systems	✔	**SAv-Gd-157**		in-house	
Gd-158	TIGIT	MBSA43	eBioscience	✔	TIGIT	MBSA43	eBioscience	✔
Tb-159	GITR	110416	R&D Systems	✔	**SAv-Tb-159**		in-house	
Gd-160	PD-1	eBioJ105	eBioscience	✔	PD-1	eBioJ105	eBioscience	✔
Dy-161	Granzyme K	GM6C3	Santa Cruz Biotech	✔	**SAv-Dy-161**		in-house	
Dy-162	Granzyme A	CB9	Biolegend	✔	CD161	HP-3G10	Biolegend	✔
Dy-163	BTLA	MIH26	Fluidigm (DVS)	✔	BTLA	MIH26	Fluidigm (DVS)	✔
Dy-164	LAG-3	874501	R&D Systems	✔	LAG-3	874501	R&D Systems	✔
Ho-165	**SAv-Ho-165**		in-house		**SAv-Ho-165**		in-house	
Er-166	**SAv-Er-166**		in-house		**SAv-Er-166**		in-house	
Er-167	TIM-3	874501	R&D Systems	✔	TIM-3	874501	R&D Systems	✔
Er-168	**SAv-Er-168**		in-house		**SAv-Er-168**		in-house	
Tm-169	**SAv-Tm-169**		in-house		**SAv-Tm-169**		in-house	
Er-170	2B4	C1.7	Biolegend	✔	2B4	C1.7	Biolegend	✔
Yb-171	**SAv-Yb-171**		in-house		**SAv-Yb-171**		in-house	
Yb-172	4-1BB	4B4-1	Biolegend	✔	OX40	443318	R&D Systems	✔
Yb-173	**SAv-Yb-173**		in-house		**SAv-Yb-173**		in-house	
Yb-174	CD160	688327	R&D Systems	✔	CD160	688327	R&D Systems	✔
Lu-175	**SAv-Yb-175**		in-house		**SAv-Yb-175**		in-house	
Yb-176	CD127	A019D5	Biolegend	✔	CD127	A019D5	Biolegend	✔
Ir-191/193	DNA Intercalator		Fluidigm (DVS)		DNA Intercalator		Fluidigm (DVS)	
Pt-194	CD8α	SK1	Biolegend		CD8α	SK1	Biolegend	
Pt-195								
Pt-198	CD4	SK3	Biolegend		CD4	SK3	Biolegend	
Bi-209	CD16	3G8	Fluidigm (DVS)		CD16	3G8	Fluidigm (DVS)	
One-SENSE category	**Differentiation+TNFR**				**Differentiation+TNFR**			
	Exhaustion				**Exhaustion**			
	Function				**Trafficking**			

Table 2. Antibody staining panel for mass cytometry and parameters for high-dimensional cytometric data analysis (Continued).

List of metal conjugated antibody and streptavidin (SAv) used for cellular marker staining and highly multiplex combinatorial pMHC tetramer strategy used in this report. Colored boxes indicate the parameters in different T cell categories used in One-SENSE analysis. Checked parameters were analyzed by *t*-SNE and Diffusion map.

3.6. Streptavidin (SAv) production and metal labeling

Streptavidin with nine free cysteines residues separated by glycine linkers were used for recombinant expression as described (44, 121). Briefly, purified streptavidin was made in-house and stored in 10 mM TCEP in 20 mM HEPES (pH 7.2) buffered saline with 50% glycerol after refolding. For every DN3 polymer, 100 mM of metals were added for labeling. Metal-polymer mixture was incubated for 1 hour in 37°C water bath, and then exchanged into fresh L-buffer (Fluidigm DVS) using 3kD Nanosep concentrator (PALL Life Science) and spin at 14,000 xg at 4°C for 45 min. Streptavidin was diluted and 50 μg streptavidin protein was used for each metal-coupled DN3 MAXPAR chelating polymer in L-buffer (Fluidigm DVS). Streptavidin and metal-polymer were mixed and span down at 14,000 xg for 1 hour and 15 min to drive the reaction with high polymer and protein concentration. Mixture was further incubated at 37°C for 2 hours and transferred to a new 30kD concentrator (Merck) to perform several washes with EDTA-free W-buffer (Fluidigm DVS). SAv-metal was adjusted to final concentration at 200 μg/ml prior the formation of tetrameric pMHC complex.

3.7. Generation of HLA-A*11:01 monomer and 562-plex pMHC library

The inclusion bodies of HLA-A*1101 were produced (42, 122), and refolded with a UV-cleavable peptide H-RVFA(J)SFIK-OH, where J is ANP (3-Amino-3-(2-nitrophenyl)propionic acid) linker. The protein was purified and biotinylated, and stored in PBS + 50% glycerol at -20°C. Peptide exchange was performed at 0.1 mg/ml of HLA-A*1101 monomer in 100 μl PBS with 25 μM of peptide of interest in a 96-well plate. The reaction was exposed to 365 nm UV irradiation for 5 min twice using UVP CL-1000 Ultraviolet Crosslinker, the plate was further sealed and stored at 4°C overnight to complete the exchange.

3.8. 562-plex combinatorial (Quadruple/Triple SAv-metal coded) pMHC tetramers

Each SAv-metal was diluted into 20 μg/ml in EDTA-free W-buffer on the same day of tetramerization of pMHC. Two different configurations of quadruple SAv-metal coding for 562-plex pMHC tetramers were generated using a R-based script **(Fig. 5)** for a 14-choose-4 scheme (1001 combinations). The script was then loaded onto TECAN Freedom EVO200 automatic liquid distribution robot to prepare the designed combinations of quadruple SAv-metal mixtures. To reach a 1:4 ratio of streptavidin to pMHC, quadruple SAv-metal mixtures were added to the corresponded pMHC monomer in a stepwise manner of four additions, each has 10 min incubation at room temperature. 10 μM D-biotin was added into the reaction at the end for another 10 min at room temperature to saturate unbound streptavidins. The 562-plex pMHC tetramers were combined and concentrated down to 5 μg/ml (123) per pMHC tetramer in 10% FBS CyFACS buffer using Amicon 50kDa cut-off concentrator (Millipore). The combinatorial streptavidin codings were re-scrambled for every independent 562-plex combinatorial pMHC tetramer staining experiment.

For selected experiments, a 9-choose-3 (84 combinations) or 8-choose-3 (56 combinations) scheme were used to cover 120-plex (40 peptide clusters) or 50-plex (17 peptide clusters) combinatorial triple coded pMHC tetramers staining preferentially selected **(Table 1)** for more phenotypic analysis, or *in vitro* functional assay and ETV-treated HBeAg seroconversion longitudinal cohorts**.**

3.9. Highly multiplex pMHC tetramer, antibody staining and CD8 T cell enrichment

Cryopreserved PBMC were thawed and washed with complete RPMI (10% FBS, 1% penicillin/streptomycin/L-glutamine, 1% 1M HEPES, 0.5 mM β−mecaptoehanol) (Gibco, Invitrogen), and rest for 3 hours at 37°C.

After the recovery, cells were harvested and seeded on a non-treated 96-well plate, and about 10 million cells per patient were used and split evenly in two separated wells for two configurations of 562-plex combinatorial pMHC tetramer staining. 50μM dasatinib was incubated with cells for 30 min at 37°C 5% CO_2, to prevent the downregulation of TCR (44, 123) Cells were washed with CyFACS buffer (2 mM EDTA + 0.05% sodium azide + 4% FBS in PBS) and incubated with 200 mM cisplatin (Pt-195) for 5 min on ice, or rhodium (Rh-103) for 20 min at room temperature for viability measurement. After wash once with CyFACS buffer, cells from the same donor in separated wells were stained with 50 μl of cocktail containing the same 562-plex pMHC tetramers but completely different SAv-metal coding configurations for 1 hour in room temperature in the presence of 1:100 Fc block (Biolegend). Cells were washed twice with CyFACS buffer after incubation, and resuspend in 50 μl of T cells or CD8 T cells enrichment kit (STEMCELL) antibody cocktail in 1:10 in CyFACS buffer for 30 min on ice. Cells were then washed, and stained with 50 μl of primary antibody cocktail **(Table 2)** for 30 min on ice. Excessive antibodies were removed by washing the cells twice with CyFACS buffer, and cells were resuspend with 4 μl of enrichment beads (STEMCELL) + 46 μl of CyFACS buffer for 15 min on ice. After the staining, cells were washed with PBS and fixed with 200 μl of 2% PFA (paraformaldehyde, Electron Microscopy Sciences) overnight at 4°C. On the next day, PFA was removed and cells were incubated with permeabilization buffer (Biolegend) at room temperature for 10 min, and then resuspended with 50 μl of intracellular antibody cocktail for 30 min at room temperature. For subsequent dual mass-tag cellular barcoding, 2 mM bromoacetamidobenzyl-EDTA (BABE; Dojindo) with 0.5 mM $PbCl_2$ was dissolved in HEPES buffer, and each sample was given a unique combination of metal-barcode (BABE-Pd-102, BABE-Pd-104, BABE-Pd-106, BABE-Pd-108, BABE-Pd-110) on ice for 30 min. After 5 min incubation with CyFACS buffer on ice, cells were labeled by Iridium DNA interchelator (Ir-191/193, Fluidigm DVS) in 2% PFA at room temperature for 20 min. Cells were then washed with CyFACS buffer

and CD8 T cells were negatively selected using EasySep™ Magnet (STEMCELL) according to manufacture's instruction. Enriched cells were washed twice by MilliQ water and ready for mass cytometry acquisition.

3.10. Mass cytometry and data pre-processing

All experiments were acquired by CyTOF2 (Fluidigm DVS) systems. Cells were wash by MilliQ water twice, filtered, and immediately acquired by mass cytometry with an acquisition rate of 300~350 cells/sec. 2% of Four EQ beads (Fluidigm DVS) were mixed with cell suspension. To normalize signal variations of CyTOF2, the output FCS files were normalized based on the added beads as previously described (124). Normalized FCS files were further loaded onto a Unix-based R-written script and all zero values were randomized into values between 0 to -1 using uniform distribution.

3.11. Self-validated automatic deconvolution of antigen-specific T cells

After data pre-processing, lived $CD8^+$ T cells were gated using FlowJo v9.7.6 (Tree Star Inc.) and individual samples were de-barcoded based on the dual mass-tag cellular barcodes using Boolean gates. Two SAv-metal coding configurations from the same donor were barcoded and exported independently. For optimal automatic identification of tetramer positive cells, multiple safety parameters and thresholds were built and subjectively defined using an R-written script, respectively **(Fig. 5)**. Briefly, thresholds for each SAv-metal channel were manually defined by gating a tetramer negative population for all fourteen SAv-metal channels. Based on thresholds (Threshold X=*Tx* and Threshold Y=*Ty*) of every SAv-metal channel, the safety factors then objectively identify the tetramer positive population using the pre-set geometric criteria (Y/X Slope=*k*, X/Y Slope=*k*, and Width=*w*) **(Fig. 5)** (44). All antigen-specific $CD8^+$ T cells identified by highly multiplex combinatorial pMHC tetramer

strategy in this report have to firstly pass both the thresholds and safety factors. Secondly, the corresponded four SAv-metals coded on each pMHC tetramer must have exclusive and higher metal intensity than rest of the ten SAv-metal channels. The deconvolution algorithm excluded any tetramer positive cells that have less, or more than four SAv-metals coding. The tetramer positive cells identified in two different SAv-metal coding configurations of the same donor were further calculated for their signals correspondence by using statistical simulation **(Fig. 5)**, with $p<0.05$ was considerate a confident detection. Finally, antigen-specific $CD8^+$ T cells who passed all the abovementioned tests with frequency >0.002 of total $CD8^+$ T cells were preferentially selected for further high-dimensional data analysis.

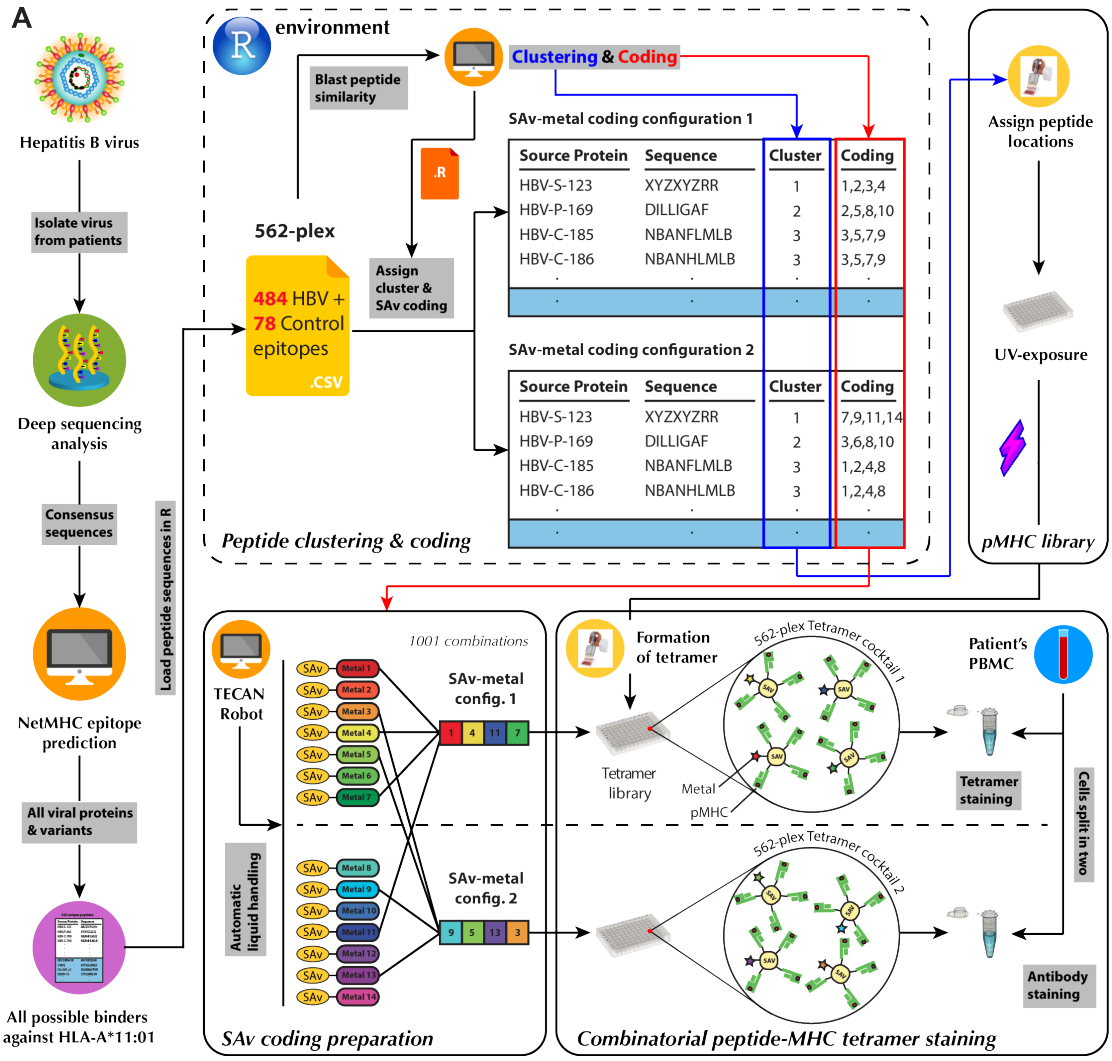

Figure 5. Comprehensive epitope mapping strategy against hepatitis B virus (HBV).

Overview of the experimental workflows include HBV viral genome deep sequencing, generation of 562-plex pMHC tetramer library, schematic of highly multiplex combinatorial pMHC tetramer strategy using mass cytometry, the rationale of two SAv quadruple coded configurations of pMHC tetramers and an unsupervised self-validated pMHC tetramer deconvolution algorithm.

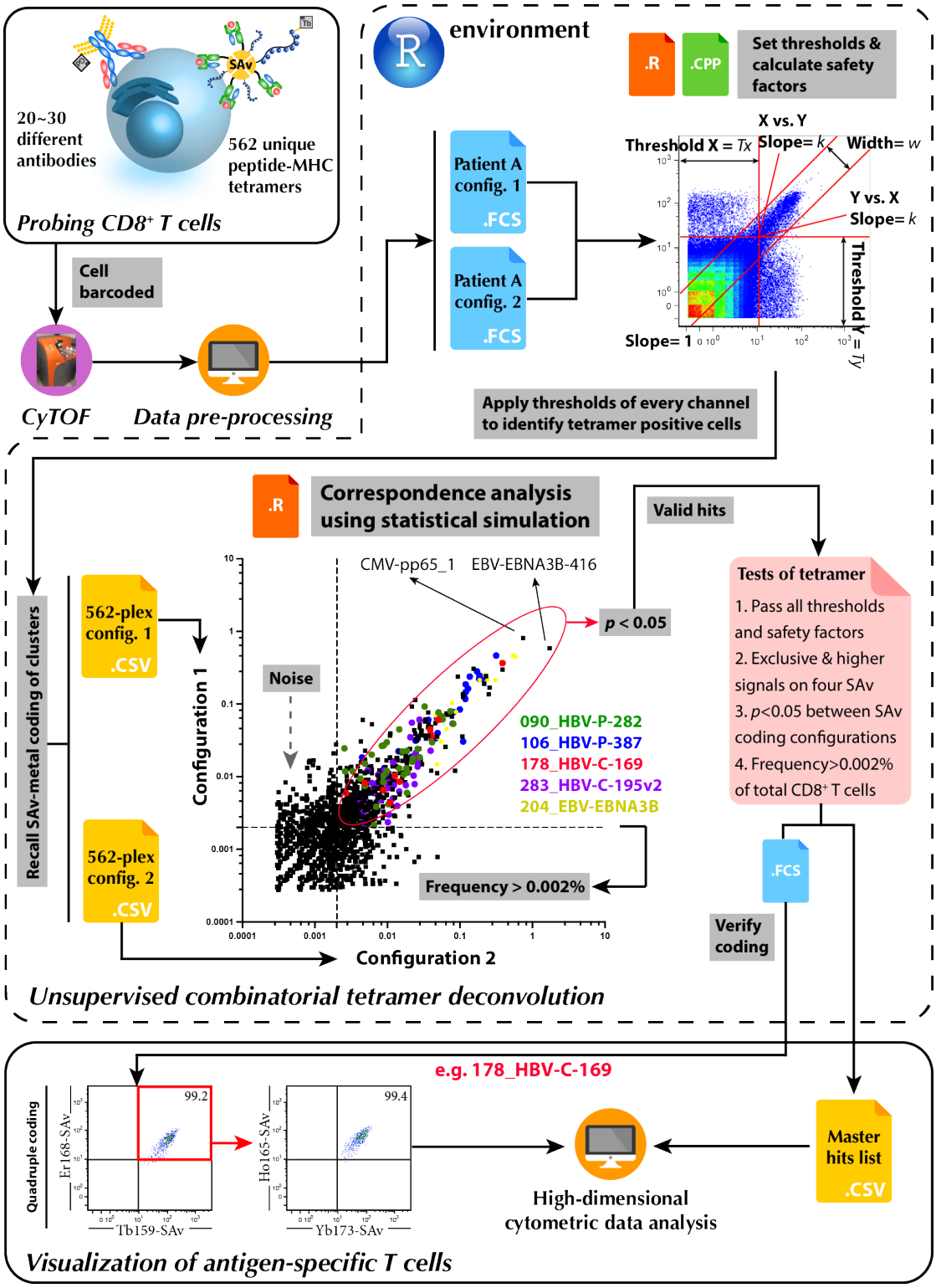

Figure 5. Comprehensive epitope mapping strategy against hepatitis B virus (HBV) (Continued).

3.12. High-dimensional cytometric data visualization and trajectory

Validated antigen-specific $CD8^+$ T cells were exported individually from each donor for dimensionality reduction analysis. Detailed methodology for *t*-SNE (110), One-SENSE (116) and Diffusion map (119) can be found else where. Briefly, *t*-SNE and One-SENSE were performed using custom R scripts based on "flowCore" and "Rtsne" packages downloaded from The Comprehensive R Archive Network (CRAN). All data were transformed using the "logicleTransform" function and *w*=0.25, *t*=16409, *m*=4.5, *a*=0 as input parameters to roughly match scaling historically used in FlowJo (112, 116). Cellular markers analyzed by *t*-SNE, One-SENSE and Diffusion map were indicated **(Table 2)**. For One-SENSE, cellular markers in each T cell category ("Differentiation+TNFR", "Exhaustion" and "Trafficking") were subjectively assigned for categorical analysis. Aligned heatplots represent the distribution of marker positive cells in percentage on each "bin" on the axis (category) constructed by cells residing in small ranges of values. Positive population of markers was manually defined and markers of the same category were combined for each dimension using 250 bins (116). 3D Diffusion map was applied for putative cell trajectory analysis using "diffusionMap" package loaded R script. Three visualized cell trajectories were projected by Diffusion map and path for each arm was subjectively drew from naïve cell to terminal differentiated cells. The distances were computed and 100 nearest neighbors identified along each path using "knn.index" function ("FNN" package). The average local expressions of these 100 nearest neighbors along each path were calculated and constructed for nine inhibitory and memory markers, respectively.

The 3D visualizations of Diffusion map, t-SNE and One-SNESE were built from numerous consecutive 3D images supported by "rgl" package based on the three dimensions of each high-dimensional data

analysis. The continuous image sequences were subsequently combined by Sequimago (AppleScript) to generate 3D movies.

3.13. Flow cytometry and cell sorting

Cells were prepared as the same fashion as mass cytometry experiments. After incubation with dasatinib, cells were washed with PBS and incubated with 50 μl of Live/Dead-Pacific Orange (Thermo Fisher) on ice for 20 min in dark. For single fluorochrome-tag pMHC tetramers, peptide-exchange and tetramer formation were done using the same method as metal-tag pMHC tetramers in dark. PE-SAv (eBioscience), PE-Cy7-SAv (eBioscience), PE-Cy5-SAv (eBioscience), BV650-SAv (BD) and APC-SAv (Biolegend) were diluted to 20 μg/ml in PBS and added into pMHC monomer loaded with different peptides in the same manner as mentioned above. Cells then washed, and stained by tetramer cocktail in the same condition as mass cytometry experiment in dark. After two washed with FACS buffer, cells were stained with primary antibodies, Pacific Blue-CD14 (Biolegend), Pacific Blue-CD16 (Biolegend), Pacific Blue-CD19 (Biolegend), Alexa Fluor 700-CD3 (Biolegend), FITC-CD4 (Biolegend) and QD605-CD8 (Thermo Fisher) in FACS buffer for 30 min on ice in dark. Cells were then washed twice, filtered, and analyzed by LSRFortessa (BD). Fluorochrome-tag tetramer positive cells were stained using the same method and live-sorted using Aria II 5 lasers system (BD).

3.14. TCR high-throughput sequencing

Five populations, including four different tetramer-stained virus-specific $CD8^+$ T cells plus the bulk $CD8^+$ T cells from each donor were live-sorted, and genomic DNA were freshly extracted using Qiagen Blood & Tissue kit according to manufacturer's instruction. Cells from three donors per patient group, with five groups and 75 samples (5

populations per donor) in total, were used for TCR sequencing. Briefly, CDR3 region of TCRβ chain were amplified using a bias-controlled two-step multiplex PCR (125) by ImmunoSEQ platform (Adaptive Biotechnologies). The first PCR amplified the CDR3 region of sorted T cells, followed by adding the adaptor sequences in second PCR, and subsequently sequenced by next-generation sequencing (NGS). Productive reads were generated from the reduction of amplification and sequencing bias (126). 1000, 5000, 1500, 2000 and 10000 cells were live sorted for HBV_{pol282}-, HBV_{pol387}-, $HBV_{core169}$-, $HBV_{core195}$-specific and total $CD8^+$ T cells, respectively.

3.15. TCR repertoire spectratyping and motif analysis

TCR sequences exported from ImmunoSEQ Analyzer and the genes were defined by IMGT/HighV-Quest (127) nomenclature. CDR3β length analysis was calculated by Prism using Gaussian fit with the null hypothesis “one curve fits all”. The null hypothesis was rejected with statistical significance. Unipro UGENE (128), an integrated bioinformatics interactive platform for multiple sequence alignment was used to perform MUltiple Sequence Comparison by Log-Expectation (MUSCLE) (129) alignment. TCR rearrangements were further phylogenetically grouped using Phylip neighbor joining method with Jones-Taylor-Thornton distance matrix. TCR motif groups that clustered by the phylogeny tree were exported, and the Sequence Logo was constructed using The MEME Suite (130) motif discovery function, GLAM2 (131). Each phylogeny tree structure was uploaded to Dendroscope (132) to calculate the root distances. 3D Principal Component Analysis (PCA) for HBV_{pol282}-specific TCR was visualized using Jalview (133) with BLOcks SUbstitution Matrix (BLOSUM).

3.16. Enzyme-linked immunosorbent assay (ELISA)

Paired serum samples from patients were serially diluted in PBS, and level of HBeAg, HBsAg, HBeAb, HBsAb and HBcAb were determined

using quantitative sandwich ELISA kits (Abnova and MyBioSource) according to manufacturer's instruction.

3.17. *In vitro* virus-specific CD8$^+$ T cells expansion

PBMC from patients were thawed and recovered, and then resuspend in AIM-V medium (with 10% human AB serum, 1% penicillin/streptomycin/L-glutamine, 1% 1M HEPES) (Gibco, Invitrogen) with 20 IU/ml of recombinant human IL-2 (R&D system). Cells were pulsed with corresponded HBV or control peptides at 1 μM per 1 million cells in 200 μl medium in 96-well round bottom tissue culture plate and cultured for 10 days at 37°C. Half of the medium was replaced as supplementary every three days without any peptide. On day 10, cells were restimulated with or without the corresponded peptides for 7 hours in the presence of 150 ng/ml phorbol-12-myristate-13-acetate (PMA), 1μM ionomycin, Brefeldin A (eBioscience), monensin (eBioscience) and 0.5 μg/ml anti-CD107a at 37°C. After incubation, cells were collected and then stained with the 50-plex pMHC tetramers **(Table 1)** and surface antibody. Intracellular cytokine staining was performed on the second day as indicated in **(Table 1)**. All staining, cellular barcoding, and CD8 T cell enrichment were done in the same manner as *ex vivo* staining described above.

3.18. Statistical analysis

The *t*-tests were done in two-tailed Mann-Whitney. Non-parametric ANOVA was used for group comparison. *P* values were calculated using Prism software (Graphpad).

4. RESULTS

4.1. Comprehensive HBV epitope mapping

To generate a comprehensive pMHC library targeting HBV, was isolated and deep sequenced from a series of longitudinal CHB patient cohort to determine viral consensus sequences using next-generation sequencing (NGS). These sequences were then loaded onto the NetMHC (version 3.4) platform to predict possible A*11:01 binders. We took all epitopes above the predictive “weak binding” threshold across the whole viral genome and variants, resulting 484 unique putative A*11:01-restricted HBV epitopes **(Fig. 5)**. Combined with 78 known A*11:01-restricted epitopes derived from other common antigens, a total of 562 peptides are listed in **Table 1**. Sequence homology was analyzed to group similar peptides into the same cluster by a pairwise matching algorithm **(Table 1)**. The following 284 peptide clusters were subsequently assigned for unique combinations of quadruple streptavidin-metal (SAv-metal) coding randomly chosen from fourteen streptavidin (SAv)-metal channels of mass cytometry panel **(Fig. 5)**. This critical step reduces the false interpretation of possible cross-reactive epitopes, such as sequence variants. The coded 562-plex pMHC tetramers library was pooled and simultaneously stained on each patient’s peripheral lymphocytes to probe the antigen specificities. To increase confidence of detection, patient’s cells were evenly divided and independently interrogated by the same 562-plex pMHC tetramers library but two entirely different SAv-metal coding configurations **(Fig. 5 and Table 1)**. Together with >26 cellular markers **(Table 2)**, the signals of 562-plex pMHC tetramers on every cell were determined by mass cytometry. We applied a self-validated automatic combinatorial tetramer deconvolution algorithm to objectively identify quadruple coded tetramer positive cells **(Materials and Methods, Fig. 5)**. Importantly, the correspondences between matching tetramers from two SAv-metal coding configurations were calculated using simulation analysis **(Fig. 5)**. In this report, we cautiously enumerated the validated antigen-specific

CD8$^+$ T cells for those who pass all the deconvolution criteria with p<0.05 between two configurations **(Fig. 5 and Table 1).**

We hypothesized that the antigen-specific T cell response could vary across different clinical stages and mediate the disease progression during natural chronic viral infection. Therefore, we applied this strategy to map potential T cell epitopes on three CHB patient groups (IT, IA and InA) and one group of acutely resolved patients (R). Among all, we observed more epitopes derived from polymerase (P) and core (C) compared to envelope (S) and x (X) protein, including four epitopes with the most dominant response **(Fig. 6A)**. These were HBV-P-282 (cluster 90, 4 peptides), HBV-P-387 (cluster 106, 1 peptide), HBV-C-169 (cluster 178, 7 peptides), and HBV-C-195v2 (cluster 283, 1 peptide) **(Fig. 6B, and Table 1)**. Our analysis therefore focused on these epitopes.

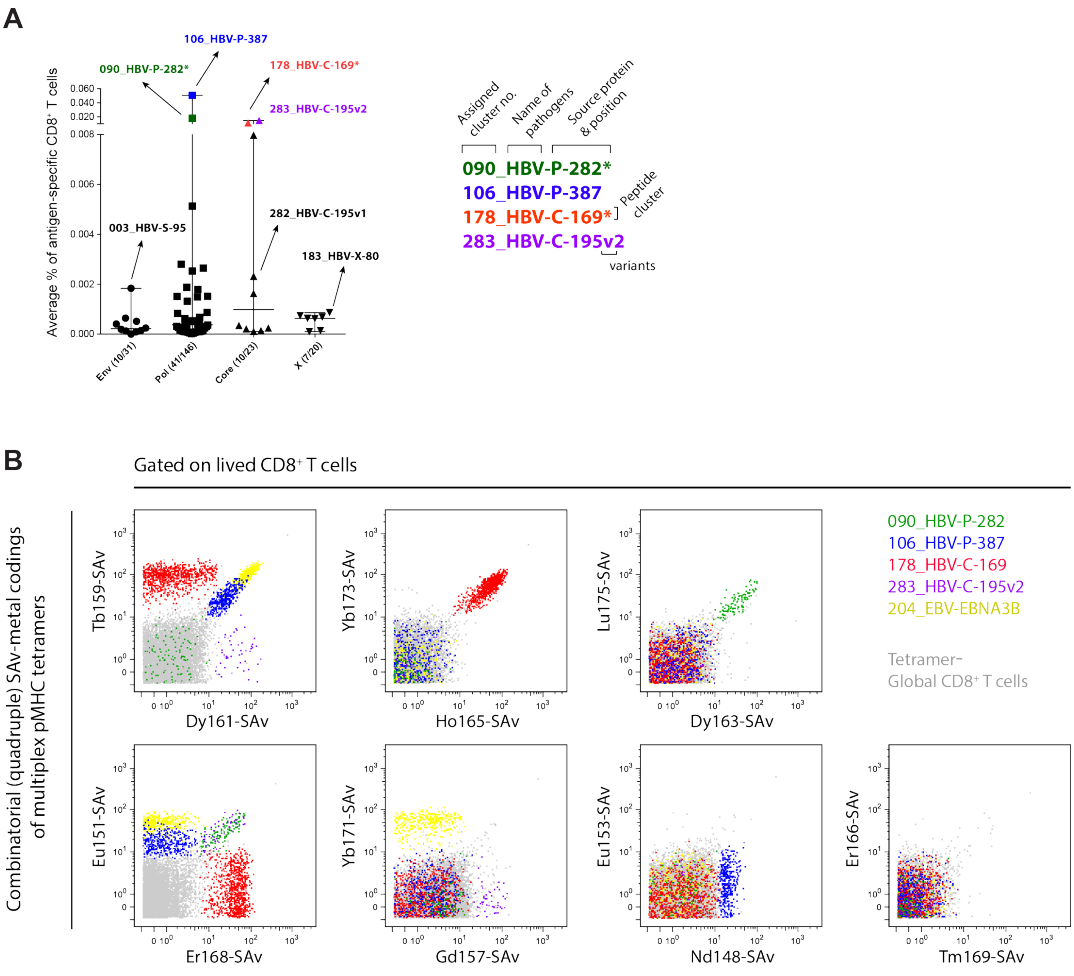

Figure 6. Detection and the frequency of four dominant antigen-specific CD8$^+$ T cells in CHB.

(A) Overall frequency of detected antigen-specific CD8$^+$ T cells in four different HBV viral proteins. (B) Representative dotplot of combinatorial pMHC tetramer staining and the signal quality from a CHB donor.

We performed several experiments to verify our findings by testing these epitopes in parallel with healthy cord blood (CB) and non-A*11:01 donors (including CHB, HD and CB) **(Fig. 7A and B)**, and further reproduced the pMHC tetramer staining using flow cytometry **(Fig. 8)**. All of them showed consistent results.

Figure 7. Validation of highly multiplex combinatorial pMHC tetramer strategy in HLA-A*11:01 and non-HLA-A*11:01 donors.

(A) Cells from donors were stained with selected 120-plex (Table 1) of pMHC tetramers coded with three different metal-tag SAv using two different sets of SAv coding configurations. Cells were stained and gated on $CD3^+$, $Dump^-$ ($CD4^+CD19^+CD16^+$) and $CD8^+$. MR1-restricted MAIT cells were gated on $CD3^+Dump^-CD8^+CD45RA^-CD161^{hi}$. Bar graphs indicate the frequency of parent cells for each epitope. HD=healthy donor. CB=cord blood. CHB=chronic hepatitis B.

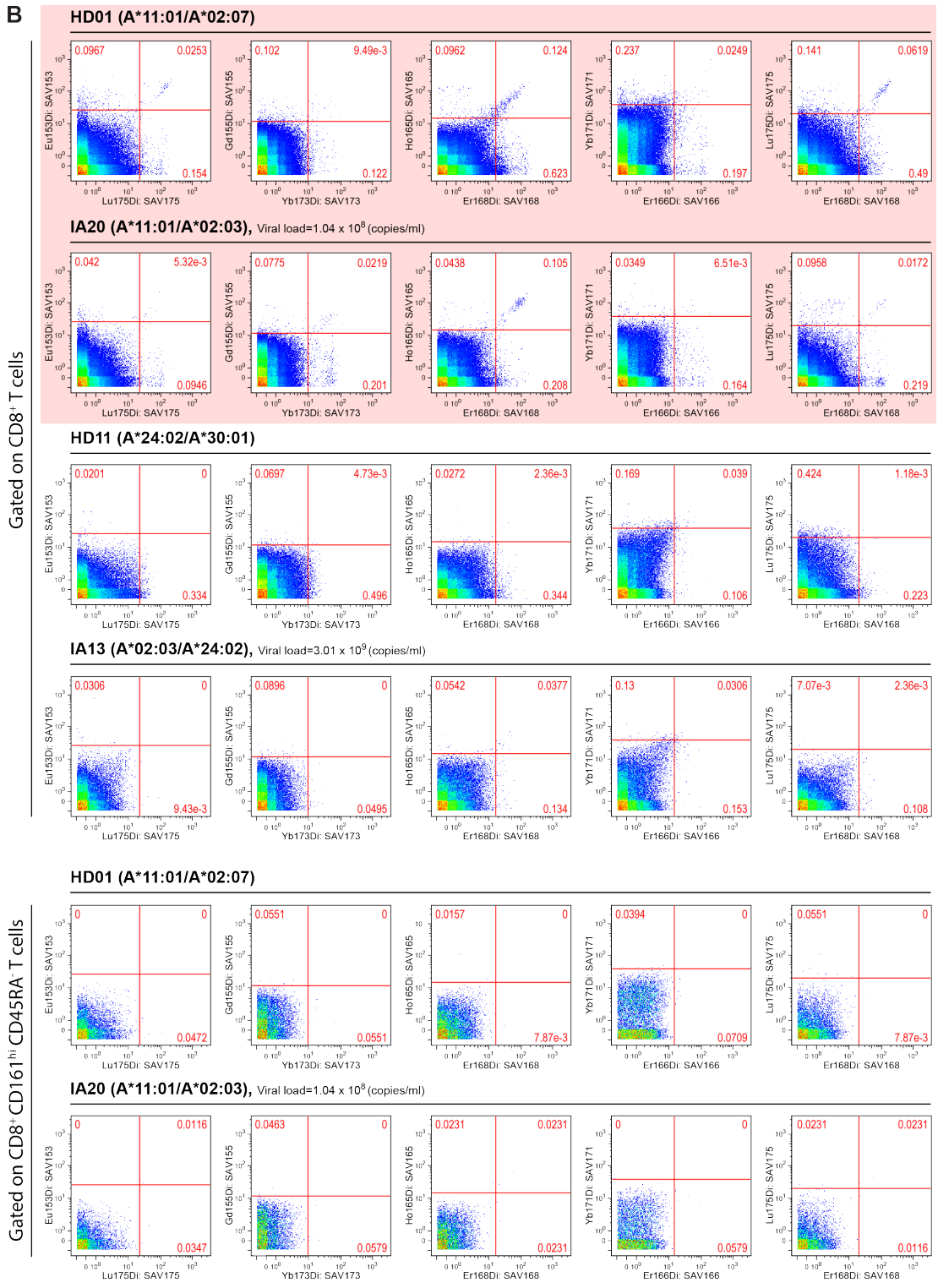

Figure 7. Validation of highly multiplex combinatorial pMHC tetramer strategy in HLA-A*11:01 and non-HLA-A*11:01 donors (Continued).

(B) Validation of the staining quality of highly multiplex combinatorial pMHC tetramer using metal-tag SAv between HLA-A*11:01 versus non-

HLA-A*11:01 donors. Dot plots show the tetramer positive cells and their signal of coded SAv by different combinations of nine metal-tag SAv.

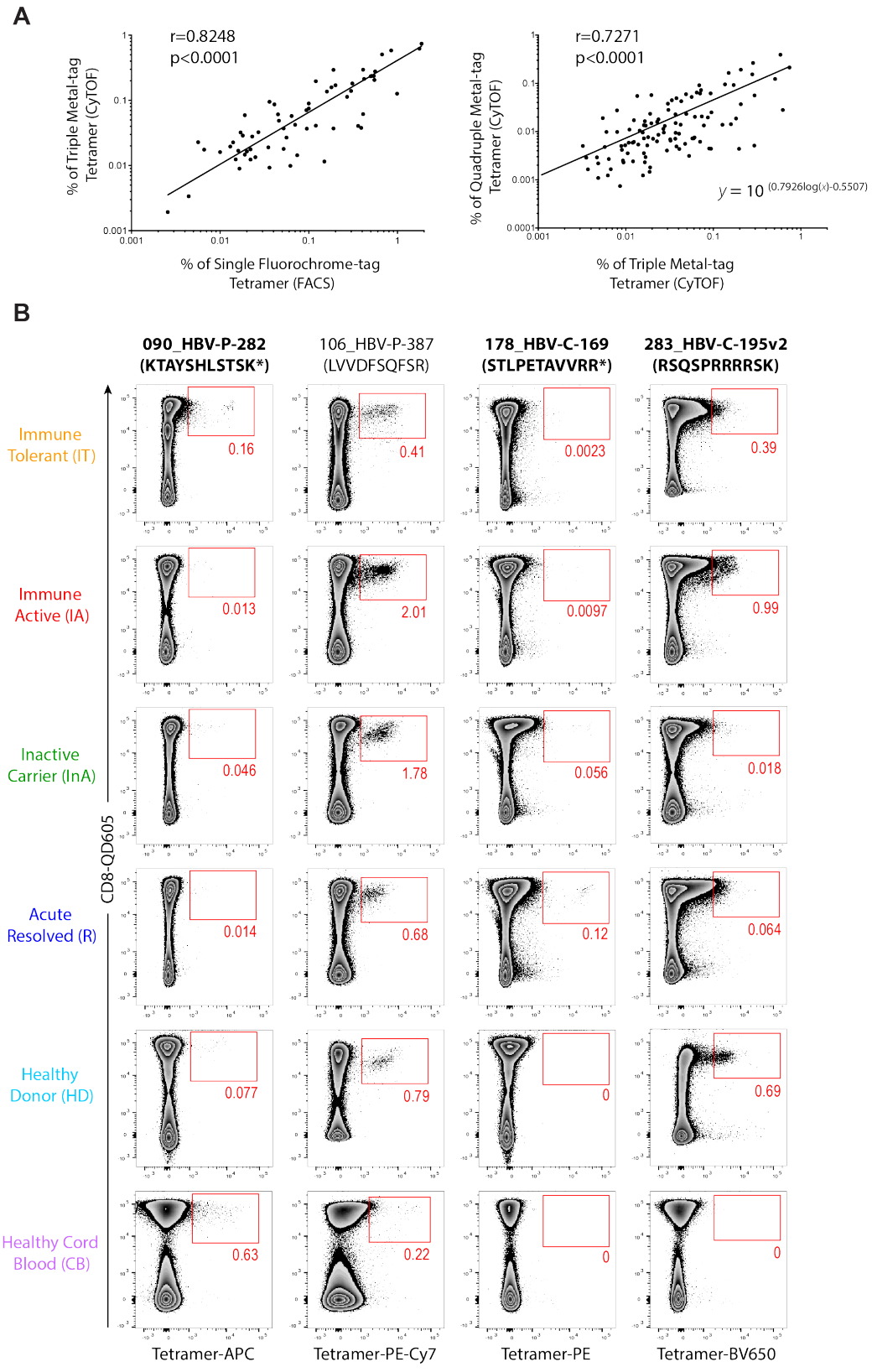

Figure 8. Reproducibility of detected HBV epitopes using flow cytometry.

(A) The correlations of FACS (single-coded) versus CyTOF (combinatorial-coded) detected frequency (B) Representative FACS dotplots of selected HBV epitopes across various patient groups. Numbers indicate the frequency of total $CD8^+$ T cells.

Unexpectedly, the total magnitudes of detected epitopes did not significantly differ between patient groups **(Fig. 9)**. However, across the differential frequencies of these epitopes, the HBV-C-169 was significantly elevated in patients associated with viral suppression or clearance (InA and R) **(Fig. 10)**. We were also intrigued by the observation that HBV-P-282 was detected in most of the patients but significantly increased in CB as possible naïve precursors, whereas the frequency of HBV-C-195v2 augmented in patients with high viremia (IT and IA) yet significantly diminished in InA and R. Of note, the previously identified HBV-P-387 (37, 134) showed strong responses regardless of patient groups including 5/10 HD. We postulated such counterintuitive observation could be due to subclinical infection without the development of anti-HBc antibody (HBcAb), as has been previously reported (135, 136) **(Fig. 11)**.

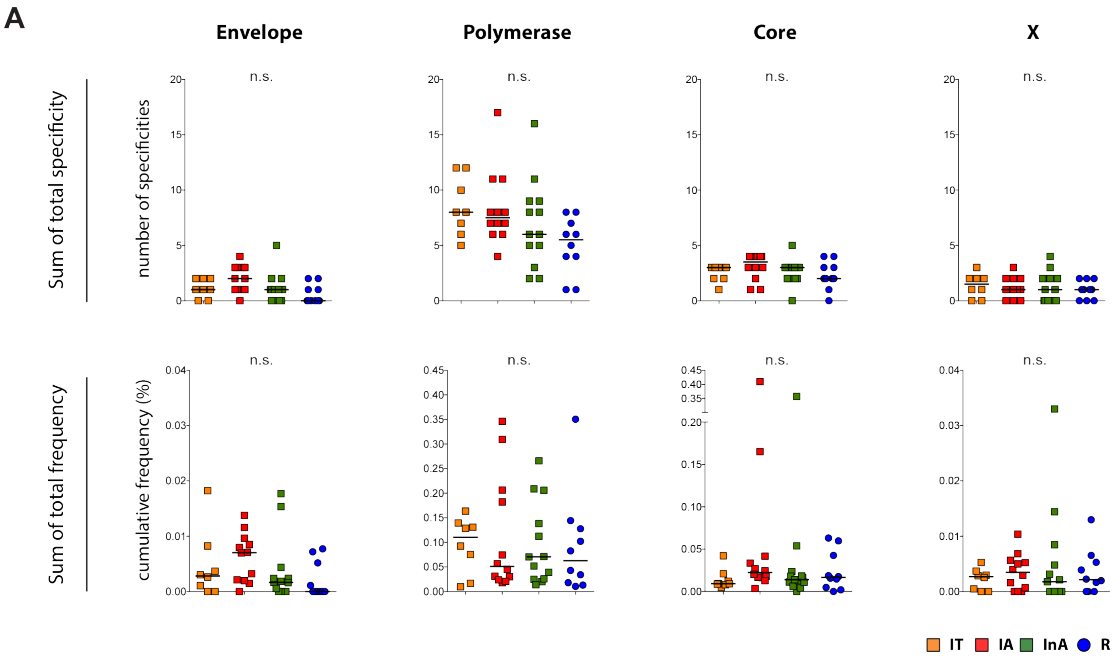

Figure 9. Total antigen-specific CD8$^+$ T cells response in various clinical stages during HBV infection.

(A) Upper panel, sum of total detected HLA-A*11:01-restricted specificities against each hepatitis B viral protein (envelope, polymerase, core and x) across various clinical stages. Lower panel, sum of total frequency (%) of antigen-specific CD8$^+$ T cells against each hepatitis B viral protein. n.s. = no significance. Statistical analysis was determinate using nonparametric One-way ANOVA.

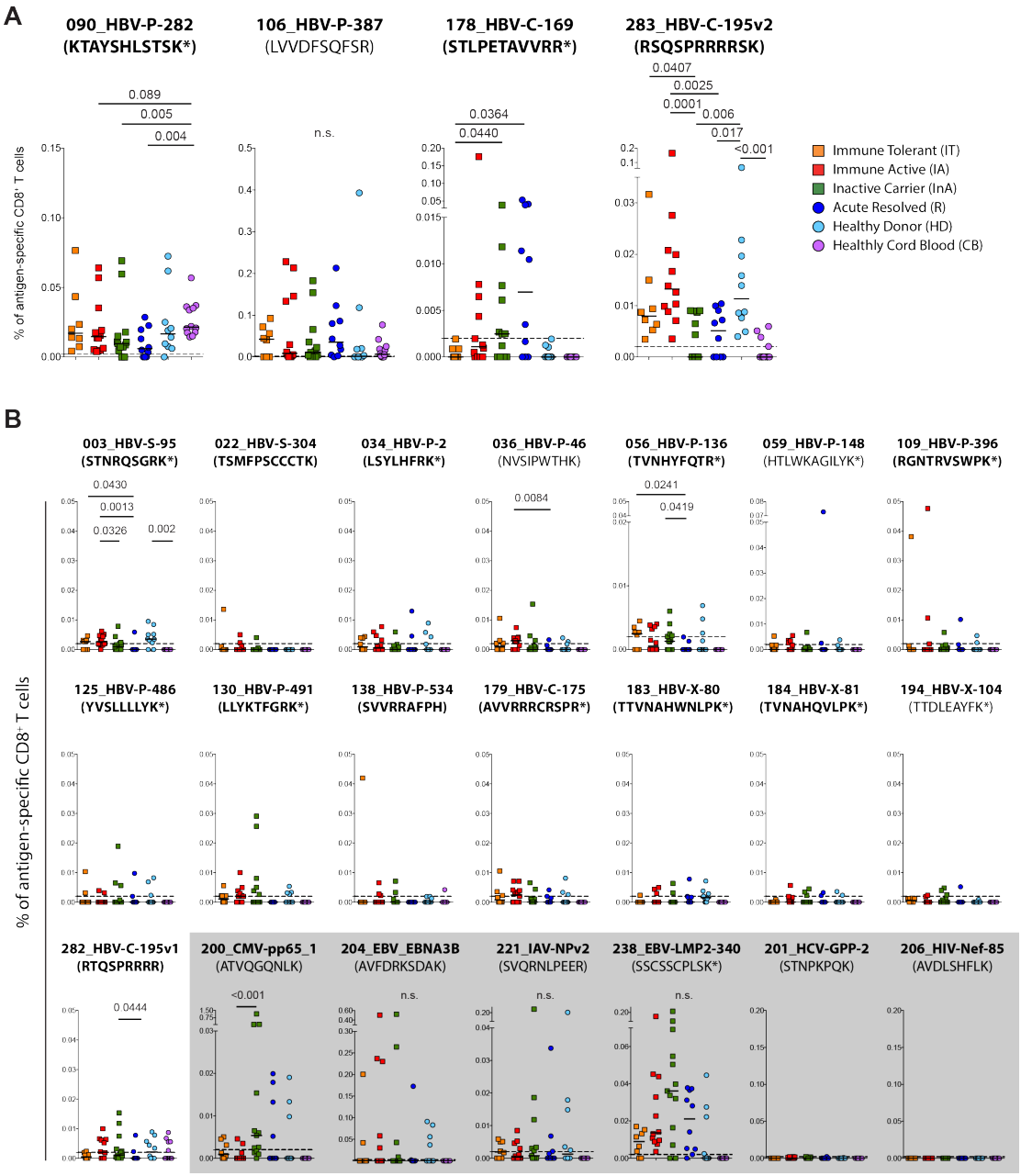

Figure 10. Total antigen-specific CD8$^+$ T cells response in various clinical stages during HBV infection.

(A) Differential frequency of four dominant antigen-specific CD8$^+$ T cells across various patient groups. (B) Magnitude of selected HBV-specific CD8$^+$ T cells detected by highly multiplex combinatorial pMHC tetramer strategy across various clinical stages of HBV infection. Plots show the frequency of antigen-specific CD8$^+$ T cells for fifteen predictive HBV epitope clusters and six known control viral epitopes (shaded box). Epitope sequences in bold face indicate previously unpublished sequences. * means this epitope cluster contains more than one peptide (Table 1). Dash lines on the y-axis are 0.002. Statistical significance was measured by non-parametric One-way ANOVA. n.s.= no significance.

A

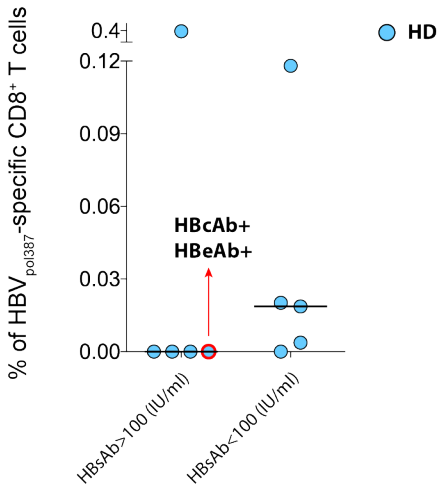

Figure 11. HBV serological status and the relationship with HBV$_{pol387}$-specific CD8$^+$ T cells in healthy donors.

(A) Frequency of HBV$_{pol387}$-specific CD8$^+$ T cells of healthy donors (HD) in different HBV serological (HBsAb, HBcAb and HBeAb) status. Levels of serum antibodies against different HBV viral antigens were defined by ELISA. Red circle indicates the only individual who was tested positive for HBcAb and HBeAb.

Importantly, the responses of these antigen-specific $CD8^+$ T cells (HBV_{pol282}, HBV_{pol387}, $HBV_{core169}$ and $HBV_{core195}$) were verified by different sets of experiments independently including flow cytometry, as well as their seemingly responsiveness upon stimulation of corresponded viral peptides (**Fig. 12)**. Regardless of the HBV epitopes, such significant expansions were mainly seen in IA and InA but not IT and HD.

Lastly, unsupervised high-dimensional data analysis *t*-SNE (110) demonstrated a remarkable heterogeneity of these HBV-specific $CD8^+$ T cells differing between patient groups, contrasting to the steady phenotype of EBV_{EBNA3B}-specific $CD8^+$ T cells **(Fig. 13)**. Thus, our comprehensive epitopes mapping and validation experiments identified several A*11:01-restricted virus-specific $CD8^+$ T cells against HBV with diverse phenotypic profiles.

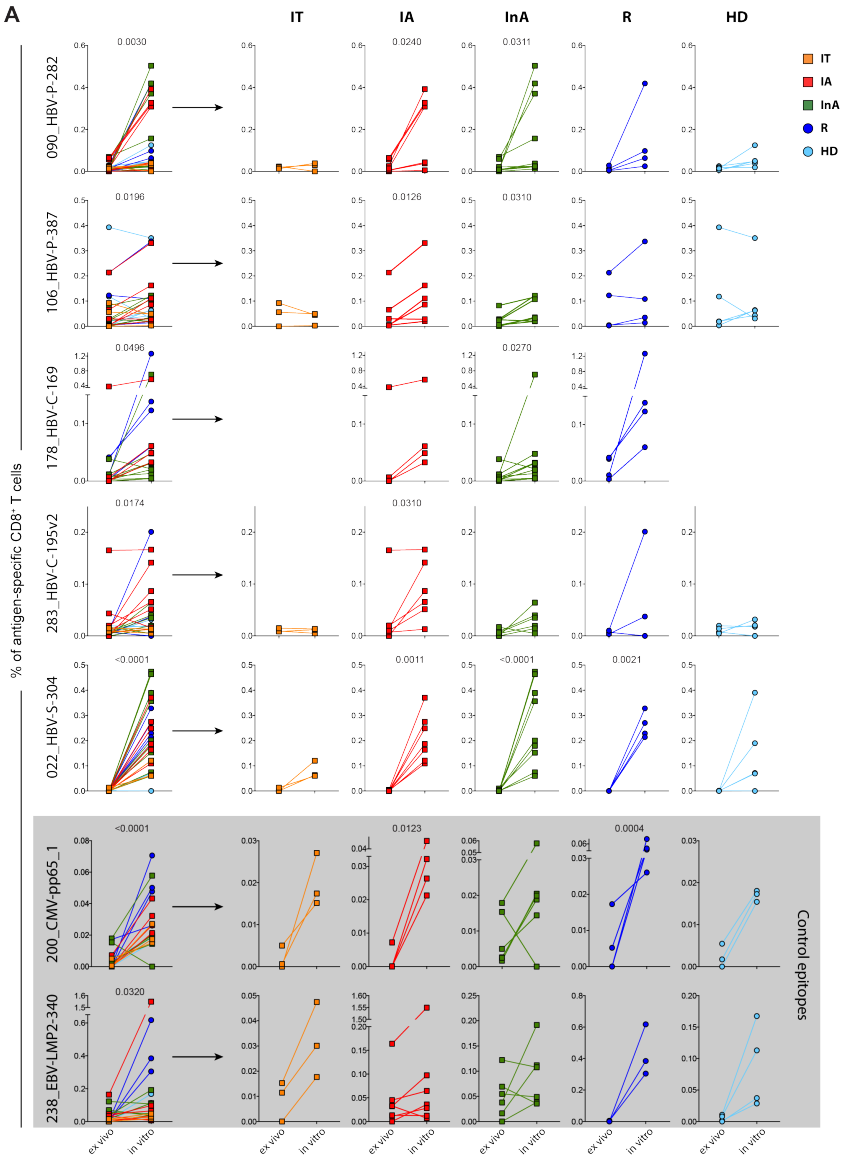
A
IT
IA
InA
R
HD
090_HBV-P-282
106_HBV-P-387
178_HBV-C-169
283_HBV-C-195v2
022_HBV-S-304
200_CMV-pp65_1
238_EBV-LMP2-340
Control epitopes
% of antigen-specific CD8+ T cells
ex vivo
in vitro

Figure 12. *In vitro* expansion of antigen-specific CD8$^+$ T cells upon peptide stimulation.

(A) PBMCs from different patient groups were expanded by corresponded viral peptides for 10 days. Frequency of antigen-specific CD8$^+$ T cells were determined as the same as ex vivo pMHC tetramer staining experiment. Number above each graph indicates the significant p value and defined by nonparametric Two-way ANOVA to compare between groups.

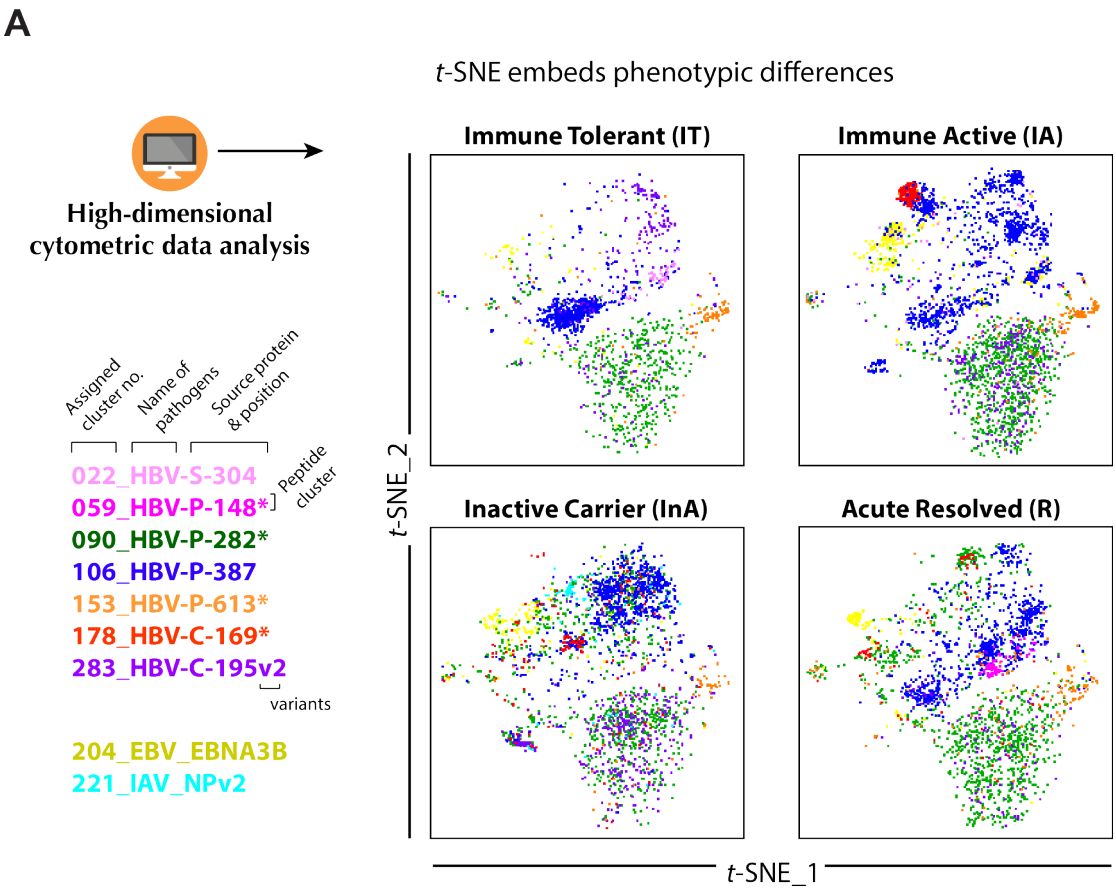

Figure 13. *t*-SNE illustrated the phenotypic diversity of selected antigen-specific CD8$^+$ T cells across various patient groups.

(A) Valid antigen-specific CD8$^+$ T cells were analyzed by dimensionality reduction algorithm *t*-SNE. Selected antigen-specific CD8$^+$ T cells were plotted and colored coded as indicated. Dotplots showed the representative of n=3 in each patient group. Parameters that were used for *t*-SNE analysis are indicated in Table 2.

4.2. Development of One-dimensional Soli-Expression by Nonlinear Stochastic Embedding (One-SENSE)

Rapid progress in single-cell analysis methods allow for exploration of cellular diversity at unprecedented depth and throughput. Visualizing and understanding these large high-dimensional datasets poses a major analytical challenge. A dimensionality reduction analysis, *t*-SNE (110), has been showed to perform exceptionally well on high-dimensional mass cytometry (112, 137). However, one major limitation of *t*-SNE is that the values on the axes of the plots are arbitrary and have no biological meaning. In particular, the function that *t*-SNE minimizes is invariant under rotations of the low-dimensional map, which implies that *t*-SNE visualizations can be arbitrarily rotated (138). Furthermore, even arbitrary directions in the visualizations have no meaning in the sense that they do not consistently indicate the same change in the underlying parameters.

One major goal in T cell biology is to directly assess the relationships between different types of cellular proteins whose expressions are associated to various T cell properties, and testing related hypothesis, such as T cell memory versus exhaustion. To this end, we have developed and proposed One-SENSE (116), a high-dimensional analysis method that facilitates this type of T cell categorical analysis. It measures cellular parameters assigned to manually predefined categories, and a one-dimensional map is constructed for each category using *t*-SNE **(Fig. 14)**. An advantage of this approach is that each dimension (axis) is informative and can be annotated through the use of heatplots aligned in parallel to each axis, allowing for simultaneous visualization of two categories across a 2D plot. The cellular occupancy of the resulting plots allows for direct assessment of the relationships between the categories. Although *t*-SNE is becoming widely used for its ability to map cells into two-dimensional space with high resolution (102, 112, 116), *t*-SNE also performs remarkably well even when mapping is restricted to a single dimension

(138). To address this and quantitatively compare the performance of *t*-SNE in mapping high dimensional mass cytometry data into lower dimensional projections, a neighborhood preservation analysis was performed **(Fig. 15A)**. Following *t*-SNE analysis (and mapping to various numbers of dimensions), the *k*-nearest neighbors were identified for the same cells and the fraction matching those identified for the same parameters was calculated as the neighborhood preservation ratio for each cell. This analysis shows that one-dimensional *t*-SNE is already more effective than three-dimensional PCA and performs to level that is ~78% of maximum for *t*-SNE at any number of dimensions **(Fig. 15B)**. We have applied this analysis approach on human peripheral T cell and explored the heterogeneity of functional $CD8^+$ T cells and regulatory T cells (Treg) (116). One-SENSE was proven to be more sensitive than *t*-SNE **(Fig. 14)** in separating meaningful T cell subpopulations using various T cell categories, and successfully identified previous unappreciated T cell functional heterogeneity (116, 117) and the diverse human resident memory T cells (T_{RM}) trafficking profiles (117).

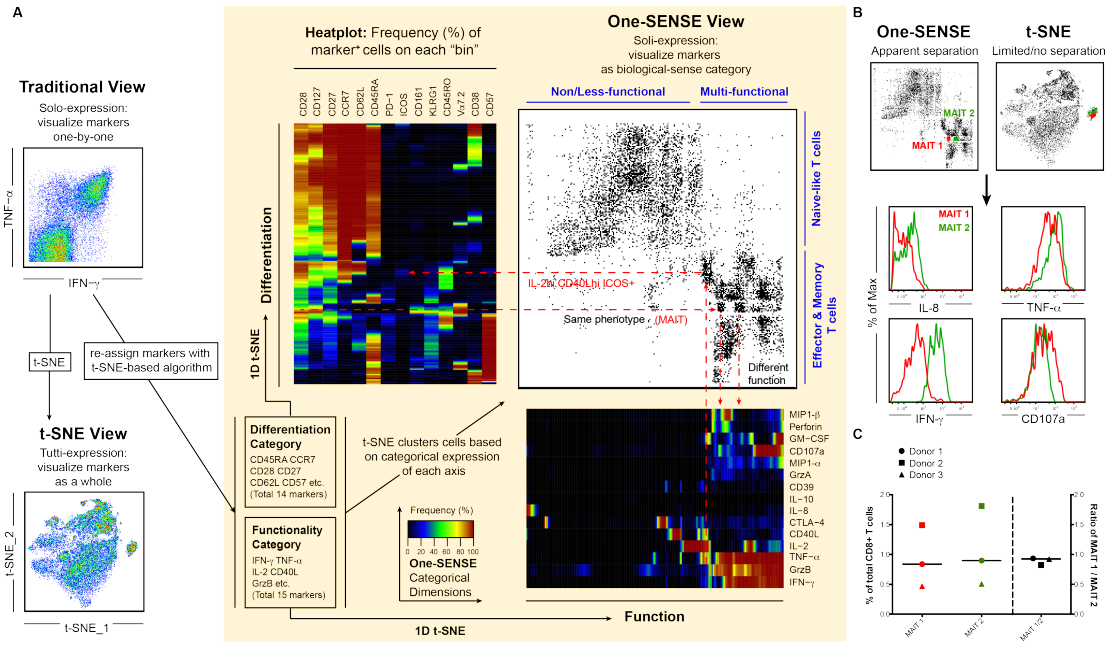

Figure 14. The rationale and representation of One-SENSE.

Human PBMCs isolated from three healthy donors were stained and acquired by mass cytometry for dimensionality reduction analysis. Total $CD8^+$ T cells were exported and analyzed by *t*-SNE and One-SENSE in parallel. (A) Plots show comparison of protein marker visualization

between *t*-SNE (Tutti-expression) and One-SENSE (Soli-expression) in different dimensions. Protein markers were assigned to various immunological categories based on previous studies. Shown is a One-SENSE view of $CD8^{+}$ T cells displaying "Differentiation" against "Function". Cells are aligned to a range of 250 bins (column of cells) on the categorical dimensions (axes) that are composed of cellular protein expression. Each categorical dimension is a one-dimensional *t*-SNE analysis. Heatplots indicate the frequency of marker positive cells in each bin. One-SENSE shows non-functional/naïve T cells are mainly located in the upper left corner of the map, while multifunctional effector and memory T cells have diverse combination clusters on the opposite area. Cellular features of clusters can be described by the coordination of *cis* and *trans* co-expression from each axis. (B) Comparison of One-SENSE and *t*-SNE on MAIT cells is shown (top). Histograms (bottom) of the indicated markers are shown for the gated populations of MAIT cells. (C) The frequency and ratio of MAIT 1 and MAIT 2 population identified between donors using One-SENSE.

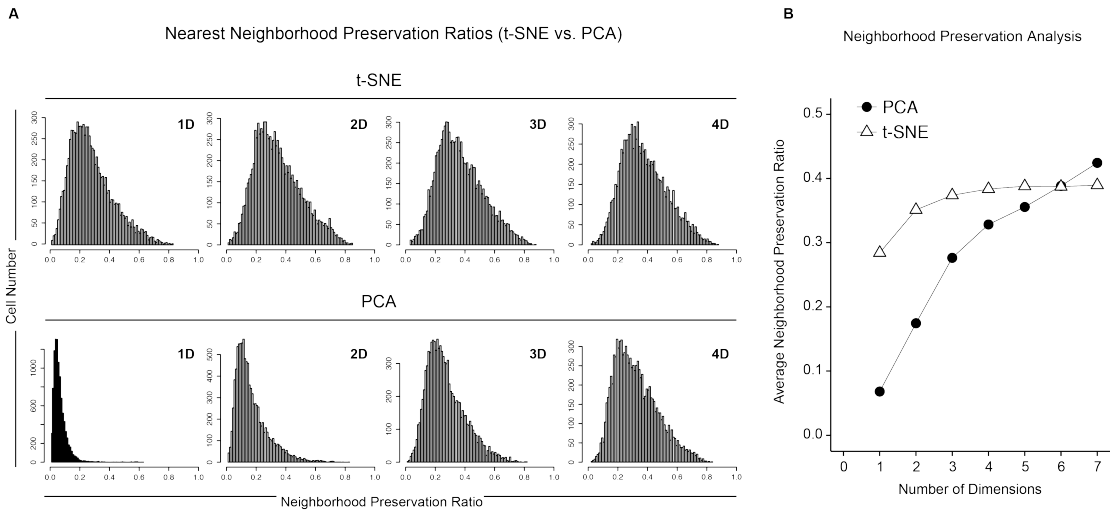

Figure 15. Neighborhood preservation analysis of *t*-SNE vs. PCA used at varying degrees of dimensionality reduction.

To quantitatively assess the performance of *t*-SNE compared to linear PCA at various mapping dimensionalities, a neighborhood preservation analysis strategy was used. $CD8^{+}$ T cells (10,000 random events sampled from 3 different donors as in **Fig. 14**) were used and 37 parameters for each cell (all parameters used for **Fig. 14**). For each cell, the nearest 100 neighbors were identified in 37 dimensions. The same cells were mapped into one to seven-dimensional space using *t*-SNE or PCA. Based on these results the 100 nearest neighbors were also identified and the ratio of these cells matching those identified using all 37 dimensions was calculated to assign a neighborhood preservation ratio. (A) Histograms of the neighborhood preservation ratio for this 10,000 cells dataset are plotted for the one to four-dimensional t-SNE

and PCA mappings. (B) Average neighborhood preservation ratios are plotted for one to seven-dimensional *t*-SNE vs. PCA mappings. Note that one dimensional *t*-SNE outperforms three-dimensional PCA on this dataset (in terms of neighborhood preservation) and that gains in performance coming from the use of 2 or more dimensions of *t*-SNE are modest compared to that achieved by just a single dimension. Specifically, *t*-SNE performance in one dimension is already at >70% of the maximal performance possible for higher dimensional *t*-SNE mapping of these data. Note though that *t*-SNE performance in >3 dimensional mappings can improve by increasing the number of degrees of freedom of the student-t kernel (116, 138).

4.3. Diverse interrelations of exhaustion and memory by One-SENSE

By co-staining nine major inhibitory receptors (63) with pMHC tetramers, we found a wide array of expression profiles on these selected virus-specific $CD8^+$ T cells. Expression of 2B4 was seen in most of the detected epitopes, while there were very minimum expression of LAG-3, TIM-3 and CTLA-4 **(Fig. 16 and 17)**. Moderate-to-low levels of HVEM were also universally expressed, which may associate with cellular memory (88, 139). Besides HVEM and BTLA, we did not find HBV_{pol282}- and $HBV_{core195v2}$-specific $CD8^+$ T cells expressing other inhibitory receptors **(Fig. 17 and 18)**. Interestingly, HBV_{pol387}-specific $CD8^+$ T cells significantly upregulated CD160, 2B4 and TIGIT with the diminished BTLA, apart from the dominance of PD-1 and TIGIT on $HBV_{core169}$-specific $CD8^+$ T cells **(Fig. 16, 17A and 18)**.

A

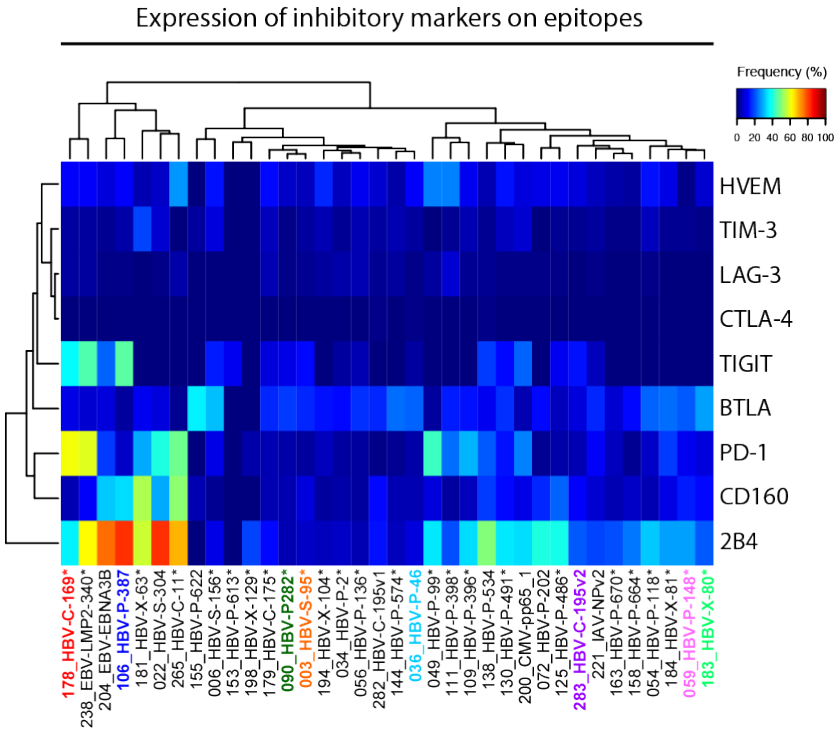

Figure 16. Overview of the expressions for nine major inhibitory receptors.

(A) Heatmap showed the diverse expression pattern of inhibitory receptors on different antigen-specific CD8+ T cells against HBV epitopes. Plot indicates the frequency of inhibitory receptors for each epitope.

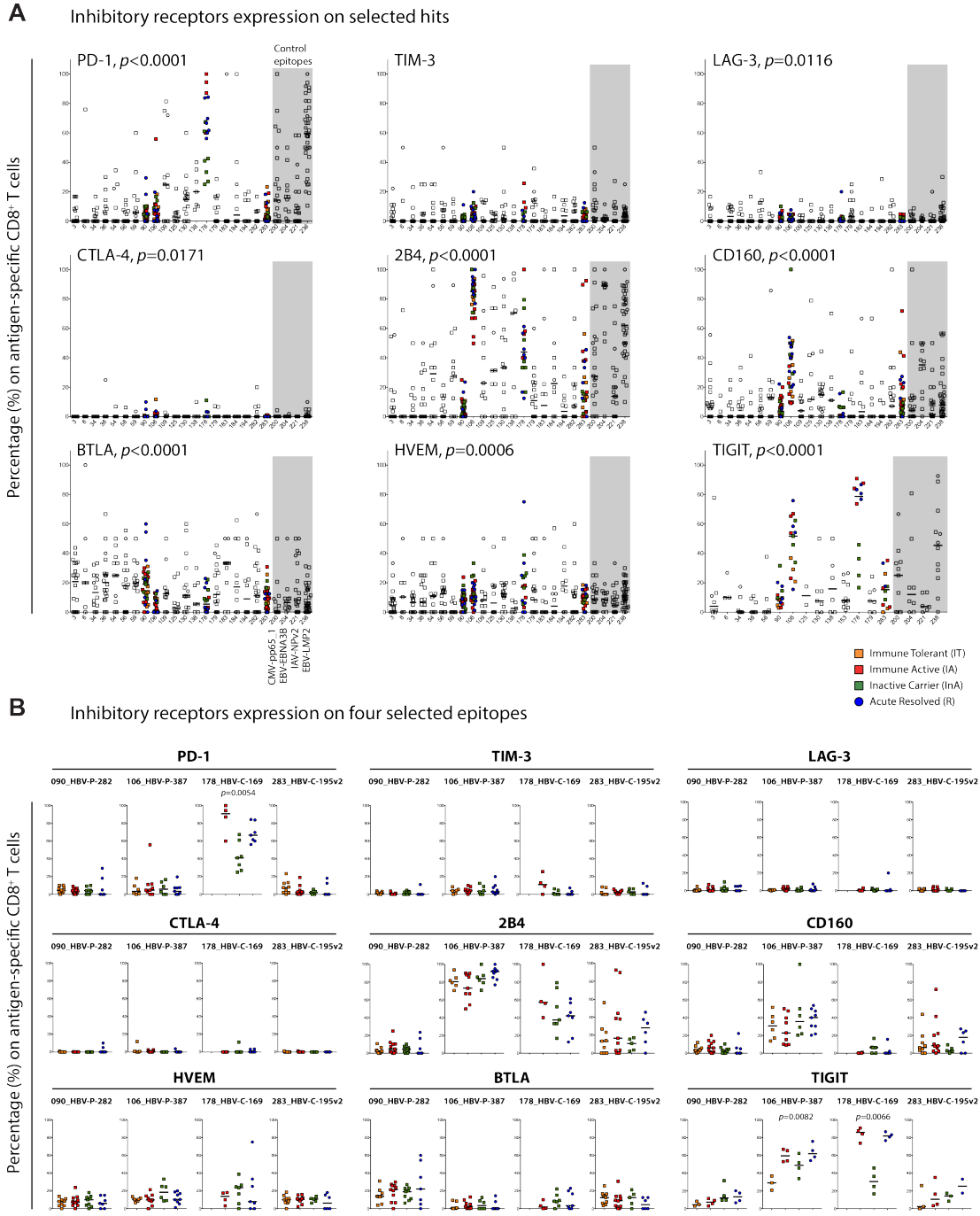

Figure 17. Expression levels of nine different inhibitory receptors on antigen-specific CD8$^+$ T cells.

(A) Expression level on selected hits. Numbers on x-axis indicate the cluster number of each specificity (epitopes) (see Table 1). Shaded area

are control viral epitopes. (B) The inhibitory receptors on four dominant antigen-specific $CD8^+$ T cells (090_HBV-P-282, 106_HBV-P-387, 178_HBV-C-169 and 283_HBV-C-195v2) were further compared across various clinical stages of HBV infection. Related to Figure 2B. Individual dots on four high profiles hits are color coded as indicated. Statistical analysis was calculated using nonparametric One-way ANOVA.

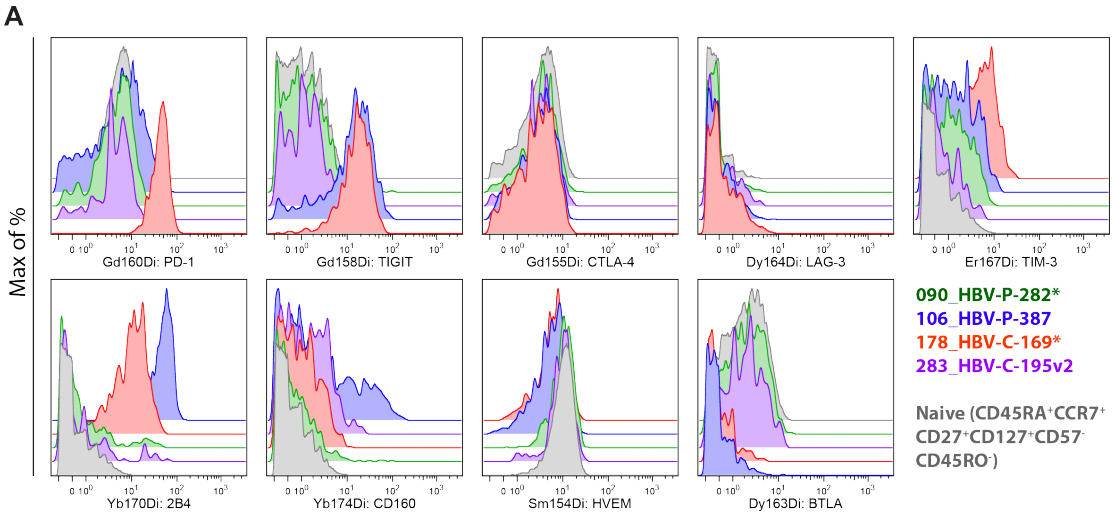

Figure 18. Comparison of nine inhibitory receptors on four dominant virus-specific $CD8^+$ T cells.

(A) Histograms showed the discrepancy of the expression levels for four dominant virus-specific $CD8^+$ T cells against HBV. Greys are the tetramer negative naïve cells from the same donor as indicated in the legend.

By referring the *t*-SNE plots of these epitopes **(Fig. 13)** with the expression level of inhibitory receptors **(Fig. 19),** such diversity can be illustrated.

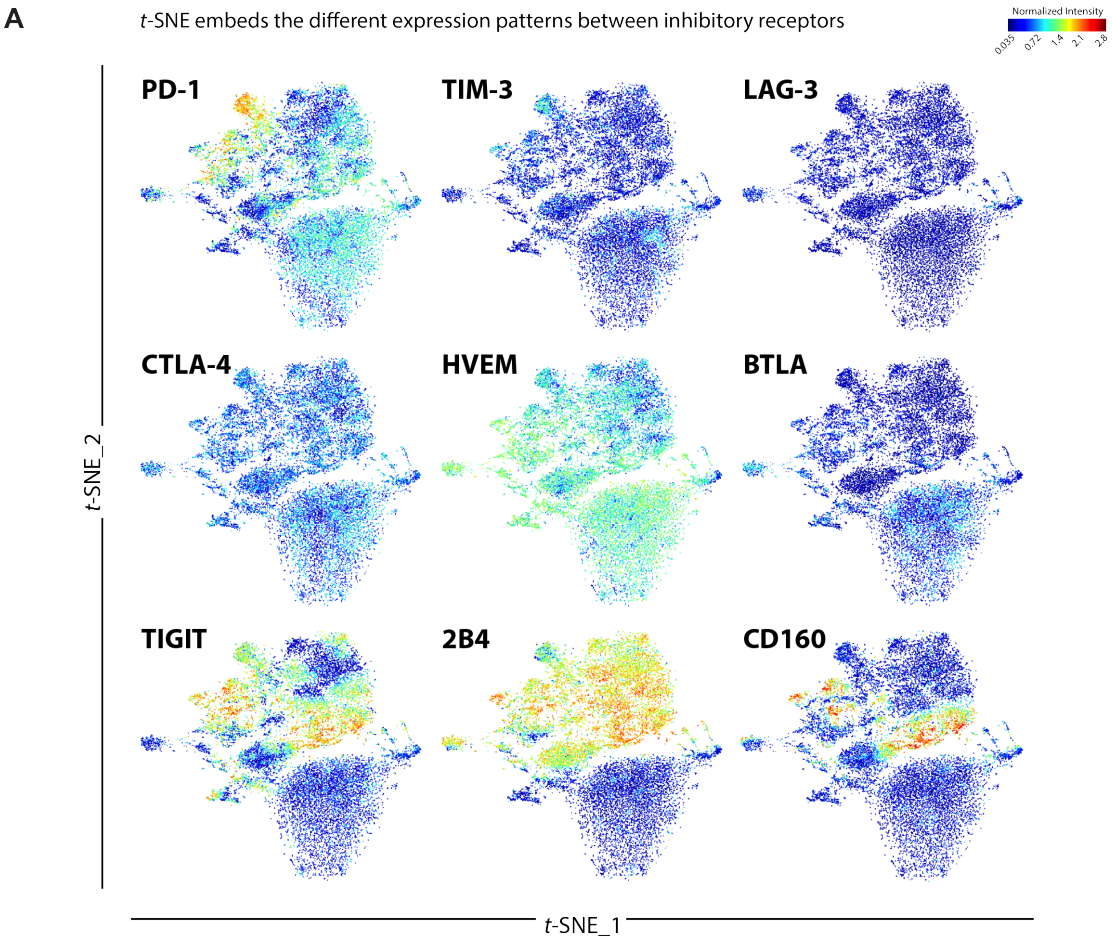

Figure 19. Expression levels of nine inhibitory receptors using *t*-SNE analysis.

(A) The distribution and expression pattern of nine different inhibitory receptors on *t*-SNE map. Each dot represents the antigen-specific $CD8^+$ T cell. Plots were generated by combining all detected antigen-specific $CD8^+$ T cells from 4 patients per group (IT, IA, InA, R and HD) using highly multiplex combinatorial pMHC tetramer strategy.

To directly investigate the relationship between exhaustion- and memory-associated markers, we employed One-SENSE (116), which benefits from user-defined categories (cellular properties) that are biological meaningful and suitable for testing hypothesis with intuitive visualization. Most importantly, One-SENSE clusters cells and objectively displayed all possible protein co-expressions based on each T cell category **(Fig. 20)**. We delineated the immunome of virus-specific $CD8^+$ T cells into three categories, as “Differentiation+TNFR” (markers of differentiation and tumor necrosis factor receptor superfamily), “Exhaustion” (inhibitory receptors) and “Trafficking” (chemokine receptors). These dimensions called out the cellular clusters, and such striking heterogeneity was readily shown in 3D or 2D plots. Composed by all detected virus-specific $CD8^+$ T cells, there were approximately 6~9 different co-expressions of inhibitory receptors across various patient groups. Between these discrepancies, one had the most number of inhibitory receptors ($HVEM^{int}2B4^+TIGIT^+CD160^+PD\text{-}1^{lo}$), and was mainly contributed by subpopulation of HBV_{pol387}- and EBV_{EBNA3B}-specific $CD8^+$ T cells. Additionally, we found that the majority of PD-1-expressing cells did not express CD160 but co-expressed 2B4 and TIGIT. This heterogeneity can be best presented by HBV_{pol387}- and $HBV_{core169}$-specific $CD8^+$ T cells. The former had a very homogeneous memory and trafficking profile with four distinct inhibitory receptors co-expressions in IT **(Fig. 20)**. However, several subpopulations from IA, InA and R, one exhaustion profile can correspond to three or even more differentiation and trafficking phenotypes. This presents a multifactorial composition between inhibitory receptors against cellular differentiation and trafficking profiles across the events of chronic viral infection. Noteworthy, the absence of CD39 on HBV-specific $CD8^+$ T cells marked their difference from HCV- and HIV-specific $CD8^+$ T cells (140), suggest they might be less vulnerable for apoptosis (141).

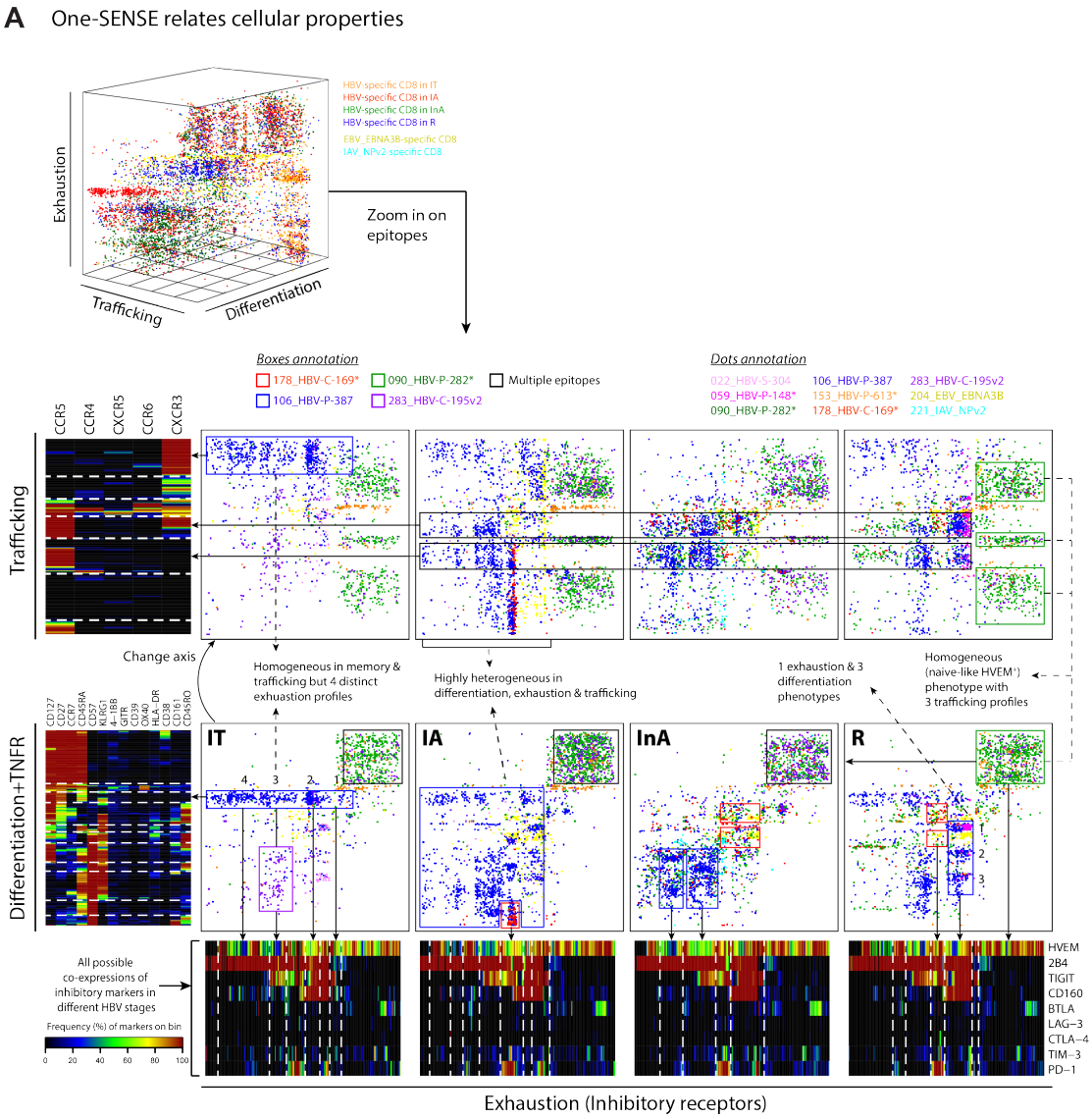

Figure 20. Categorical analysis using One-SENSE uncovers the relationships between exhaustion- and memory-associated markers of virus-specific CD8$^+$ T cells.

(A) One-SENSE to dissect the phenotypic profiles of virus-specific CD8$^+$ T cells by three different T cell categories, as “Differentiation+TNFR”, “Exhaustion” and “Trafficking”. Virus-specific CD8$^+$ T cells were color coded by patient groups in 3D, or by different specificity in 2D. Cells were aligned by 250 bins on each axis (categorical dimension) and corresponded heatplots were shown. The different combinations of protein co-expressions segregated the cell cluster from each category and the frequency of such expression levels were shown. Boxes annotated the epitope who mostly enriched in given regions.

4.4. Multifactorial exhaustion and memory atlas of HBV_{pol387}-specific $CD8^+$ T cells

Of all of the epitopes, we were most interested by HBV_{pol387}- and $HBV_{core169}$-specific $CD8^+$ T cells, having the higher degrees of heterogeneity across various clinical stages. Indeed, HBV-P-387 (LVVDFSQFSR) (37, 134) and one of the epitope in HBV-C-169 (STLPETTVVRR) (37, 134, 142, 143) were previously described without available phenotypic data. Using *t*-SNE, we found seven different major cellular clusters within HBV_{pol387}-specific $CD8^+$ T cells that against this single epitope **(Fig. 21A)**. Surprisingly, ~80% of HBV_{pol387}-specific $CD8^+$ T cells from IT were significantly enriched in *t*-SNE cluster 6 (C6) comparing to other patient groups **(Fig. 21A-C)**. HBV_{pol387}-specific $CD8^+$ T cells from other patient groups conversely concentrated in distinct regions on *t*-SNE map as C7, C3 and C5, from IA, InA and R, respectively **(Fig. 21A and C)**. By separating these major subpopulations, C6 of HBV_{pol387}-specific $CD8^+$ T cells possessed the highest memory profile with $CXCR3^{hi}CD27^{hi}CD127^{hi}$ but $CCR7^{lo}CD45RA^{int}$ **(Fig. 21B)**. Holding similar phenotypes, C3 and C5 had intermediate level of these memory markers with the addition of CCR5, KLRG-1 and CD57, suggesting they were later-stage effector cells. Minimal enrichment of C7 in IA was highlighted by the unique co-expression of high CD45RO, CCR4 and HVEM with central memory phenotype, indicating a diverse differentiation status. All cellular clusters expressed 2B4 besides C7, while C1 solely upregulated PD-1 and C4 and C5 had selective expression of CD160 and TIGIT. Furthermore, patients from IT and InA were better stratified by unsupervised pairwise measurement of these *t*-SNE clusters due to the significant enrichment of C6 and C3, respectively **(Fig. 21D).** Lastly, the heterogeneous HBV_{pol387}-specific $CD8^+$ T cells can be further explored and validated using One-SENSE to describe the different numbers of phenotypic profiles **(Fig. 22)**.

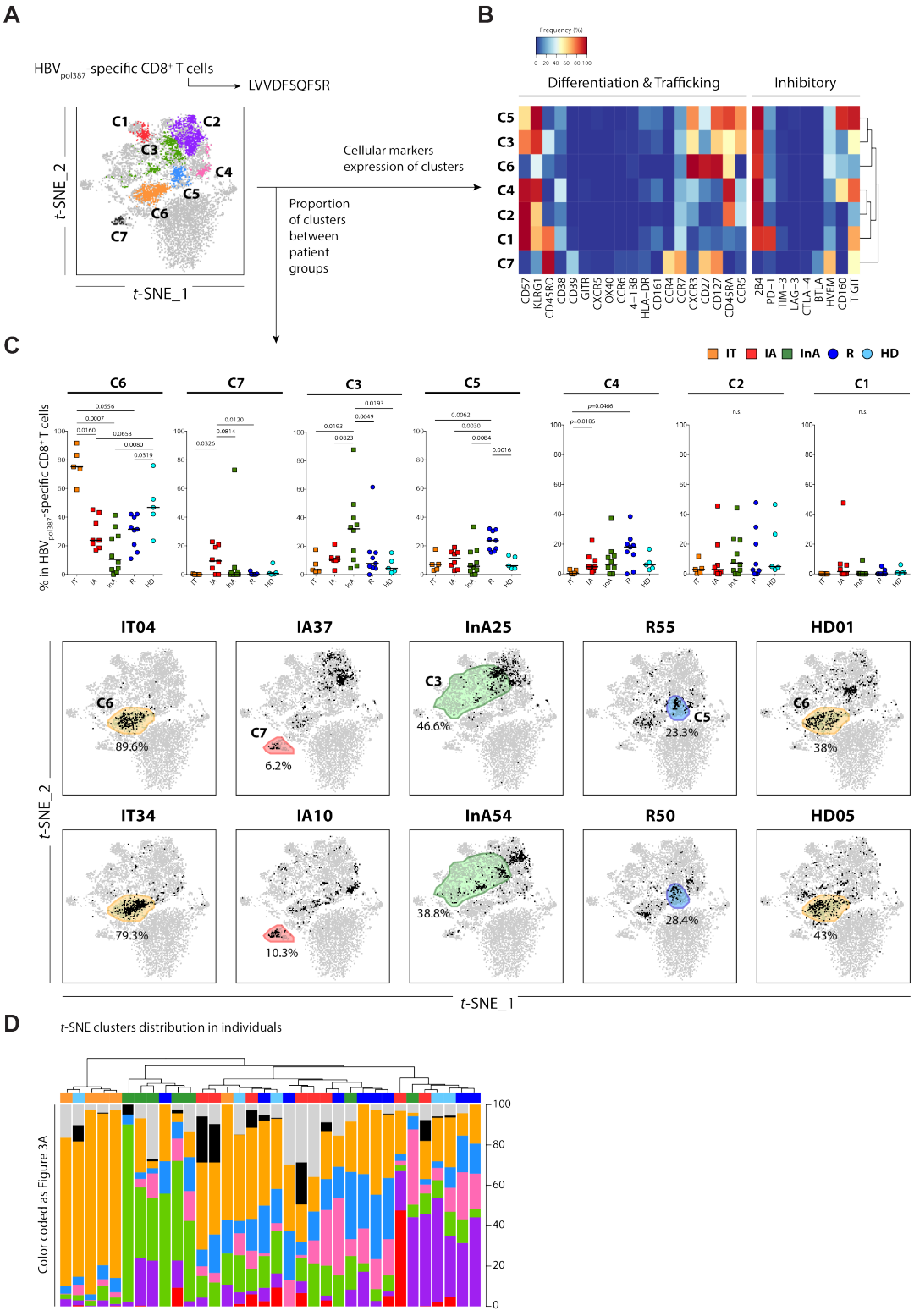

Figure 21. Unsupervised high-dimensional and clustering analysis showed the multifactorial phenotypes of HBV_{pol387}-specific $CD8^+$ T cells across various patient groups.

(A) *t*-SNE dissected HBV_{pol387}-specific $CD8^+$ T cells into seven major cellular clusters. (B) Expression level of cellular markers on HBV_{pol387}-

specific $CD8^+$ T cells. (C) Proportion of t-SNE cluster of HBV_{pol387}-specific $CD8^+$ T cells across the various patient groups. Two representative plots per patient groups show HBV_{pol387}-specific $CD8^+$ T cells were enriched in distinct *t*-SNE regions. Statistical analysis was determined by nonparametric One-way ANOVA. n.s. = no significance. Black dots represent HBV_{pol387}-specific $CD8^+$ T cells from the indicated individual donors. Grey dots are combined of al antigen-specific $CD8^+$ T cells of twenty donors including all patient groups. Numbers indicate the percentage of each highlighted cluster (color coded as in Fig. 21A) within HBV_{pol387}-specific $CD8^+$ T cells. (D) Unsupervised hierarchical clustering analysis clustered individual patient based on the Euclidean distances between the proportional *t*-SNE cellular clusters and color coded as in Fig. 21A).

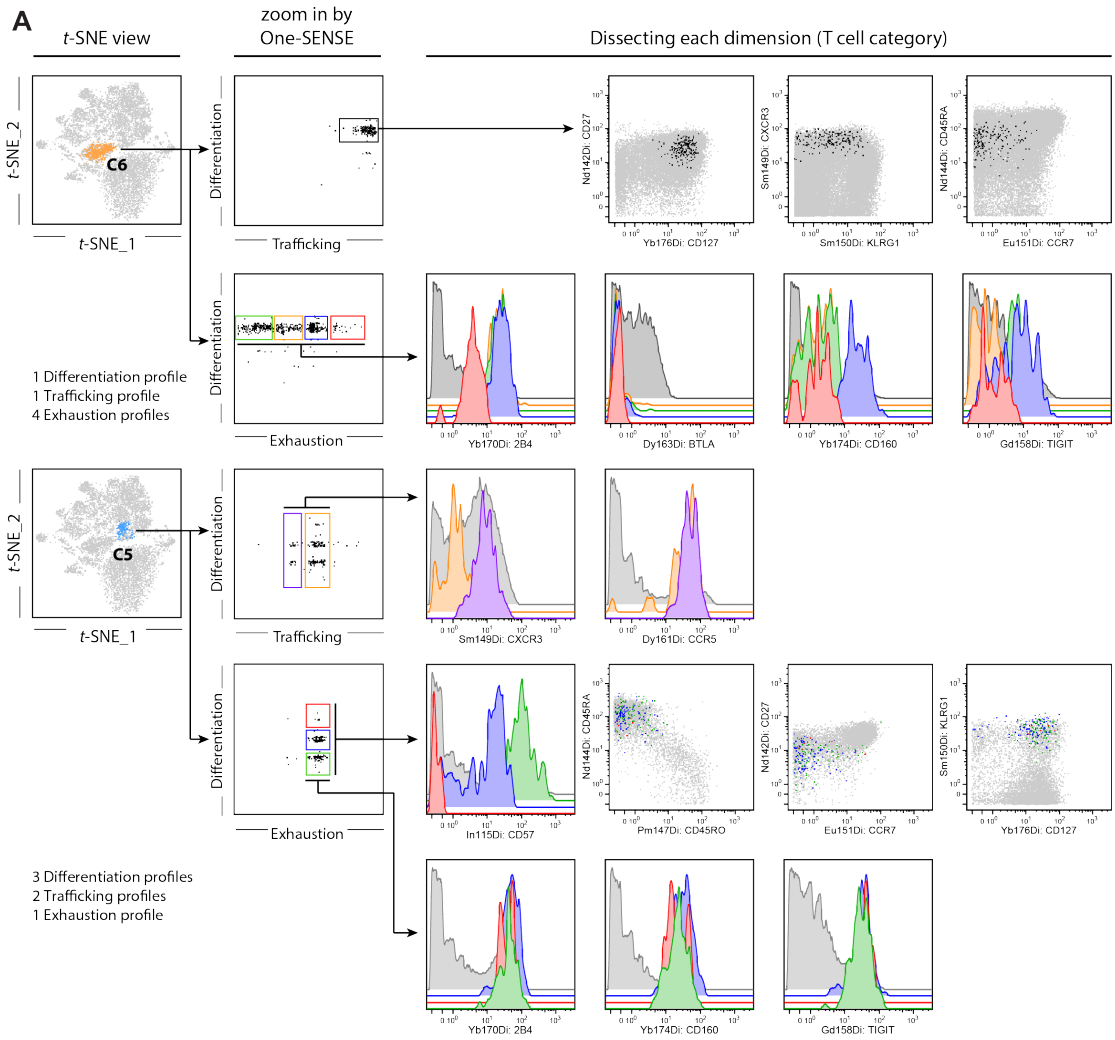

Figure 22. One-SENSE analysis of HBV_{pol387}-specific $CD8^+$ T cells for further investigation of selected *t*-SNE-defined cellular clusters.

(A) Dissecting the highly heterogeneous immune profiles (Differentiation, Trafficking, and Exhaustion) of HBV_{pol387}-specific $CD8^+$ T cells analyzed by One-SENSE. Each *t*-SNE cluster (related to Figure 21A) was analyzed by One-SENSE to further reveal the heterogeneity of subpopulations within each cluster of the same antigen-specific $CD8^+$ T cells. One-SENSE outperform *t*-SNE by identifying the rare differences on each T cell category that are biological meaningful. The differences between subpopulations that separated by One-SENSE can also be validated using dotplots or histograms and were color-coded as indicated. Plots show that the different dominant cluster (in Fig. 21A) of HBV_{pol387}-specific $CD8^+$ T cells in different patient groups possess distinct composition of three immune profiles, including “Differentiation”, “Trafficking”, and “Exhaustion”.

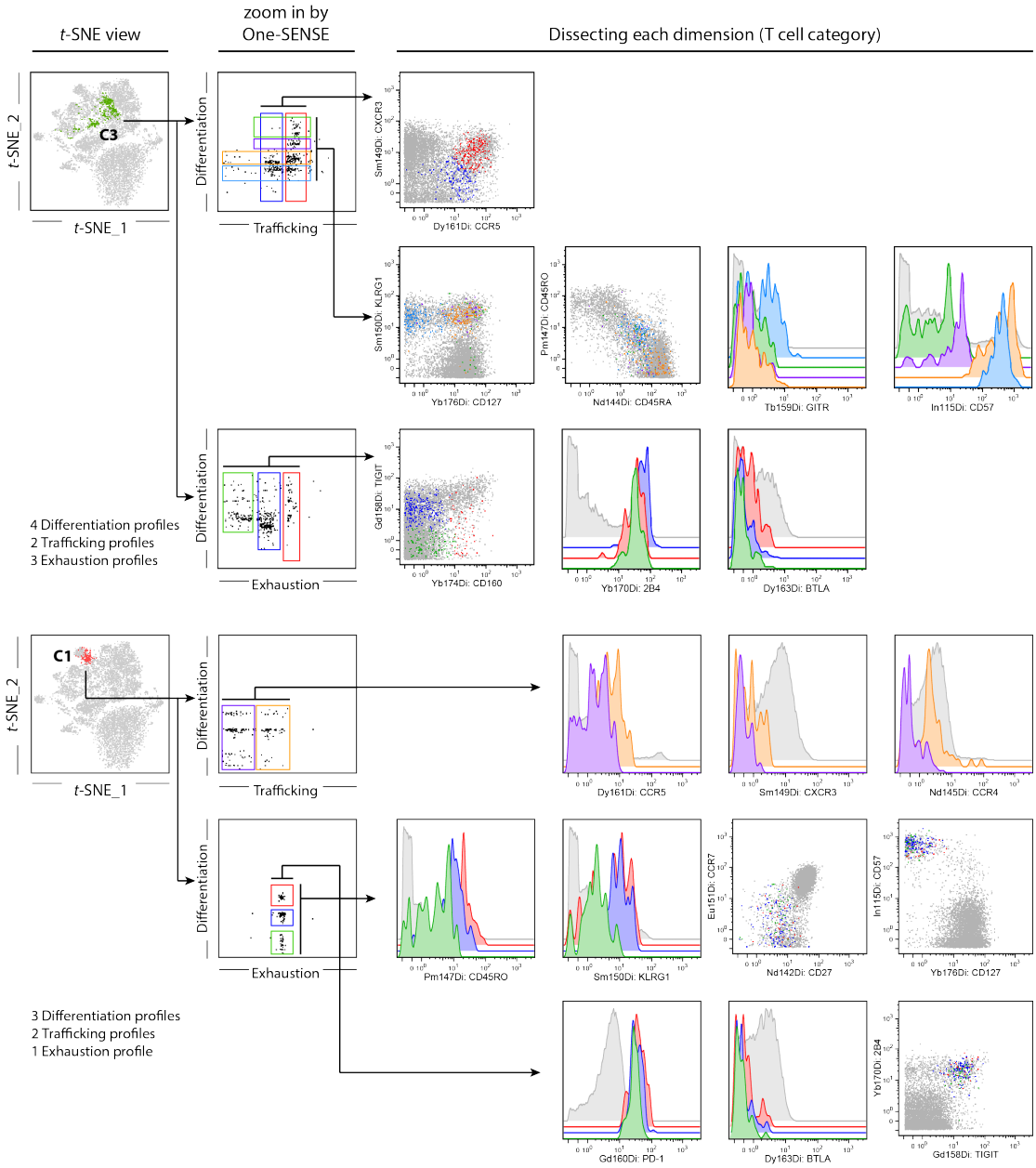

Figure 22. One-SENSE analysis of HBV_{pol387}-specific $CD8^+$ T cells for further investigation of selected *t*-SNE-defined cellular clusters (Continued).

4.5. Immunodominant $HBV_{core169}$-specific $CD8^+$ T cells are associated with viral clearance

Comprised of seven similar peptides **(Table 1),** $HBV_{core169}$-specific $CD8^+$ T cells had both significant greater frequency **(Fig. 10A)** and a stepwise increment of pMHC tetramer intensity toward acute resolved patients **(Fig. 23)**. As support for the *t*-SNE analysis **(Fig. 24A)**, unsupervised hierarchical clustering segregated individuals into different clinical stages based on the cellular profiles of $HBV_{core169}$-specific $CD8^+$ T cells, which was not observed for EBV_{EBNA3B}-specific $CD8^+$ T cells analyzed in parallel **(Fig. 24B)**. Compared to the unique expression of CD57 in IA, several memory-associated markers (CD27, CD28, CD45RO, CD127 and CXCR3) on $HBV_{core169}$-specific $CD8^+$ T cells were significantly and gradually enhanced in InA and R **(Fig. 24B and C).** We also observed a significant reduction of PD-1 and TIGIT on $HBV_{core169}$-specific $CD8^+$ T cells in InA **(Fig. 17B and 24B)**. Indirectly evidenced by the increased pMHC tetramer intensity, the preferential upregulation of PD-1 in clinical stages of high but fluctuating viral load during ongoing viral clearance is in line with study in LCMV (90, 91). Together, this suggests that elevated expression of PD-1 was the consequence of continual TCR-viral epitope engagement leading to the selection of high affinity T cell clones.

A

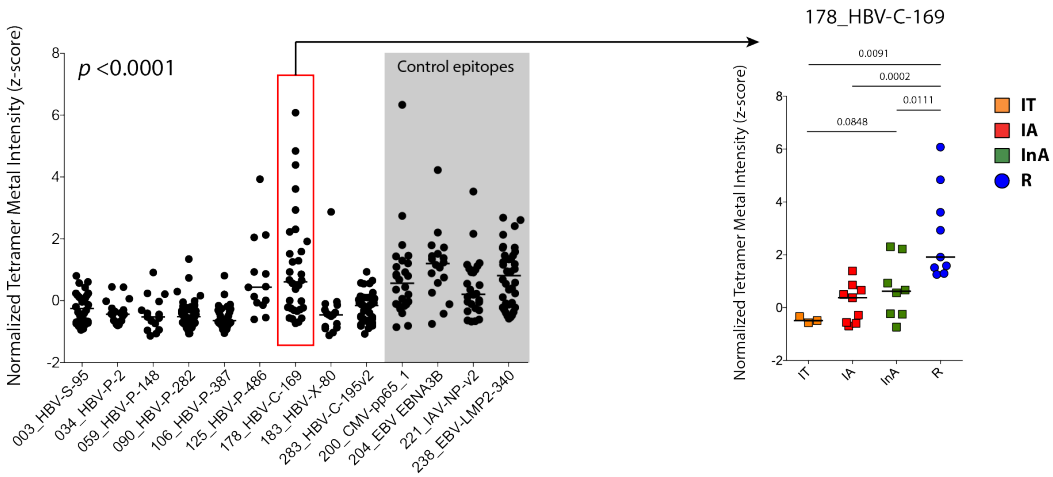

Figure 23. Significant elevation of pMHC tetramer intensity of $HBV_{core169}$-specific $CD8^+$ T cells in acute resolved patients.

(A) Tetramer intensity was quantified by averaging the median numbers of metals of four different SAv-metals coded on tetramer positive cells. Plots show the normalized value (z-score) of tetramer intensity on different selected virus-specific $CD8^+$ T cells (left), and $HBV_{core169}$-specific $CD8^+$ T cells (right) across various patient groups.

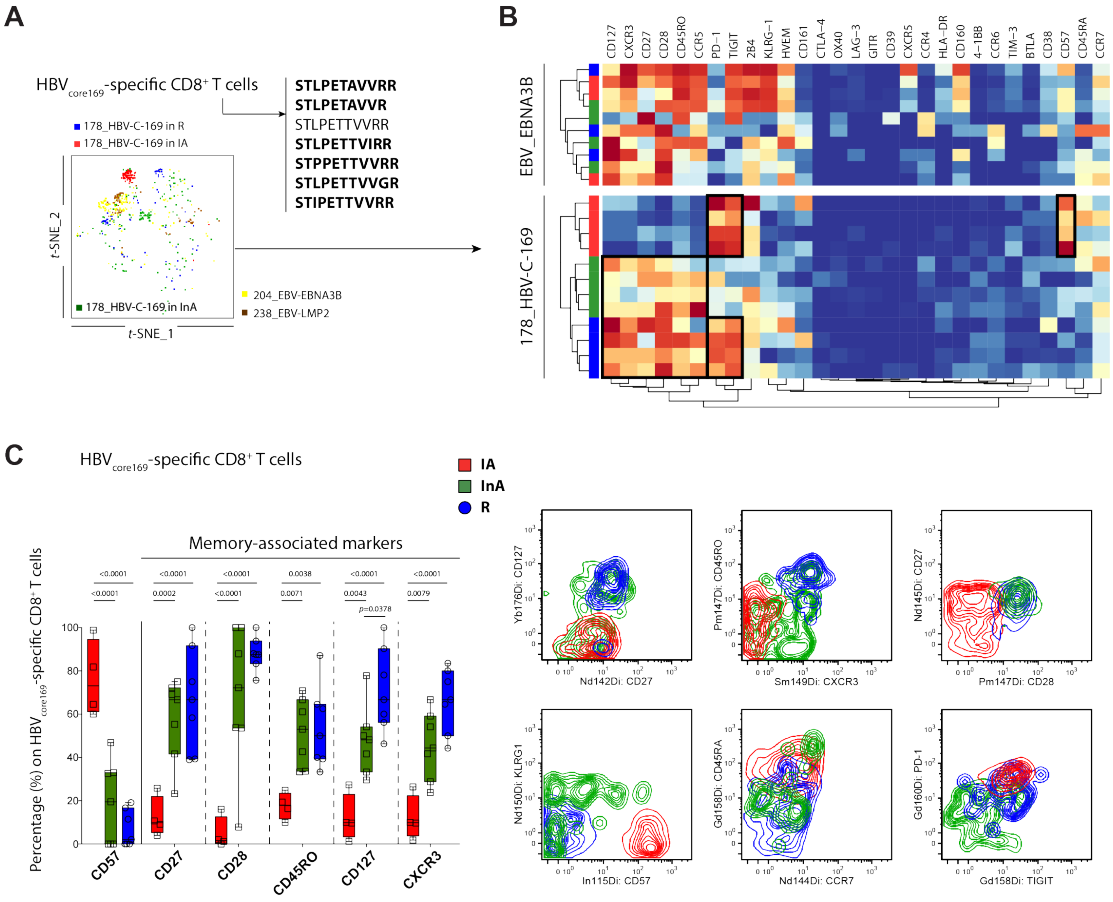

Figure 24. Differential phenotypic analysis of $HBV_{core169}$-specific $CD8^+$ T cells in various patient groups.

(A) High-dimensional *t*-SNE analysis showed the diverse phenotypic difference of $HBV_{core169}$-specific $CD8^+$ T cells in various patient groups. This antigen-specific $CD8^+$ T cells comprised of seven different peptides based on the sequence homology **(Materials and Methods)**. Bold faces are previously unknown sequences. (B) Hierarchical clustering of cellular markers expression of EBV_{EBNA3B}-specific $CD8^+$ T cells (upper panel) and $HBV_{core169}$-specific $CD8^+$ T cells (lower panel). Individual patient was color-coded. (C) Bar graph indicates the discrepancy of T cell memory-associated markers (CD27, CD28, CD45RO, CD127 and CXCR3) and CD57 expressed on $HBV_{core169}$-specific $CD8^+$ T cells. Error bars are range, and values from individuals are imposed. Right panel, contour plots show the expression level of markers on $HBV_{core169}$-specific $CD8^+$ T cells between representative patients from different clinical stages. Patient groups are color coded as indicated. Statistical

significance was measured by non-parametric ANOVA to compare groups.

4.6. Diffusion map projects the cellular dynamics between exhaustion and memory

Next, we sought to address how the exhaustion and memory profiles of virus-specific T cell are altered over the course human chronic viral infection. As the temporal expression of cellular proteins is intrinsically imprinted in the timing of cellular programming, we took the major subsets of HBV_{pol387}- and $HBV_{core169}$-specific $CD8^+$ T cells from disease events across time and measure cellular transition by Diffusion Map (119). It computes all possible differentiation paths to reconstruct the cellular progression using diffusion distance. Strikingly, we found three distinct hypothetical cellular routes (here we refer to memory arm) branching from naïve cells to the nearly identical ends **(Fig. 25)**. Arm 2 seems to link to viral clearance as the $HBV_{core169}$-specific $CD8^+$ T cells of R and IA, and the C7 (IA) of HBV_{pol387}-specific $CD8^+$ T cells shared this trajectory. Contrarily, $HBV_{core169}$-specific $CD8^+$ T cells found in InA and most of the HBV_{pol387}-specific $CD8^+$ T cells populated arm 1. The two separated arms were emerged from naïve cells by the enriched C6 and C7 of HBV_{pol387}-specific $CD8^+$ T cells that had high memory profiles, whereas arm 3 was uniquely occupied by CMV_{pp65_1}- and IAV_{NPv2}-specific $CD8^+$ T cells **(Fig. 25A).** Building from Diffusion Map, we plotted the local expression of exhaustion- and memory-associated markers for each arm **(Fig. 26A)**. We found a profound asynchrony of inhibitory receptors in arm 2 compared to arm 1 and 3, who had closely synchronized expression of TIGIT and CD160 **(Fig. 26B)**. In addition, these oscillating inhibitory receptors interrelated to the differential expression of memory-associated markers, mainly contributed by CXCR3, CD45RO, CCR5, CD127 and KLRG-1. Taken together, our analysis hypothesizes a remarkable expression dynamic connecting exhaustion and memory manifolds between virus-specific cellular progression and HBV clinical stages.

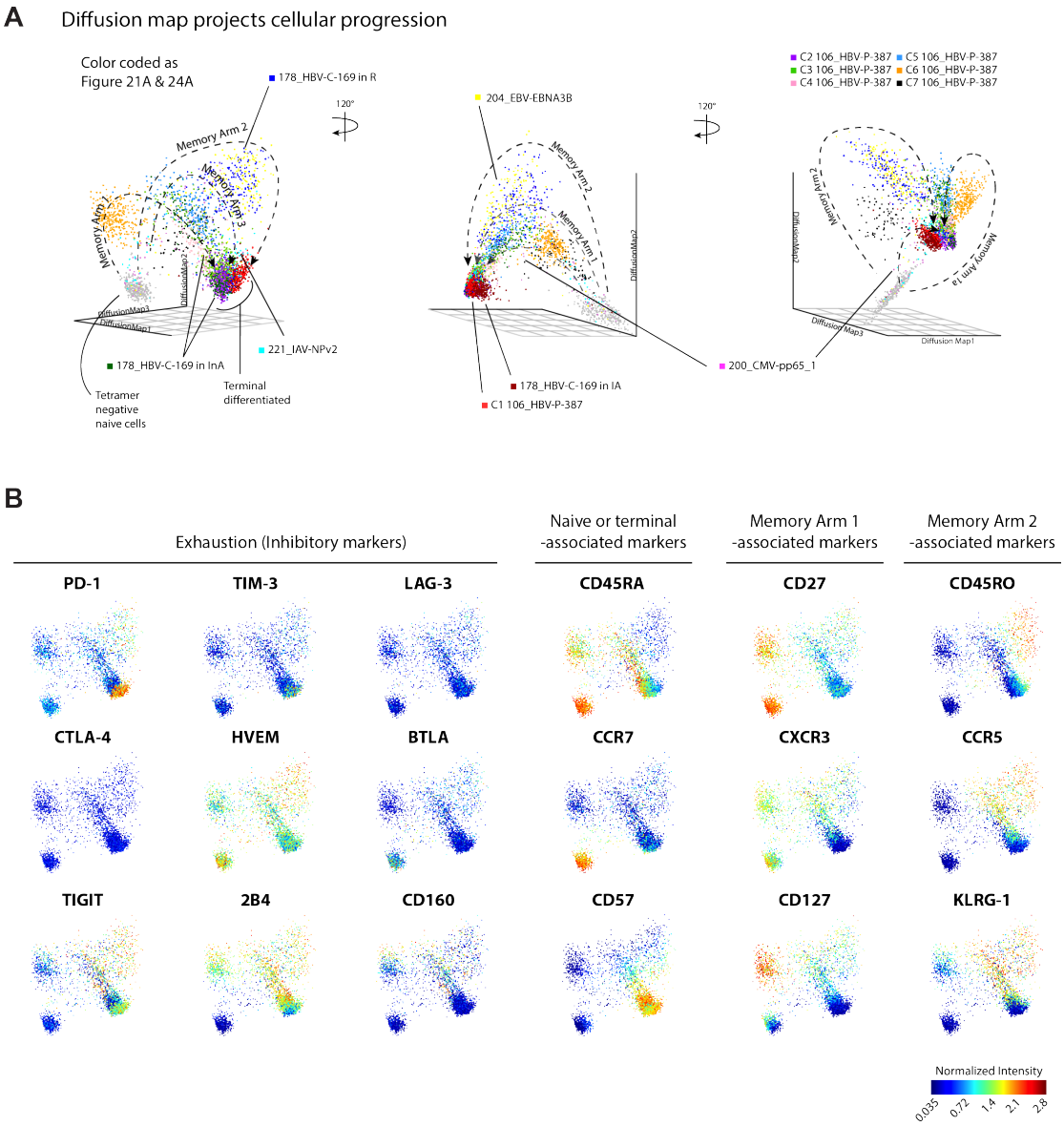

Figure 25. Putative trifurcation in 3D cellular trajectories of HBV_{pol387}- and $HBV_{core169}$-specific $CD8^+$ T cells using Diffusion map.

(A) Major cellular subsets of HBV_{pol387}- and $HBV_{core169}$-specific $CD8^+$ T cells identified by *t*-SNE (Fig. 21A and 24A) were analyzed by Diffusion map. 3D plots showed the distinct pathways of antigen-specific $CD8^+$ T cells. Different antigen-specific $CD8^+$ T cells were color-coded as shown. Naïve cells were gated on tetramer-, $CD45RA^+CCR7^+CD27^+KLRG\text{-}1^-CD57^-CD45RO^-$. (B) Plots from the same Diffusion map analysis displayed the various expression patterns of exhaustion- and memory-associated markers that linked to different trajectories.

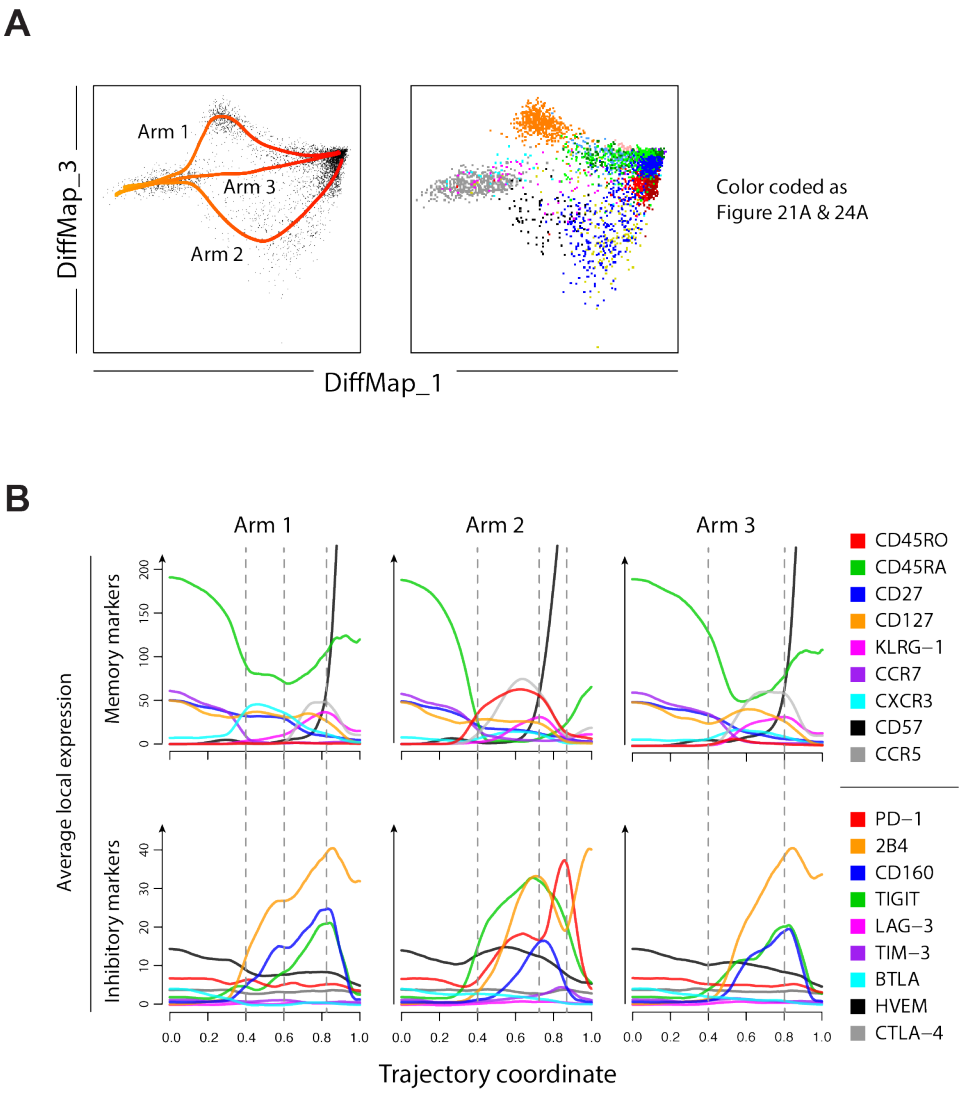

Figure 26. Asynchrony and oscillating expression of exhaustion- and memory-associated cellular proteins in each antigen-specific CD8$^+$ T cells trajectory.

(A) Three arms of Diffusion map trajectory were subjectively defined (left), and 100 nearest neighbor cells along each arm in three-dimensional space were included and calculated the average local expression of nine inhibitory receptors (related to Fig. 25A). Plot (right) was color-coded to indicate the various subsets of antigen-specific CD8$^+$ T cells. (B) The local expression of memory (upper)- and exhaustion (lower)-associated markers showed an asynchrony and oscillating expression pattern on each arm of trajectory.

4.7. HBV_{pol282}-specific $CD8^+$ T cells are pre-existing naïve precursor

The conserved but rare frequency of HBV_{pol282}-specific $CD8^+$ T cells across donors (144) **(Fig. 10A)** prompted us to further examine this epitope containing four previously unknown viral peptides. In conjunction with the previous observation in EBV and CMV (145), the pre-existing frequency of HBV_{pol282}-specific $CD8^+$ T cells was significantly higher in healthy CB than adult **(Fig. 10A)**. *t*-SNE further revealed a divergent naïve-like phenotype of cells specific for this epitope **(Fig. 27)**, suggesting they are virus-specific $CD8^+$ naïve precursors as described in other virus infections (145-147). Indeed, HCV-specific naïve precursors were observed in HCV-seronegative individuals and responsive to vaccination (147). Unlike in adult blood, HBV_{pol282}-specific $CD8^+$ T cells from cord blood were significantly located in a different *t*-SNE cluster that were reminiscent of naïve recent thymic emigrants (naïve RTE-like cells) and were $CD38^{hi}CXCR3^+CD127^+CD27^+CD95^+$. Importantly, the HBV_{pol282}-specific cells also expressed $TIM\text{-}3^+CD28^{hi}CD62L^{hi}CD49d^+$, which distinguishes them from the global $CD8^+$ T cells in cord blood. Adult blood-derived HBV_{pol282}-specific cells expressed $CD45RA^+CCR7^+CD28^+CD27^+$ $CD62L^+CXCR3^+CD95^-CD122^-$, which is a phenotype that is consistent with the previous described memory T cells with a naïve phenotype (T_{MNP}-like cells) (148). These cells were also distinct from the naïve RTE-like cells in that they conversely expressed $CD38^{lo}TIM\text{-}3^-BTLA^+CD160^+$. Intriguingly, the lower BTLA and CD160 (inhibitory ligands for HVEM) on HBV_{pol282}-specific $CD8^+$ T cells in cord compared with cells from adult blood might imply these cells are more prone to activation. Although we failed to observe significant phenotypic differences between HBV_{pol282}-specific $CD8^+$ T cells from CHB versus HD, we saw a trend toward to effector phenotype in CHB. Further experiments on this epitope to better characterize their phenotypic and functional differences in various clinical stages are needed. It is also therefore a great interest to

investigate this epitope during HBV infection from mother to infants (149-151).

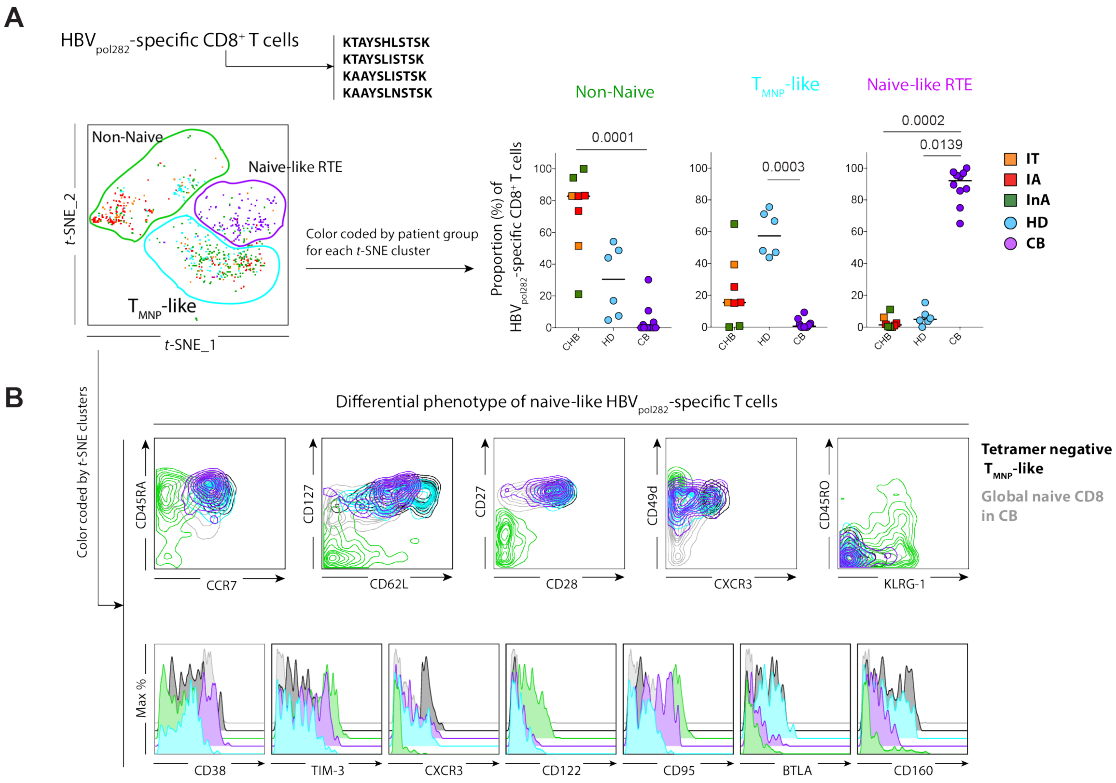

Figure 27. Naive-like HBV$_{pol282}$-specific CD8$^+$ T cells in adult and cord blood.

(A) *t*-SNE analysis showed a differential phenotypes of HBV$_{pol282}$-specific CD8$^+$ T cells between adult versus cord blood. Graphs (right) are the proportion of HBV$_{pol282}$-specific CD8$^+$ T cells from each individual located in three different *t*-SNE clusters. Clusters were color-coded as in *t*-SNE map. Individual dots were color-coded by patient groups. (B) Graphs were plots by total HBV$_{pol282}$-specific CD8$^+$ T cells inside each color-coded *t*-SNE cluster. Non-Naive, green. T$_{MNP}$-like, cyan. Naïve RTE-like, purple. Upper row showed the naive-like phenotype with CXCR3$^+$ of these subsets. Histograms (lower row) indicated the differential expression of cellular markers that separated these three subsets of HBV$_{pol282}$-specific CD8$^+$ T cells.

4.8. Nonlinear correlation of functional capacity and inhibitory receptors on virus-specific CD8$^+$ T cells

HBV is a non-cytopathic virus that however induces liver immunopathology due to the cytolytic immune response targeting infected hepatocytes. To address the functional capacity and the expressions of inhibitory receptors upon antigen recall, we pulsed patient's cells with the corresponded viral epitopes **(Fig. 12)**. Using three T cell categories, One-SENSE reconstructed virus-specific CD8$^+$ T cells into highly heterogeneous functional subsets defined by categorical analysis that can be visualized and labeled **(Fig. 28)**.

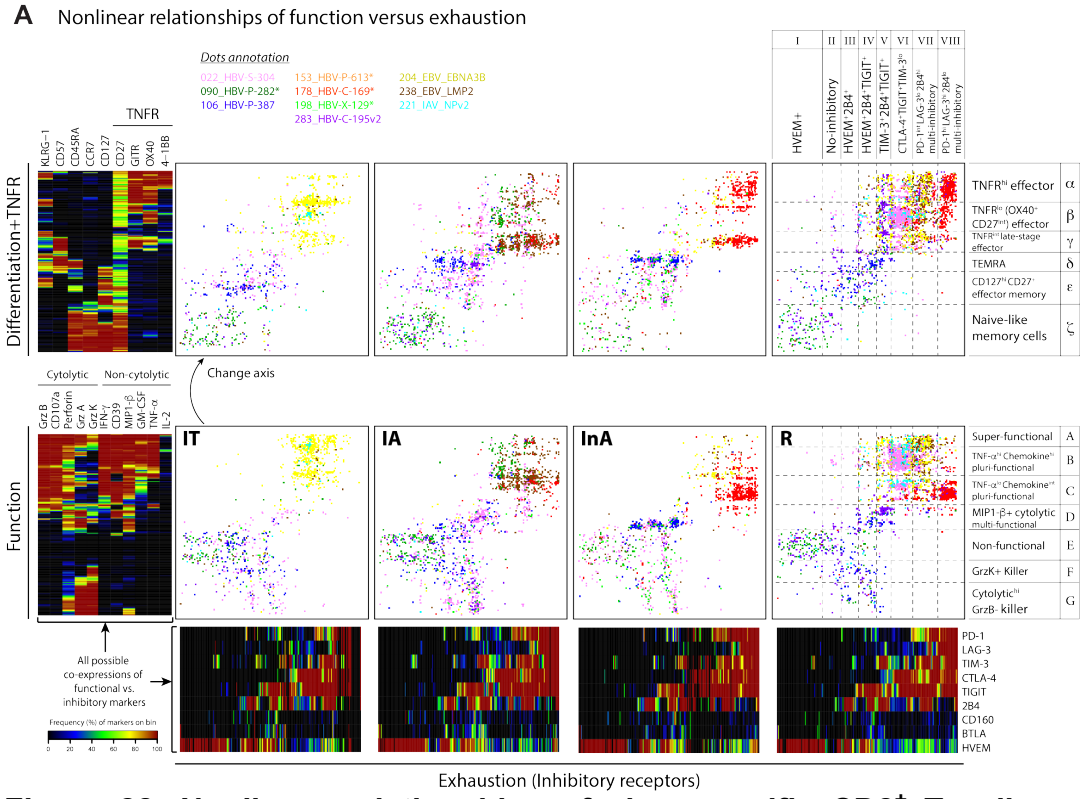

Figure 28. Nonlinear relationships of virus-specific CD8$^+$ T cells multi-functionality and inhibitory receptors by One-SENSE.

Patient's PBMCs across various clinical stages were pulsed by corresponded viral peptides for 10 days and intracellular cytokines staining (ICS) was performed. (A) One-SENSE composed of three T cell categories (Function, Exhaustion and Differentiation+TNFR) visualized the diverse multi-functional virus-specific CD8$^+$ T cells subsets , which corresponded to the different co-expressions of inhibitory receptors. Dots indicate each single virus-specific CD8$^+$ T cells as color-coded. The different subsets for each categorical dimension was manually labelled based on the aligned One-SENSE heatmaps.

Regardless of patient groups, the multi-functional subset (D) was contributed mainly by HBV_{pol387}-, $HBV_{core195}$- and HBV_{env304}-specific $CD8^+$ T cells expressing MIP-1β^+GrzA$^+$GrzK^{lo}Perforin$^+$ but CD107a^{lo} **(Fig. 28 and 29A),** indicating their low cytolytic activity. Surprisingly, we also found these cells in subsets of GrzA$^+$GrzK$^+$Perforin^{Int} (FG) without the secretion of degranulation marker CD107a, suggesting an alternative form of T_{EX} that were perhaps regulated by 2B4 and TIGIT but not PD-1 (III-V). Indeed, the co-expression of GrzA$^+$GrzK$^+$ was correlated with 2B4$^+$TIGIT$^+$ **(Fig. 28 and 29B)**. Adding to the dissimilar usages of inhibitory receptors, CD160 and HVEM were largely reduced on cells with effector functions by TCR stimulation. The sustained HVEM (I) was mostly expressed by the non-functional (E) subset of HBV_{pol282}-specific T_{MNP} **(Fig. 29B)**. Such naïve-like unresponsive T cells may present a different type of T cell dysfunctionality, perhaps contributed by their higher level of BTLA and CD160 prior to TCR stimulation **(Fig. 27)** (152, 153). We also found a dramatic expansion of HBV_{env304}-specific $CD8^+$ T cells upon peptide stimulation **(Fig. 12)**. Comparing to CHB, these cells from R had significant enrichment in pluri-functional subset (B) **(Fig. 29A and 30)** with IFN-γ^+TNF-α^{hi}MIP-1β^{hi}GM-CSF^{hi}, giving their non-cytolytic function and cell recruiting ability. Most similar to EBV- and IAV-specific $CD8^+$ T cells, HBV_{env304}-specific $CD8^+$ T cells were PD-1$^-$ LAG-3$^-$TIM-3^{lo} (VI). Moreover, $HBV_{core169}$-specific $CD8^+$ T cells were in the unique pluri-functional (C) region despite reciprocally expressed five inhibitory receptors including PD-1 **(Fig. 28)**. Remarkably, $HBV_{core169}$-specific $CD8^+$ T cells from R significantly co-producing various non-cytolytic functions (IFN-γ^+TNF-α^{lo}MIP-1β^+GM-CSF^{int}) (C) **(Fig. 29A and 30)** (21, 25) but low of Granzyme A and K **(Fig. 28-30)**. In addition, these cells exhibited high levels of TNFR costimulatory receptors (OX40, GITR, 4-1BB and CD27), suggesting the greater activation and memory status (154). However, the cells from IA had contrasting pattern of functional subset compared with patients of R, elevated in subset D but diminished in subset C **(Fig. 29)**. Evidenced jointly by our *ex vivo* profiling and *in vitro* functional data, and in line with previous *in vivo*

mouse model (155), we conclude this immunodominant A*11:01-restricted $HBV_{core169}$-specific $CD8^+$ T cells is the analogue of A*02:01-restricted $HBV_{core18-27}$-specific $CD8^+$ T cells who has therapeutic implication.

In general, our analysis displays complex orchestrations rather than a simple relationship between inhibitory receptors and functional capacity on virus-specific $CD8^+$ T cells upon antigen recall in CHB. Contrasting to the model of “Hierarchical T cell exhaustion”, such dysfunctionality was not entirely the consequence of the linear accumulation of inhibitory receptors, indicating these cells were not completely functional inert (63), and were retained to fulfill specialized functionality and viral control.

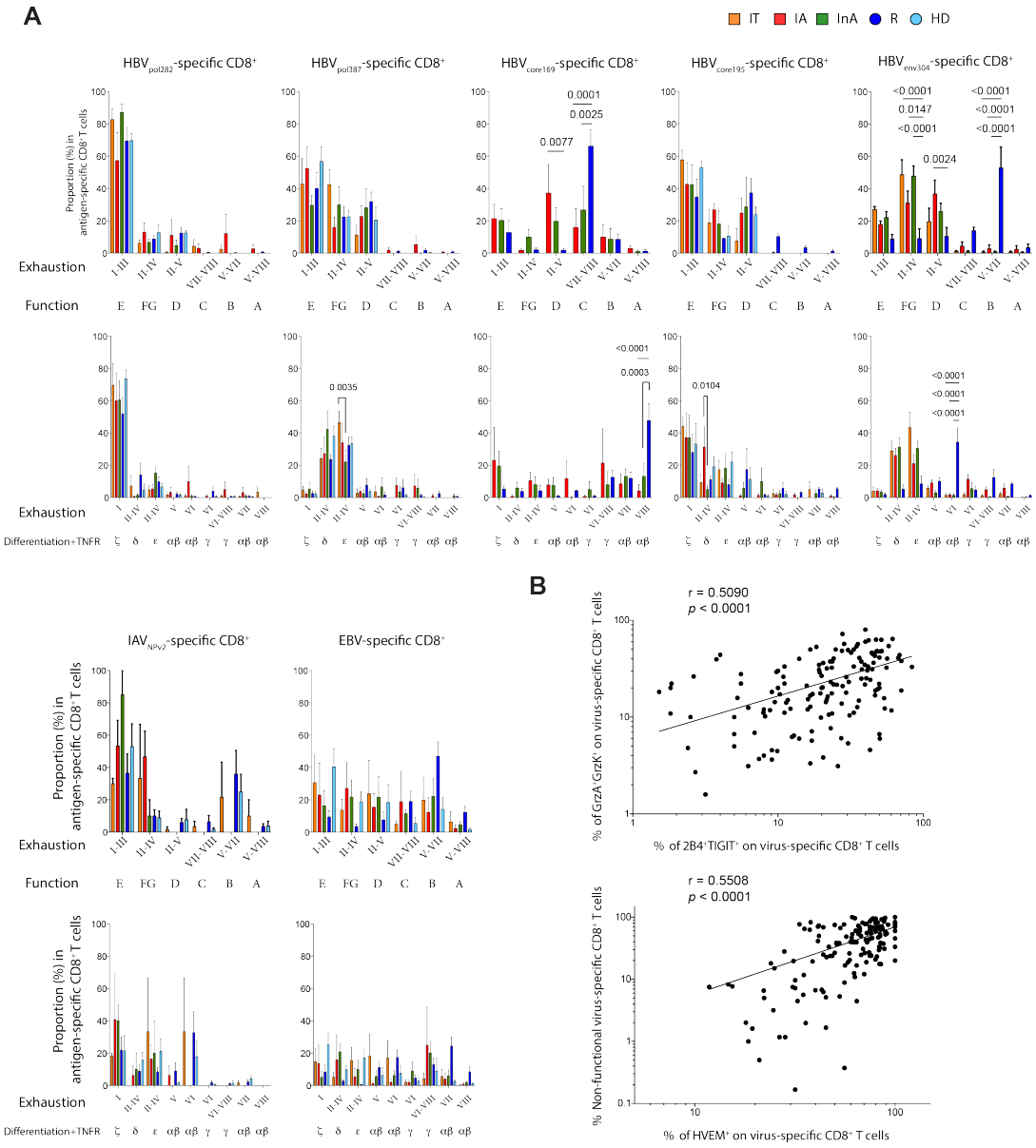

Figure 29. Highly heterogeneous multi-functional subsets of virus-specific CD8$^+$ T cells and their exhaustion and differentiation status after TCR-viral epitope engagement.

One-SENSE subsets were defined and labelled (Fig. 28) based on three different categorical dimensions and their co-expressing proteins. (A) Bar graphs show the proportion of each One-SENSE subset in different virus-specific CD8$^+$ T cells between various patient groups. Error bars indicate SEM. n=3~5 for each patient groups as color-coded. Statistic significances were determined by non-parametric ANOVA. (B) Cytolytic function of co-producing Granzyme A and K correlated to the co-expression of 2B4 and TIGIT on virus-specific CD8$^+$ T cells. Proportion of Non-functional (E) **(Fig. 28)** subset was connected to the maintaining expression of HVEM on virus-specific CD8$^+$ T cells. Dots were the different virus-specific CD8$^+$ T cells from different patients.

A

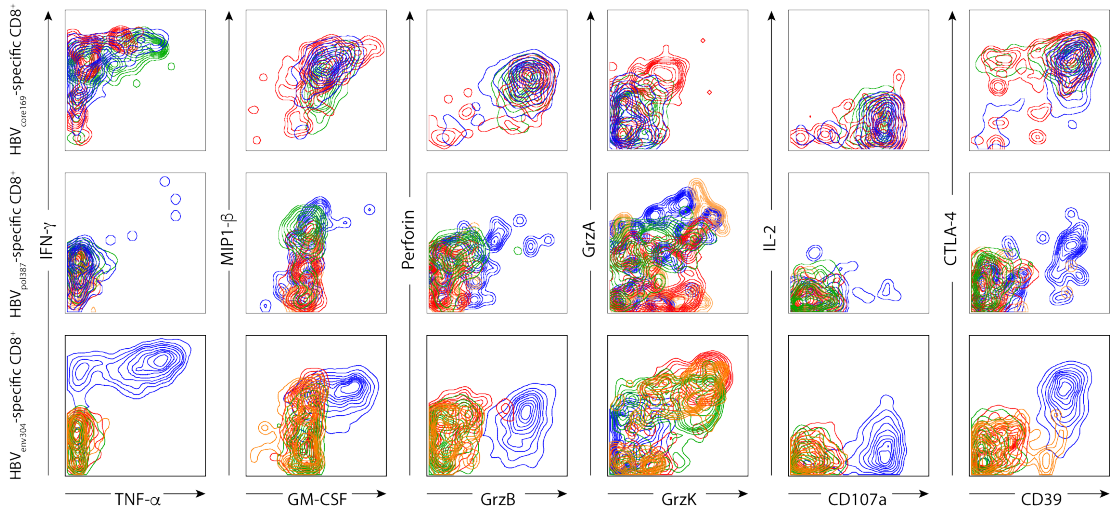

Figure 30. Multi-functionality of selected HBV-specific CD8$^+$ T cells.

(A) Representative contour plots of $HBV_{core169}$- (upper), HBV_{pol387}- (middle) and HBV_{env304}- (lower) specific CD8$^+$ T cells showed the heterogeneous multifunctionality in various patient groups. Related to Figure 28 and 29.

4.9. Diverse epitope-specific T cell receptor (TCR) spectratype linked to HBV clinical stages in an epitope dependent manner

The foundation of antiviral immunity is the recognition of viral epitopes by $CD8^+$ T cells through the presentation of peptide-major histocompatibility complex (pMHC). By interacting their $\alpha\beta$ T cell receptor (TCR) and pMHC, antigen-specific $CD8^+$ T cells can therefore identify infected cells and trigger effector function. TCR repertoire against various virus, such as HIV, CMV and IAV, has been intensely investigated in great detail (156, 157). However, many studies were focused on few dominant alleles such as those restricted by HLA-A*02:01, HLA-B*27 and HLA-B*57. How such TCR repertoire is selected over the continual viral antigen binding during human chronic HBV infection in the context of A*11:01 has not yet reported.

To understand the virus-specific TCR repertoire as it related to the status of chronic viral infection, we live-sorted **(Fig. 8B)** four selected A*11:01-restricted HBV-specific $CD8^+$ T cells, including HBV_{pol282}-, HBV_{pol387}-, $HBV_{core169}$- and $HBV_{core195}$-specific $CD8^+$ T cells, across various clinical stages. Epitope-specific TCRs were sequenced using next-generation sequencing (NGS) and analyzed based on IMGT/HighV QUEST (127) (International ImMunoGeneTics) nomenclature. We observed higher clonality of these sorted virus-specific $CD8^+$ T cells compared to total $CD8^+$ T cells from the same donors, which supported the quality of cell sorting **(Fig. 8B and Fig. 31A)**. Importantly, the three HD who were seemingly subclinically infected had overall higher degree of TCR repertoire diversity, distinguished them from ongoing HBV-infected patients in molecular level. Interestingly, the clonality of virus-specific TCR was associated with the observed frequency of $HBV_{core169}$-specific $CD8^+$ T cells, suggesting the selective expansion of T cell clonotypes during the course of CHB. In contrast to total $CD8^+$ T cells, the TCR repertoire from each virus-specific population was mainly

contributed by the top 3 TCR rearrangements besides patients from IT **(Fig. 31B)**.

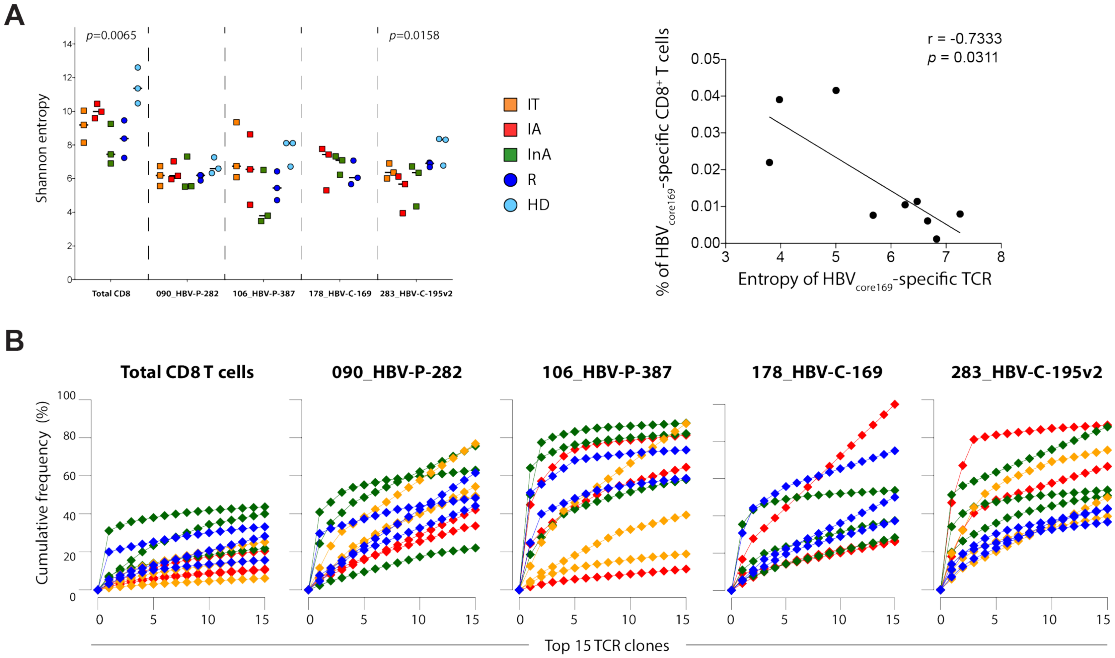

Figure 31. The clonality of T cell receptor (TCR) repertoire of selected HBV-specific CD8$^+$ T cells in epitope dependant manner.

(A) Shannon entropy was calculated for total CD8$^+$ T cells, HBV$_{pol282}$-, HBV$_{pol387}$-, HBV$_{core169}$- and HBV$_{core195}$-specific TCR and color-coded by patient groups. Each dot is one individual. The correlation between the frequency and TCR diversity of HBV$_{core169}$-specific CD8$^+$ T cell. (B) The accumulative frequency of top 15 TCR rearrangements for each population was shown. Each line is one individual.

Delving into the molecular level, we observed the diverse TCRβ V (Variable) and J (Joint) region segments usages of these HBV-specific $CD8^+$ T cells. Of note, the CDR3β of naïve-like HBV_{pol282}-specific $CD8^+$ T cells were uniquely paired by *TRBV05* gene as the top TCR Vβ usage **(Fig. 32),** which was not seen in other virus-specific $CD8^+$ T cells. This *TRBV05* from HBV_{pol282}-specific TCR was largely contributed by *TRBV05-01*, and diminished in patients from IA with different TCR characteristics, suggesting a functional non-redundant role of *TRBV05* in HBV_{pol282}-specific $CD8^+$ T cells. This lower frequency of *TRBV05* in IA might be related to the slight differences in HBV_{pol282}-specific $CD8^+$ T cell functionality that we observed upon antigen recall **(Fig. 29A)**. Besides the Vβ usage, HBV_{pol282}-specific $CD8^+$ T cells selectively used *TRBJ02-06*, instead of *TRBJ02-07,* which was the predominant Jβ segment in other epitope-specific TCR. Perhaps it attributed to their unique naïve precursor phenotype.

The highly individualized TCR repertoire can be observed in HBV_{pol387}-specific $CD8^+$ T cells, which may have been a reflection of their highly heterogeneous cellular phenotypes across different clinical stages **(Fig. 21)**. Indeed, we only plotted TCR rearrangements that were more than 1.5% for an accessible visualization. Therefore, many rare TCR rearrangements largely from IT (except one outlier from IT) and HD were not presented as they have more diverse TCR clonotypes, in contrast to other patient groups who had a more biased TCR repertoire of HBV_{pol387}-specific $CD8^+$ T cells **(Fig. 31B and 32)**. Interestingly, the particular homogeneous cellular phenotype of HBV_{pol387}-specific $CD8^+$ T cells from IT had a differential usage of *TRBV06-05* and *TRBJ01-06* **(Fig. 32 and 33A).** In line with the highly memory-like profile of HBV_{pol387}-specific $CD8^+$ T cells in IT and HD **(Fig. 21)**, and their closer position to the global naïve cells on Diffusion trajectory **(Fig. 25 and 26)**, this diverse TCR repertoire might suggest they were less differentiated with lower level of responsiveness during TCR-viral epitope engagement **(Fig. 12 and 29A)**. The peculiar but biased Vβ and Jβ pairing **(Fig. 32)** and the selective expansion of TCR clones **(Fig. 31)** of HBV_{pol387}-

specific TCR for IA and InA supported their highly heterogeneous effector phenotypes between individuals and patient groups **(Fig. 21)**, inferring a more committed effector and differentiated status.

We also found a preferential expansion of Vβ and Jβ usage in $HBV_{core169}$-specific TCR. Patients from InA and R had TCRs with biased usage of *TRBV09*, *TRBV07-08* and *TRBV06-01*, with the top 3 Jβ of *TRBJ02-07*, *TRBJ01-01* and *TRBJ01-06*. In addition, the characteristics of these different epitope-specific CDR3β lengths were largely dissimilar between patient groups but not in total $CD8^+$ T cells **(Fig. 32 and 33B)**. It has been reported that CMV-specific TCR exhibited preferential usages of a given Vβ gene that do not share between individuals and such massive repertoire is functionally redundant (158-162). In sharp contrast to IAV-specific TCR, which presented a more restricted Vβ usage and clonotypes in the context of A*02:01 (158, 163). Similar to our analysis, $HBV_{core169}$-specific response in InA and R that linked to viral suppression or clearance were biased towards the usage of only a few Vβ genes. Shared $HBV_{core169}$-specific TCR Vβ usages could also be found between individuals **(Fig. 32)**. These important features underline the epitope-specific TCR usages in persistent viral infection from acute viral infection. Surprisingly, significant differences in the frequencies of $HBV_{core195}$-specific TCRs using *TRBV06* were observed for IT and IA patients **(Fig. 32)**. This may be related to the similar pattern we observed in the frequencies of the same antigen-specific T cells across the same patient groups **(Fig. 10A).** Lastly, unlike the $HBV_{core195}$-specific TCRs in R having more diverse repertoire composed of various rearrangements **(Fig. 31B and 32),** $HBV_{core195}$-specific TCRs from InA were dominantly formed by *TRBV07* or *TRBV15* pairing with *TRBJ02-07*, or by *TRBV09* pairing with *TRBJ01-06*.

Figure 32. Distinct pairing of Vβ and Jβ gene segment and covariation in HBV epitope-specific TCR.

Circos plots display combinations of all V-J pairings (>1.5%) of four selected HBV epitope-specific T cell receptor. (A) Circos plots were

generated based on the individual TCR rearrangement for all patients in each group (n=3 per group). Outer circle is the ranked gene usages in proportion for each family (V and J). Red is V gene segment while blue is J gene segment. Inner circle showed the TCR rearrangements contributed to the use of this gene from each individual patient and color-coded as indicated. Bands are TCR rearrangements coming from the same or different patient using this particular V-J pairing. Band width indicates the productive frequency of each given TCR rearrangement. Selected V gene usages between different patient groups were shown to compare their TCR characteristics.

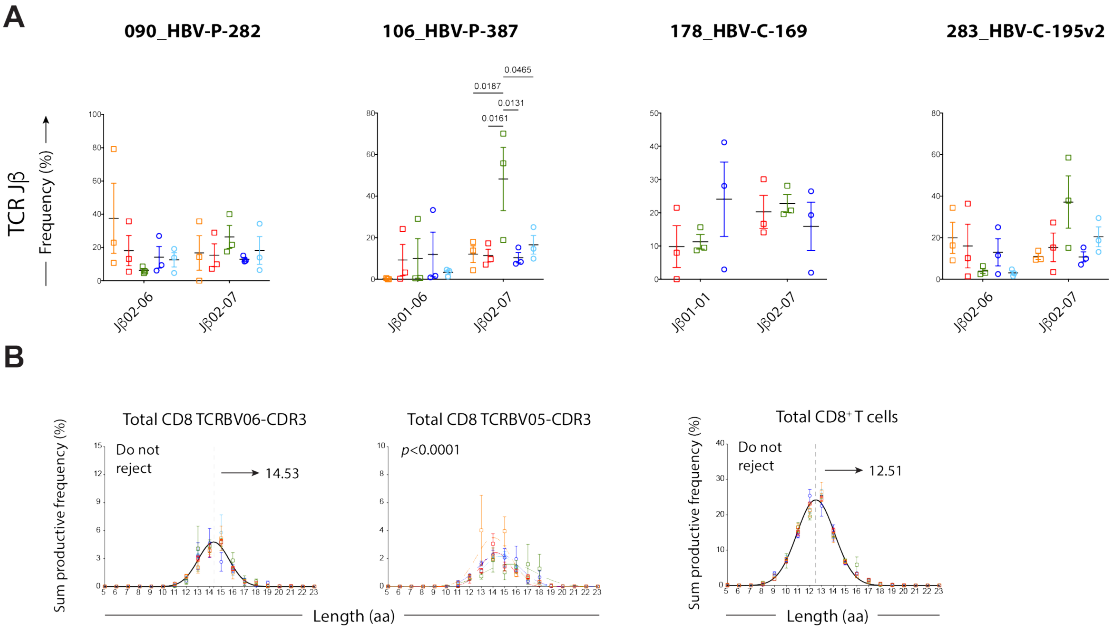

Figure 33. Distinct usage of Jβ in HBV epitope-specific TCR and the CDR3β characteristics of total CD8$^+$ T cells.

Related to Figure 32. (A) Selected J gene usages between different patient groups were shown. (B) The CDR3β characteristics of total CD8$^+$ T cells across various patient groups. Error bars are mean and SEM. Statistical analysis was calculated using Gaussian fit with the null hypothesis “one curve fits all groups”.

4.10. $HBV_{core169}$-specific public TCR clones and motif analysis linked to viral clearance

Next, we analyzed the CDR3β characteristics of these four HBV-specific TCR. Opposing to the uniformity of bulk TCR repertoire **(Fig. 33B)**, we found completely different characteristics of the length of CDR3β between epitope-specific TCRs across patient groups **(Fig. 34A)**. Interestingly, CDR3β in R had the most consistent distribution regardless of epitope specificity, while patients in high viremia (IT and IA) were in favor of larger size CDR3β varied between different epitopes **(Fig. 34A)**. In contrast, InA contained shorter epitope-specific TCRs besides in HBV_{pol387}-specific $CD8^+$ T cells. Such preferential utility of larger CDR3β in InA and IA may be associated with their heterogeneous and highly differentiated effector phenotype, whereas the near identical HBV_{pol387}-specific CDR3β characteristics between IT and HD is in agreement with their similar cellular phenotype **(Fig. 21)**. In addition, the significant differences we observed in other three epitope-specific TCR in HD again distinguished them apart from ongoing HBV infection as possible subclinical infection.

Focusing on the $HBV_{core169}$-specific response that linked to viral clearance, we performed multiple sequence alignment using (MUltiple Sequence Comparison by Log-Expectation (MUSCLE) (128, 129) to analyze the $HBV_{core169}$-specific TCR sequence motif that covered the most abundant region. Building from the different MUSCLE alignment, phylogeny trees were generated **(Fig. 34B)** to cluster the similar motifs for each particular length of CDR3β, and the sequences of major motif groups were presented using Sequence Logo **(Fig. 34C)** (131, 164). We found numerous conserved TCR in different motif groups, especially in the CDR3β length of 12 amino acids (aa) that was dominated by patients of InA **(Fig. 34A and B)**. Intriguingly, the $HBV_{core169}$-specific TCR rearrangements in this particular length was significantly expanded comparing to other size of TCR **(Fig. 34B and D)**. Most importantly, we identified several novel $HBV_{core169}$-specific public TCR clones (165) (or

recurrent clone) within four major motif groups that shared between individuals **(Fig 34B, C and E)**. In particular, a general public clone (CASGDSNSPLHF) was dominated as the top 3 TCRs in all InA **(Fig. 34E)**. Two special public clones (CASSGGQIVYEQYF and CSRAGGRGGDYTF) were also independently shared in two out of three InA. In addition, a special public TCR from the different motif group was observed in an acutely resolved patient. The presence of public TCR clones in InA and R but absence in IA that have fluctuating high viral load suggested $HBV_{core169}$-specific public TCR clones played a functional non-redundant role for viral control. Indeed, selective TCR clonotypes have been reported to mediate viral control in HCV (166), HIV (167) and SIV (168) infection. Compelling evidence in CMV-specific responses also showed high affinity TCR driven dominant clonotype selection during persistent antigen stimulation (161, 162), which is consistent with our observations on $HBV_{core169}$-specific $CD8^+$ T cells **(Fig. 23)**.

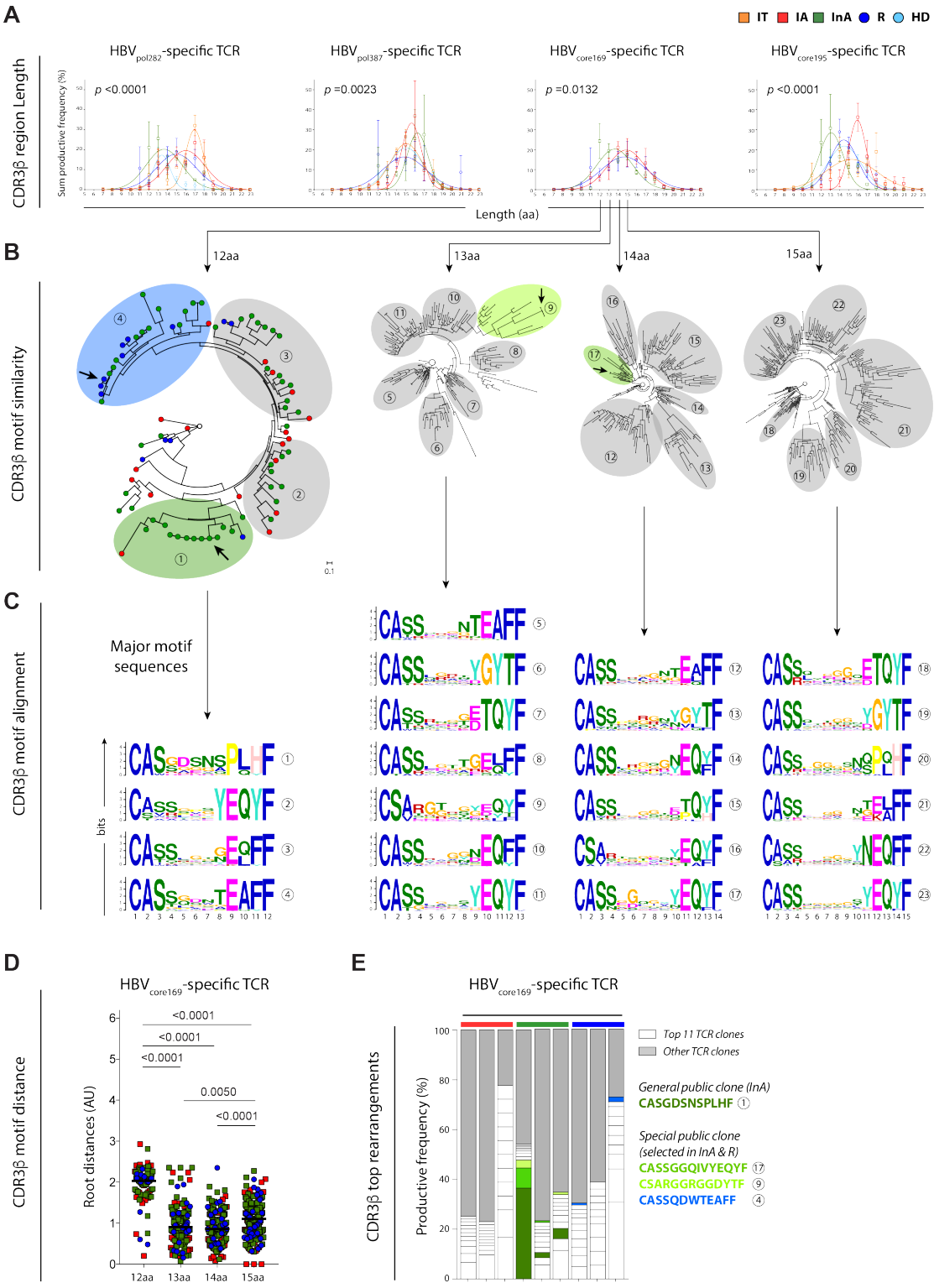

Figure 34. Epitope-specific TCR characteristics and motif analysis of HBV$_{core169}$-specific TCR reveal public clonotypes.

(A) The frequency of the CDR3β lengths for each epitope-specific TCR were calculated and plotted using Prism using Gaussian fit with the null hypothesis “one curve fits all groups”. The null hypothesis was rejected when there was statistical significance. Each curve was the different patients group as depicted. (B) HBV$_{core169}$-specific TCR sequences in

the most abundant CDR3β length (12aa to 15aa) were analyzed using MUSCLE alignment of Unipro UGENE platform, and the phylogeny trees for each length of TCR were constructed. Trees were presented in relative size as the distance legend shown. Each dot is one TCR rearrangement and color-coded but patient groups (12aa) as indicated. TCR motif groups (grey shaded) were arbitrarily defined based on the cluster of tree structure. Colored shades are the motif groups contained public TCR clones as arrow indicated. (C) The TCR rearrangements in each motif groups were further analyzed using The MEME Suite with the GLAM2 function to present the sequence logos. Numbers indicate the corresponded locations of phylogeny tree. Blue letters are hydrophobic amino acids. Greens are polar, non-charged, non-aliphatic. Purples are acidic. Reds are positively charged. (D) Arbitral root distances of TCR rearrangements for each phylogeny tree were calculated using Dendroscope. Statistical significances were determined by non-parametric ANOVA. (E) Stacked bar charts present the Top TCR clones in each individual from various patient groups. Frequency of public TCR clones were indicated, and their sequences were shown. The colors are coded as their corresponded sequences and motif groups in Figure 34B.

4.11. The presence of a HBV-specific conserved CDR3β motif is virus dependent

We further analyzed the TCR motif of the most abundant CDR3β length on HBV_{pol282}- **(Fig. 35)**, HBV_{pol387}- **(Fig. 36)** and $HBV_{core195}$-specific $CD8^+$ T cells **(Fig. 37)**. Diverse TCR motif structures were presented by Sequence Logo. Noteworthy, epitope-specific TCR in patient groups with high viremia (IT and IA) were mainly using longer CDR3β **(Fig. 34A)**, approximately 15aa to 17aa in length. Unlike $HBV_{core169}$-specific TCR which was dominantly expanded in the length of 12aa that associated with the public TCR motif and viral control, these three epitope-specific TCRs were significantly expanded for the larger TCR **(Fig. 35B)**, indicating their differential TCR usages that might attribute to the clinical stage.

Within the 17aa length of HBV_{pol282}-specific TCR, we were most fascinated by the increased numbers of TCR rearrangements who had very similar sequences in the same motif group (motif group 28) **(Fig. 35A)**. We then performed BLOcks SUbstitution Matrix (BLOSUM62) pair-wise comparison analysis for all sequences from this phylogeny tree and further digested it by Principal Component Analysis (PCA) **(Fig. 38A)**. Strikingly, PCA uniquely clustered this particular TCR motif away from all other sequences and unveiled a highly conserved motif of CASSXXXXQSRANVLTF (where X is any amino acid) with adjacent Jβ02-06 regardless of the Vβ usage **(Fig. 35A and 38)**. By searching for this conserved motif regardless of its length across all epitope-specific TCRs, we found a significant upregulation of this motif in HBV-specific TCRs in infected individuals **(Fig. 38B)**. Importantly, we neither saw the similar increments for the same epitope-specific TCR in HD that we postulated to have arisen due to subclinical infection nor from the total $CD8^+$ T cells population of both HBV-infected and HD groups. Furthermore, previous studies also reported no such TCR motif in A*11:01-restricted EBV-specific TCR (160, 169). This conserved TCR motif was significantly deployed by patients with high viremia (IT and IA)

or patients who had resolution of virus (R), suggesting this motif is virus dependent **(Fig. 38C)**. Thus, this particular CDR3β motif is highly conserved and likely selected for HBV-specific T cell response. Lastly, the majority of this motif were detected in 17aa to 18aa length and especially in naïve-like HBV_{pol282}-specific $CD8^+$ T cells. In concert with Yosef and colleagues, who recently reported that the naive-like memory YFV (Yellow Fever virus)-specific $CD8^+$ T cell population were significantly biased toward longer CDR3 lengths (170).

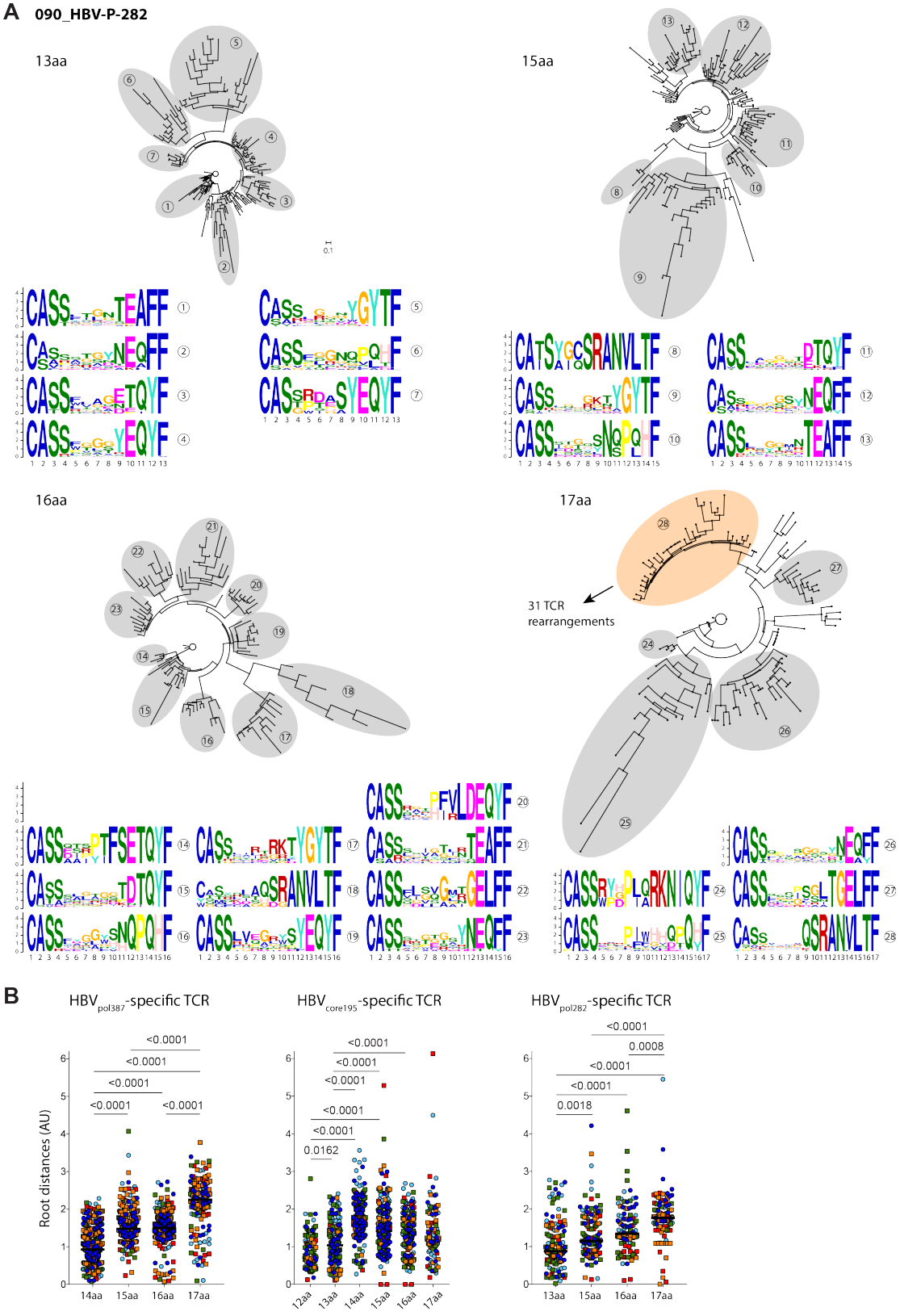

Figure 35. TCR motif analysis of HBV_{pol282}-specific $CD8^+$ T cells.

(A) The phylogeny trees of HBV_{pol282}-specific TCR were built from 13aa, 15aa, 16aa and 17aa CDR3β. Sequences for each TCR motif group were shown. Orange shaded is motif group 28 that contained 31 TCR

rearrangements with highly conserved TCR motif. (B) Arbitral root distances of TCR rearrangements for HBV_{pol282}-, HBV_{pol387}- and $HBV_{core195}$-specific TCR were calculated as in Figure 34D. Statistical significances were determined by non-parametric ANOVA.

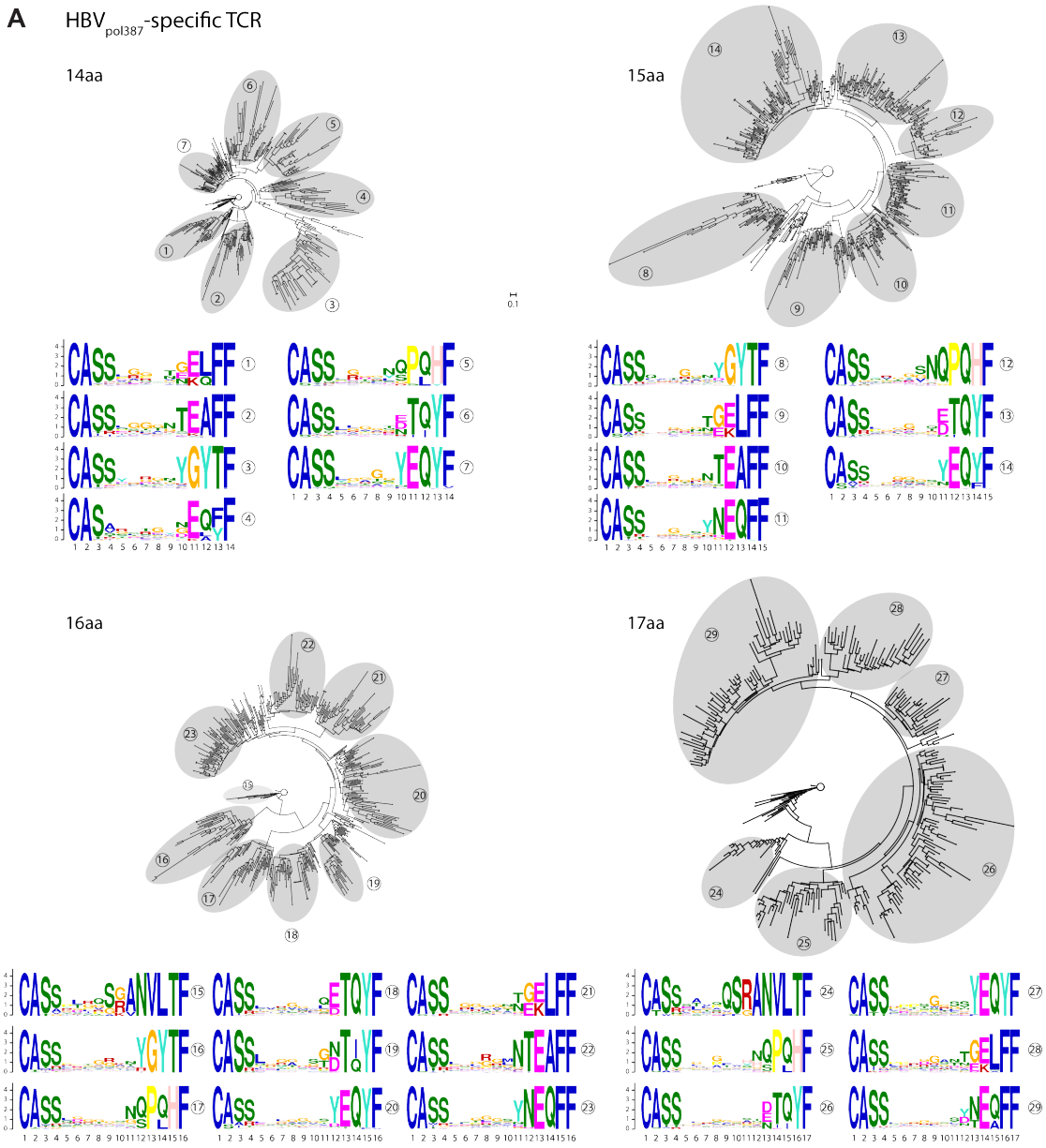

Figure 36. TCR motif analysis of HBV_{pol387}-specific $CD8^+$ T cells.

(A) The phylogeny trees of HBV_{pol387}-specific TCR were built from 14aa, 15aa, 16aa and 17aa CDR3β. Sequences for each TCR motif group were shown.

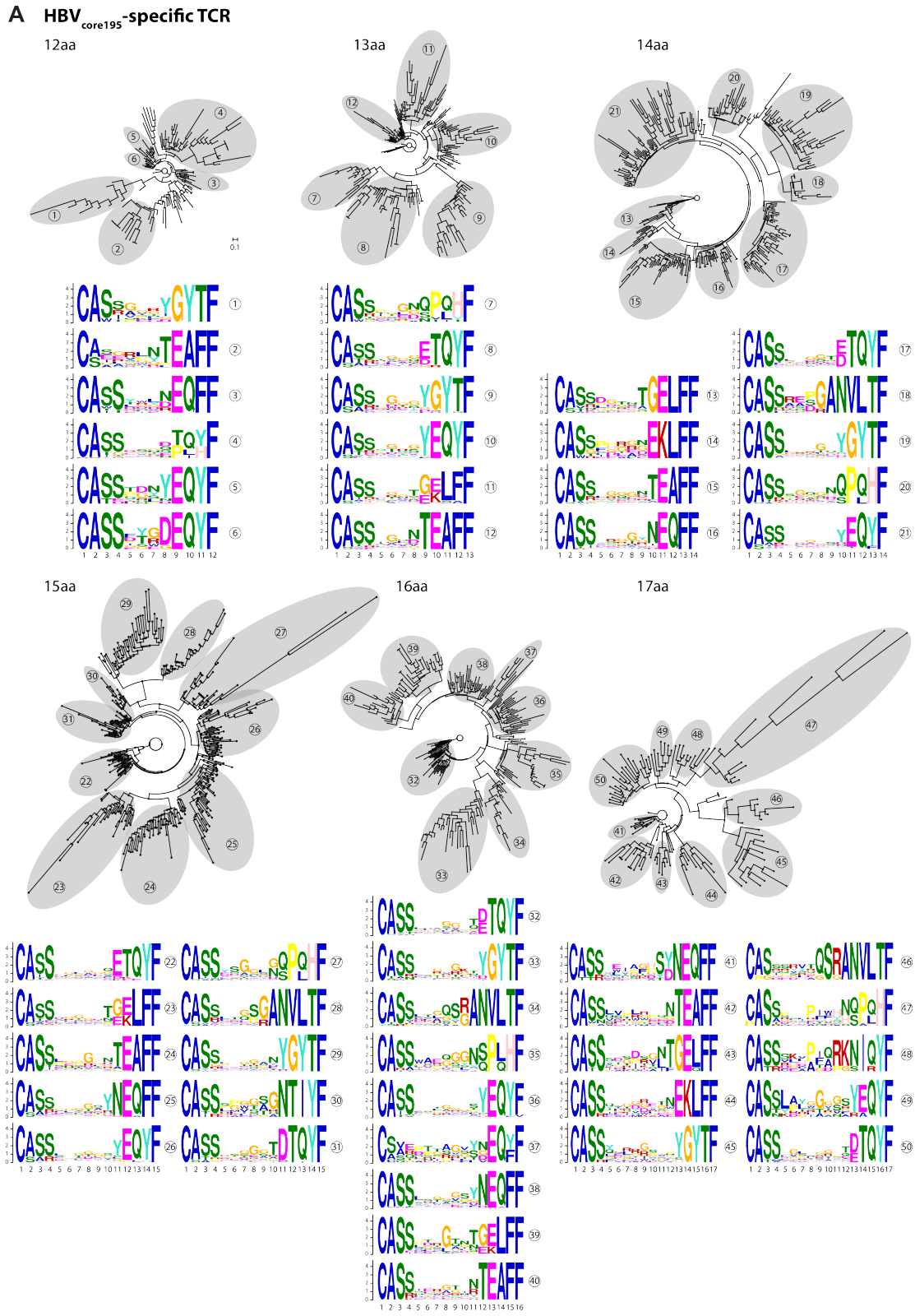

Figure 37. TCR motif analysis of HBV$_{core195}$-specific CD8$^+$ T cells.

(A) The phylogeny trees of HBV$_{core195}$-specific TCR were built from 12aa to 17aa CDR3β. Sequences for each TCR motif group were shown.

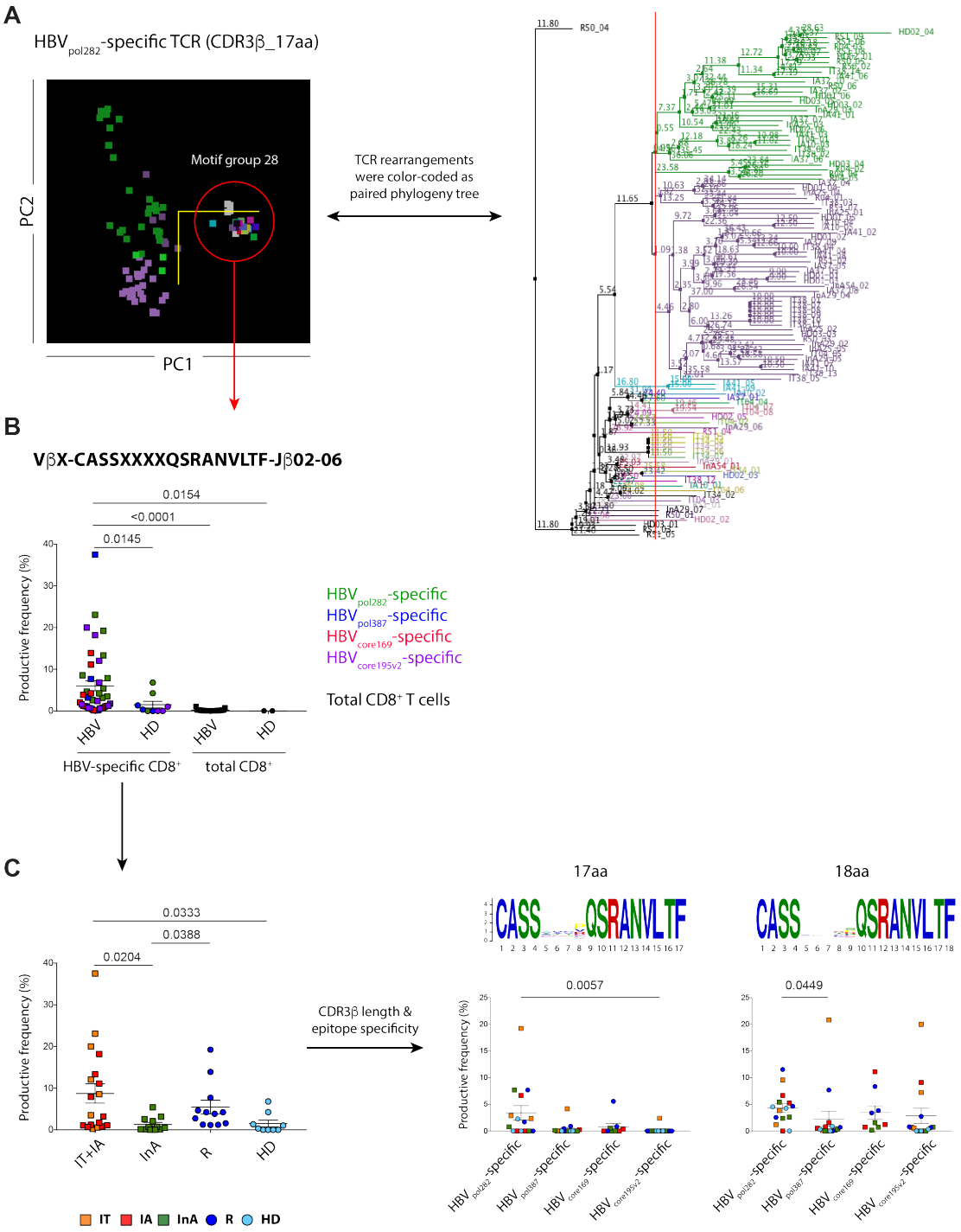

Figure 38. A virus dependent HBV-specific conserved CDR3β motif.

(A) HBV_{pol282}-specific TCR rearrangements of 17aa CDR3β were analyzed using BLOSUM62 algorithm in Jalview, a protein sequence alignment tool. TCR sequences were clustered using paired phylogeny tree and visualized in 3D PCA. (B) The composition of TCR motif group 28 was shown. Graph showed the frequency of this TCR motif in different epitope-specific TCR. Each dot is the given specificity (as color-coded) from each individual. HBV is HBV-infected individual. HD is healthy donor. Black dots are total $CD8^+$ T cells. (C) The frequency of this conserved TCR motif across various clinical stages regardless of

epitope specificity. The distribution of this motif in 17aa and 18aa CDR3β between different epitope specificities were shown. Each dot indicates an individual. The compositions for each length of CDR3β were presented. Statistical significances were determined by non-parametric ANOVA.

5. DISCUSSION

Together with a highly multiplexed combinatorial pMHC tetramer staining strategy, mass cytometry and bioinformatics, we have screened 484 unique HBV epitope candidates across the entire viral genome and variants in the context of HLA-A*11:01. High-dimensional analysis of several dominant epitope-specific T cells uncovered multifactorial exhaustion and memory manifolds that associated with the progression of chronic HBV infection. The nonlinear relationships of inhibitory receptors versus memory status and functional capacity of virus-specific T cells challenge the current notion of progressive and hierarchical loss of effector functions of T_{EX} during chronic viral infection. Our data showed a previously unappreciated level of heterogeneity of antigen-specific $CD8^+$ T cells making up the T cell response in various HBV clinical stages. Supported by the memory and functional phenotypes, we identified an immunodominant A*11:01-restricted $HBV_{core169}$-specific $CD8^+$ T cell population that appears to be the analogue of A*02:01-restricted $HBV_{core18-27}$-specific $CD8^+$ T cells linked to viral clearance with strong therapeutic potential. We also found several epitope-specific public TCR motifs that correlated with HBV infection and viral control. Here, this report unveiled the highly heterogeneity of virus-specific T cells from a broad spectrum of antigen specificity, memory and exhaustion profiles, functional capacity and TCR motif usage across the different events of disease, which have many therapeutic implications in targeting human chronic viral infection.

5.1. T cell response during the progression of HBV infection

Our report provides a new approach to circumvent the current obstacles to identify rare antigen-specific T cell populations, such as naïve-like memory T cells. Detection of HBV-specific T cells in chronic HBV patients has been very difficult due to the extremely low numbers

of cells that could be identified by traditional approaches, which are usually limited by the lack of broad specificity and a self-validated sensitivity. Such limitations were adding to the concerns and debates (171-173) on the terminology and interpretation of the different phases of HBV clinical stages.

Using multiple careful experimental and computational approaches, we identified several novel HBV epitopes. Importantly, these results were consistent throughout different experiment settings and patients, and further verified by flow cytometry. Although we detected several antigen-specific $CD8^+$ T cells in healthy donors, this is in line with previous works showing the standard serological measurement of anti-HBc antibody is insufficient to identify the subclinical infection in healthy individuals whose antigen-specific T cells were responsive to antigen recall (135, 136). While anti-HBs antibody provides protective effect, anti-HBc antibody status has been used as a marker that indicates prior as well as ongoing HBV infection. Extreme levels of anti-HBc response has been linked to acute liver damage (174, 175). In addition, the current available HBV vaccine only covers the S region of envelope protein (175), but not PreS1 who cooperates directly with the recent identified HBV entry protein sodium-taurocholate cotransporting polypeptide (NTCP) (176) to deliver infectivity. A recent survey of Taiwan cohort also showed a lower decline of HBV incidences than the expected vaccination efficacy (177). Such non-sterilizing immunity (135, 136) may explain the presence of HBV_{core}- and HBV_{pol}-specific $CD8^+$ T cells in some of the healthy donors we tested.

Conventional definitions of the different phases of CHB have lasted for decades since their first introduction. These definitions play a critical role in decision-making for the clinicians, such as identifying the different types of patients and the timing of intervention (3). However, recent arguments on using these definitions that are largely based on only few clinical parameters without direct immunological evidences is questionable and could delay early treatment opportunity (178).

Indeed, we detected comparable levels of virus-specificity and frequency regardless of patient groups, challenging the state of such Immune Tolerant (IT) and Immune Active (IA) controversy (149, 178). However, our data also showed unambiguous evidences of the differences in the features of these antigen-specific responses between groups in their phenotypic and TCR repertoires. For instance, the preferential usage of inhibitory receptors on different virus-specific $CD8^+$ T cells across patient groups, implying different states of T cell exhaustion and possible importance in choosing of checkpoint blockade strategies. Importantly, such asynchronous up- or down-regulation of inhibitory receptors correlated with the diverse expression of memory-associated markers, indicating the differential memory states of these virus-specific $CD8^+$ T cells. Furthermore, HBV_{pol387}-specific $CD8^+$ T cells in IT had similar low level of responsiveness as HD upon antigen recall compared with other patient groups who were significantly expanded. By sequencing the TCR of HBV_{pol387}-specific $CD8^+$ T cells, we saw similar patterns of CDR3β length between IT and HD, with higher diversity of their TCR usages. Taken together, this may suggest the HBV_{pol387}-specific $CD8^+$ T cells from IT were less committed and responsive, perhaps an alternative form of T_{EX} without expressing PD-1. Future experiments investigating their gene expression profiles and proliferation ability could help to better characterize the properties of this population. On the other hand, TCRs against other viral antigen showed dramatic variations across all patient groups in an epitope-dependent manner. Besides $HBV_{core169}$-specific $CD8^+$ T cells, we also observed low levels of multi-functionality of these virus-specific $CD8^+$ T cells regardless of the clinical stages. This indicates that these virus-specific $CD8^+$ T cells are not entirely functionally inert and may be retained for specialized function and viral control. In line with chronic LCMV infection, such virus-specific T_{EX} is essential in viral control, and removing this population was detrimental to the animals (59, 63). In general, by directly examining the ongoing T cell response across various clinical stages, the data we present here do not necessary support either concept in

redefining the different phases of CHB. However, it could lead to future studies in resolving this controversy.

By quantifying the intrahepatic A*02:01-restricted $HBV_{core18-27}$-specific $CD8^+$ T cells, Maini et al (22) found the similar magnitude of these cells between patients of IA and InA. The report suggested that $HBV_{core18-27}$-specific $CD8^+$ T cells in the liver of IA patients were able to recruit large infiltration of non-virus-specific $CD8^+$ T cells into HBV-infected liver, and such global T cells response may contribute to liver damage and inflammation. It could be perhaps supported by our observation that A*11:01-restricted $HBV_{core169}$-specific $CD8^+$ T cells produced several immune cells-recruiting chemokines including MIP1-β and GM-CSF, and these cells were able to secrete cytolytic functions (GrzA, GrzK and CD107a) in patients of IA. As the pathogenesis in HBV-infected liver has been considered immune mediated (179), future investigation on intrahepatic A*11:01-restricted virus-specific versus global $CD8^+$ T cells during the progression of CHB is needed.

5.2. T cell exhaustion or functional adaption?

T cells dysfunctionality can be categorized into T cell anergy, T cell exhaustion, and T cell senescence (63, 180). While they share similar dysfunctionality with partial overlapping cellular phenotypes, the underlying molecular mechanism and cellular programming are largely distinct, and may play diverse roles in the different context of disease. It has been widely known that T cell activation requires three signals including the TCR-pMHC formation, costimulation of CD28-CD80/86 axis and the autocrine IL-2 production. Anergic T cells often develop in responses to incomplete activation with low IL-2 production or lack of costimulatory signals from the B7 family (180, 181). These long-lived anergic T cells are in a hyporesponsive state that provides peripheral tolerance in different autoimmune diseases. Unlike the anergic T cells that associate with inappropriate T cell priming, T_{EX} cells arise from fully functional memory T cells (59) that however develop exhaustion

phenotypes through the continuous antigen stimulation (49, 50, 182). A hallmark of T cell exhaustion is the upregulation of multiple inhibitory receptors that linked to a progressive loss of T cell functionality (50, 63), which usually observed in chronic viral infection and tumor microenvironment. Importantly, T_{EX} are not completely functional inert and provide critical viral control, and removing such population from chronic LCMV-infected mice resulted in detrimental effect (63). On the contrary, T cell senescence (180, 183) is mainly described in the elders or CMV-infected individuals (184). The shorten telomere length and the expression of several markers associated with terminal differentiation such as CD57 and KLRG-1 mark the difference of senescent T cells from the other types of T cell dysfunctionality (180, 183, 185).

Inspired by the murine LCMV model, targeting the T_{EX}-associated inhibitory receptors, or so-called “exhaustion markers”, have drawn enormous attention. Studies and trials based on a range of diseases have revealed the extraordinary therapeutic potential and physiological mechanisms of antagonizing such coinhibitory pathways. However, inconsistent definitions of T cell exhaustion raise questions of generality of this cellular phenotype in a natural chronic viral infection. Using bimodal expression of one or two inhibitory receptors to define T_{EX} is insufficient. As we mentioned above, many reports have addressed the diversified usages of inhibitory receptors on virus-specific T cells during human chronic viral infection. Taking the advantage of One-SENSE that objectively visualized the co-expressing inhibitory receptors (63) on a wide array of HBV epitopes, we proposed a complex “Nonlinear T cell exhaustion” instead of “Hierarchical T cell exhaustion” endorsed by murine LCMV system.

The lack of small animal models and the difficult accessibility of non-human primate have been one of the obstacles in HBV research. To date, many have been introduced but none have been universally accepted as relevant. Furthermore, inconsistent data between transgenic mice and CHB patients have been also reported (1, 175, 178). Similar to HBV, a murine model of LCMV can both trigger acute

(Armstrong) or chronic (Clone 13) infection. Pioneered by Oldstone (51, 186, 187), and further established by Ahmed and Wherry (50, 52, 188), intense studies on LCMV as a classic model for chronic viral infection have advanced our understanding in chronic viral infection and drawn substantial implications. For instance, to restore the functionality of T_{EX} using PD-1 blockade in LCMV (60), HIV (58), HCV (79) and HBV (26, 27, 29). However, how many implications can be translated into human chronic HBV infection has been a major conundrum. Firstly, unlike the natural HBV infection which usually starts with very low viral load, the mice have to receive immense amount of LCMV Clone 13 (2×10^6 PFU) to successfully establish chronic viral infection. The different outcomes between vertical- and horizontal-transmission of HBV also cannot be simulated by the intravenous or intraperitoneal infection in LCMV. Lastly, HBV is a non-cytolytic highly hepatotropic virus while LCMV infects the host systematically.

During chronic LCMV infection, GP_{33}-specific $CD8^+$ T cells were maintained overtime while NP_{396}-specific $CD8^+$ T cells were largely deleted (47, 48) due to the higher avidity of NP_{396} epitope (189). In line with our observation, $HBV_{core169}$-specific $CD8^+$ T cells who has the highest tetramer intensity were entirely absence in IT patients. However, we found step-wise increased of these cells in both frequency and tetramer intensity after the disease progressed into later clinical stages (IA and InA). This suggests that these cells could be largely but not completely deleted in early phase of IT that have high viral load, and later expand possibly due to the viral mutation or the changes of immune homeostasis.

By comprehensively and simultaneously investigating hundreds of HBV-specific $CD8^+$ T cells with nine major inhibitory receptors, we showed a previously unappreciated degree of heterogeneity of virus-specific T_{EX}. Taking the advantage of One-SENSE that objectively displays all possible combinations of the co-expressing inhibitory receptors, our results challenges the current model of hierarchical T cell exhaustion endorsed by the LCMV system. Dissimilar to the previous

data showing a linear accumulation of multiple inhibitory receptors of T_{EX} in LCMV (77), our data indicates a more complex model. For instance, the non-mutually exclusive expression of CD160 and TIGIT had a very distinct pattern compared to the expression of PD-1. While most of the virus-specific effector or memory cells upregulated 2B4, naïve-like virus-specific $CD8^+$ T cells expressed HVEM (152) and low levels of BTLA, which may be associated with their naïve-like phenotype. The discrepancies on T cell subsets have also been addressed in peripheral (54), or intrahepatic (83) lymphocytes in CHB. Interestingly, we observed a higher complexity between the T cell functionality and exhaustion after TCR-viral epitope engagement. Opposing to the elevation of CTLA-4, LAG-3 and TIM-3 upon TCR stimulation, CD160 and HVEM were downregulated on cells who had increased effector functions. Together with their diverse correlations with cytolytic and non-cytolytic functionality, it implies the selective usages between these inhibitory receptors may relate to their TCR signalling and functional capacity. In line with previous works in LCMV (90, 91), the upregulation of PD-1 were only seen on virus-specific $CD8^+$ T cells who had higher tetramer intensity ($HBV_{core169}$- and EBV-specific T cells) before and after TCR stimulation, providing further evidence that the upregulation of PD-1 is the consequence of continual viral antigen binding and also a sign of T cell activation. Notably, these virus-specific cells were responsive and at least produced certain level of multi-functionality.

Combining both *ex vivo* and *in vitro* profiling across several dominant HBV epitopes, we failed to identify any particular subset that possessed all inhibitory receptors, and their differential co-expressions were not necessary linearly accumulated on dysfunctional or terminally differentiated T cells. This underscores the remarkable heterogeneity of $CD8^+$ T cells and suggests that diverse usages of inhibitory receptors are both epitope- and clinical stage-dependent. Indeed, T_{EX} requires continual antigen stimulation for survival and maintaining the virus-specific T cells pool during chronic viral infection (182). Our *in vitro* system cannot fully simulate the T_{EX} response *in vivo* during chronic

HBV infection and this needs to be further addressed. For instance, whether the upregulation of inhibitory receptors are transient or sustained *in vivo* in CHB could help to identify the bona fide T_{EX} (63).

As a valuable target in boosting T cell response in chronic viral infection, T_{EX} can be rescued to produce effector functions depending on the cellular and transcriptional heterogeneity. For instance, T-bet^{hi}Eomes^{lo} T_{EX} expressing PD-1^{Int} exhibited low intrinsic turnover but were proliferated and responsive to anti-PD-1 (57, 63). However, when viral antigen persisted, this subset gave rise to the terminal progeny of T-bet^{lo}Eomes^{hi} T_{EX} that expressed high level of PD-1, and such T_{EX} cannot be reinvigorated by PD-1 blockade. Similar heterogeneous expressions of transcriptional factors in exhausted CD8$^+$ T cells has also been reported in HCV, HIV and HBV (57, 190, 191). Furthermore, epigenetic analysis showed that this PD-1^{hi} T_{EX} acquired a stable epigenetic profiles differing from the effector and memory T cells (61). Importantly, PD-L1 blockade had limited effect on these cells in the epigenetic landscape, suggesting a committed T cell lineage. Recent studies also indicated a cell-intrinsic requirement of CD28 to reinvigorate T_{EX} upon the treatment of PD-1 blockade in chronic LCMV infection and non-small-cell lung carcinoma (NSCLC) (192, 193), and such T cell response may be TCF1-mediated (194, 195).

One reasonable explanation to the T_{EX} complexity is the phenomenon during chronic viral infection is a state of T cell functional adaption rather than exhaustion. Zehn and colleagues (196) recently proposed that such T_{EX} phenotype is tuned to minimize the tissue damage while maintaining essential immune response to keep invading pathogens in check. As HBV is a non-cytolytic virus, the liver inflammation that later leads to liver damage is most likely due to the cytolytic immune response targeting infected hepatocytes, which is termed immunopathology. This is evidenced by our data showing the low multifunctionality and non-cytolytic pluri-functionality of virus-specific CD8$^+$ T cells in IT and InA, respectively. Whereas patients in IA who have elevated liver inflammation had significant higher cytolytic multi-

functional virus-specific $CD8^+$ T cells. Perhaps the existence of the functional T_{EX} during CHB was purposely employed to confer viral control and immune homeostasis while limiting immunopathology by expressing inhibitory receptors as a functional feedback loop.

5.3. Nonlinear T cell functionality and inhibitory receptors

Isogawa et al. (21) addressed the asynchronous kinetic of HBV-specific $CD8^+$ T cells during T cell expansion and contraction phase. Adoptive transfer experiments suggested the non-cytolytic IFN-γ-producing $CD8^+$ T cells induced in the early phase upon antigen recognition was inversely related to the cytolytic Granzyme B-producing $CD8^+$ T cells that occurred on day 5 post antigen stimulation. Noteworthy, in line with the observation of LCMV Clone 13-induced T cell exhaustion (197), the usages of TCRs was neither changed prior nor post the adoptive transfer (21, 197). Indeed, the inflammation and the repetitive antigen recognition in the liver environment could alter the antigen sensitivity of T cell (198) and interrupt the sequential oscillating cycle of effector $CD8^+$ T that is critical for antiviral effector function (21). This could be argued by the fluctuating viral load and ALT level seen in patients of Immune Active phase, which usually leads to more severe clinical disease symptoms. Through the coupling of different disease phases across time and putative cellular differentiation projection, we reconstructed similar asynchrony in the expression of PD-1 and the co-expression of 2B4 and TIGIT. The latter was correlated with strong cytolytic functions after re-stimulation of the cells with corresponded viral peptide. HVEM, BTLA and CD160 that belong to the Tumor Necrosis Factor superfamily of receptors (TNFR) had different expression patterns related to naïve-like or effector memory phenotypes. Such reciprocal but partially opposing usages of these inhibitory receptors may be critical in control of various cytolytic and non-cytolytic functions that dictates HBV-associated immunopathology.

Our data showed that complexity in the profiles of co-expression of multi-functionality and inhibitory receptors were neither mutually exclusive nor inclusively expressed by certain $CD8^+$ T cell subsets. Most importantly, these cells were not functional inert and may be able to restore higher level of multi-functionality by different combinations of blockade strategies. The dysfunctionality of HBV-specific $CD8^+$ T cells we observed had both some similar and dissimilar properties when compared to LCMV. It has been shown that the downregulated IL-2 and TNF-α can be achieved by minimum expression of PD-1, whereas the intermediate level of PD-1 was sufficient to dampen the production of IFN-γ (199). However, it needs the highest amount of PD-1 to observe significant reduction of MIP-1β. Although there were similar trends, where IL-2 and TNF-α only expressed on higher level of pluri-functional HBV-specific $CD8^+$ T cells, and most of the subsets including the low level multi-functional subsets can produce MIP-1β. We found no such functionality was reduced in a linear manner. Instead, a complex mixture of functional capacities that may deliver cytolytic or non-cytolytic T cell response across clinical phases were observed.

5.4. Naïve-like virus-specific $CD8^+$ T cells

We identified a novel naïve-like HBV_{pol282}-specific $CD8^+$ T cells across patient groups and a surprising elevation in healthy cord blood donors, suggesting these cells are pre-existing naïve precursors. Similarly conserved frequencies across individuals regardless of infection status have also been reported (146), such as $HIV_{gag\ p17\ 77\text{-}85}$, $HCV_{NS3\ 1406\text{-}1415}$, $HCV_{core132\text{-}140}$ and $CMV_{pp65\ 495\text{-}503}$. Several studies also showed the HCV-specific naïve precursor can be detected in healthy individuals, and the dominant frequency against the same epitope was found in chronic HCV patients (200, 201). Although we failed to see significant increases or changes of phenotypes of these cells across the different clinical stages likely due to the size of patient cohort, they were nonetheless responsive with lower level of functionality upon antigen

recall. Comparing to healthy donors, the trend we observed in CHB patients toward to effector phenotype might suggest the possible distinct immune response of these HBV_{pol282}-specific $CD8^+$ T cells during the chronic HBV infection. Perhaps their functional capacity can be further boosted by the co-blockade of BTLA and CD160.

Previous quantification has estimated the frequency of LCMV-specific $CD8^+$ T cells naïve precursor to be 1 in 2×10^5 cells (144), and such naïve precursors were largely expanded upon viral infection. Indeed, the exposure of LCMV during embryonic life did not result a permanent deletion of virus-specific T cells, and these cells can be regenerated upon secondary challenge to protect the host (150). It has been recently shown that the fetal immune system is functional in early stage of gestation (151), and the HBV exposure in utero did not completely silence the newborn's immunity (149). Future longitudinal study on HBV vertical-transmission from mother to infant may be important to address the key features of antigen-specific naïve precursor in chronic HBV infection.

5.5. Immunodominant virus-specific $CD8^+$ T cells in viral control

Two decades ago, Bertoletti et al identified an immunodominant A*02:01-restricted HBV_{c18-27}-specific $CD8^+$ T cells that associated with viral clearance (20). It opened a new avenue for the research of adaptive immunity in the field of HBV. Given the extreme difficulty in detecting antigen-specific T cells in chronic HBV infection, many studies have focused on this epitope to advanced our understanding of HBV-specific immune response. Many therapeutic opportunities targeting adaptive immune responses have been therefore developed. However, such approaches are not eligible to patients who do not have this particular HLA alleles (202), especially in regions of high HBV prevalence, such as Asia and Africa.

Here, we identified $HBV_{core169}$-specific $CD8^+$ T cells and their association with viral control in the context of A*11:01. By thoroughly characterizing the memory phenotypes, expression of inhibitory receptors, functional capacity and epitope-specific TCR repertoire across various HBV clinical stages, we confirm here that the A*11:01-restricted $HBV_{core169}$-specific $CD8^+$ T cells is the analogue of A*02:01-restricted HBV_{c18-27}-specific $CD8^+$ T cells. We have summarized the similarity of their T cell response in **Table 3**. Overall, these $HBV_{core169}$-specific $CD8^+$ T cells expressed high PD-1 (26, 27, 38), high frequency in patients with improved clinical outcomes (24, 33, 34, 37, 39) but absence in patients with high viral load (22, 24, 26, 39), elevated level of IL-7Rα (CD127) (26, 34) in inactive carriers and acute resolved patients and produced several antiviral effector functions (24, 26, 27, 33, 34). By probing a broad spectrum of cellular proteins, we explored a more complicated virus-specific heterogeneity that governs the progression of chronic HBV infection. Conjointly with the putative differentiation trajectory, our functional data was also in agreement with the previous *in vivo* experiments showing that the oscillation of PD-1 and effector function of HBV-specific $CD8^+$ T cells was correlated with viral clearance

as the result of antigen recognition (21). It is noteworthy that patients in Immune Active category does not necessary mean the higher activity of immune response, as we observed differential cytolytic functionality but not superior when compared to inactive carriers. Thus, this term may be inappropriate and misleading.

Lastly, the upregulation of various TNFR costimulatory receptors coincided with other inhibitory receptors on $HBV_{core169}$-specific $CD8^+$ T cells upon antigen recall and suggests that their functional capacity could be further enhanced by combining an agonist and blockade therapeutic regiment. This discovery may have implications in the development of T cell based interventions as have been introduced in the context of A*02:01 (40, 41). Finally, it also implies the possible existence of such immunodominant HBV epitope targeting by other HLA alleles.

Features	*A0201-HBVcore18-27 CD8 T cells*	*A1101-HBVcore169 CD8 T cells*
Significant upregulated PD-1 expression	Boni et al 2007 JVI Schurich et al 2011 Hepatology Evans et al 2008 Hepatology	***Yes*** Higher expression compared to other HBV epitopes, and mostly in IA and R (viral clearance with ongoing liver inflammation)
Strong response in patients group associated with imrpoved clinical outcome (e.g. InA & R)	Boni et al 2007 JVI Bertoletti et al 1994 JEM Bertoni et al 1997 JCI Boni et al 2001 Hepatology Reignat et al 2002 JEM Webster et al 2004 JVI Boettler et al 2006 JVI	***Yes*** Higher frequency in InA and R patients
Transiently observed in CHB wih very low frequency	Boni et al 2007 JVI Bertoletti et al 1994 JEM Maini et al 2000 JEM Webster et al 2004 JVI	***Yes*** Limited/no in IT (high viral load, low liver inflammation), transient in IA
Higher memory profile of T cells (e.g. CD127 & CD27) in acute resovled patients compared to CHB	Boni et al 2007 JVI Boettler et al 2006 JVI	***Yes*** Plus other memory associated markers, such as CXCR3, CD28 and CD45RO in InA & R with differential expression level Versus CD57 in IA
Functional capacity expressing IFN-γ	Boni et al 2007 JVI Boettler et al 2006 JVI Schurich et al 2011 Hepatology Reignat et al 2002 JEM Webster et al 2004 JVI	**Yes** Producing IFN-γ with higher level of pluri-functionality in InA and R, Lower in IA with different cytolytic functional profile Huang et al 2016 Scientific Reports

Table 3. Comparison of A*11:01-restricted $HBV_{core169}$-specific and A*02:01-restricted $HBV_{core18-27}$-specific $CD8^+$ T cells from literatures.

5.6. Epitope-specific T cell receptor repertoire during viral infection

We sequenced four selected epitope-specific TCRs against HBV and found epitope-dependent biased TCR repertoire that varied individually. Most strikingly, several public TCR clones were shared on $HBV_{core169}$-specific $CD8^+$ T cells in patients with improved clinical outcomes, similar to their memory and functional profiles. We also identified a unique HBV-specific CDR3β sequence motif that was viral dependent, and its usage was linked to virus-specific naïve precursors.

Elegant experiments by Nikolich-Zugich and colleagues have shown that a polymorphic MHC H-2^{bm8} selected a broader HSV-8p-specific TCR repertoire than H-$2K^b$ and conferred greater protection to the host (203, 204). However, we observed a more diverse TCR repertoire in HBV_{pol387}-specific TCR for patients during Immune Tolerant phase with less responsive phenotypes, while the same epitope-specific TCRs had biased usage in inactive carriers and Immune Active patients that may connect to their more differentiated phenotypes. Furthermore, the public $HBV_{core169}$-specific TCRs were only found in patients associated with viral clearance but not in patients with high viral load and liver inflammation. It has been reported that public TCR clones can be seen in both highly diverse or skewed TCR repertoires (158, 165). Indeed, virus-specific public TCRs have been reported and widely studied in IAV, CMV and EBV (165). Significant clonal expansions of EBV-specific TCRs can also dominate in circulation for at least 18 years (205). This might pinpoint the different nature of chronic HBV infection, which elicits complicated progressions across all levels of clinical stages over decades. Perhaps, the continuous HBV epitope binding by T cells actively select the preferential TCR in the liver that can best provide viral control without causing immunopathology. This is supported by the observation that $HBV_{core169}$-specific $CD8^+$ T cells are capable of secreting multiple non-cytolytic functions such as IFN-γ, TNF-α and MIP-1β.

During the acute phase of viral infection, virus-specific T cells greatly expand and become capable of various effector functions. These cells then further develop into memory cells during the contraction phase after the elimination of virus (206). The public virus-specific TCR clones might be generated during viral clearance by selecting the clonotypes from a broad repertoire that were heavily contracted. It may explain the observation of $HBV_{core169}$-specific $CD8^+$ T cells in InA and R who significantly upregulated memory-associated markers, indicating their long-live and self-renewing ability. In conjunction with primary CMV and EBV infection (161, 207), virus-specific $CD8^+$ T cells do not express IL-7Rα (CD127) until T cell memory has been established. Furthermore, similar to $HBV_{core169}$-specific $CD8^+$ T cells, such CMV-specific TCR selection was driven by high affinity TCR-viral epitope binding (161). The public TCR clones have also been described against the same viral epitopes (158, 165). Importantly, intrahepatic and peripheral public TCR clones have been associated with viral clearance in HCV-infected chimpanzees (208). Future longitudinal studies on patients who undergo HBeAg-seroconversion could help to address the selection of virus-specific TCRs and their correlation with T cell memory and exhaustion status.

We were intrigued by an HBV-specific TCR motif that was conserved across all HBV-infected patients, but not healthy donors. These highly conserved sequences were only four amino acid differences between all detected TCR rearrangements. Surprisingly, it has preferential usage of Jβ02-06 regardless of Vβ segments. We did not find any similar TCR motif across different infectious disease or cancer by matching the sequence using a recently developed curated TCR database (209). Given that this virally dependent motif was mostly observed in HBV_{pol282}-specific $CD8^+$ T cells, we speculated the usage of this specific TCR might correlate to the naïve-like T cell phenotype and its lower responsiveness. Perhaps, it is an alternative form of T cell anergy by seizing TCR binding and retaining the T cell in a naïve-like

state. It is a great interest to investigate these particular virus-specific $CD8^+$ T cells and their TCR usage in infected infants in this manner.

Often time, the mutation of viral epitopes can lead to viral escape and therefore undermine T cell immune response. It has been shown that the mutation on A*02:01-restricted $HBV_{core18-27}$ epitope reduced the antiviral effector function by antagonizing TCR recognition (39). Attesting by HCV-infected chimpanzees, viral epitope mutation reduced the TCR repertoire diversity during chronic viral infection (208). The selective expansion of particular TCR clonotypes may benefit the patients in viral control and contribute to HBeAg-seroconversion (From IA to InA), by maintaining strong immune surveillance to keep virus in check. However, due to a significant part of TCR pool were committed to the wild type epitope, such biased TCR usage could be detrimental when virus mutated, and further leads to the reactivation events (3). This may support the notion that reactivation in CHB usually results a dramatic and severe liver damage.

6. CONCLUSION

We have demonstrated an integrated approach to map T cell epitope comprehensively against a single HLA allele and virus, by combining viral sequencing and computational prediction, highly multiplex combinatorial pMHC tetramer strategy, self-validated bioinformatics and mass cytometry. We not only identified several dominant viral epitope but also thoroughly characterized the virus-specific T cell phenotype. The high-dimensional exhaustion and memory T cell manifolds highlights the diverse cellular program across different clinical stages of chronic HBV infection. Together with the epitope-specific TCRs, our data also showed a previous unappreciated degree of T cell heterogeneity that relates to disease progression. Such highly diverse relationship between virus-specific inhibitory receptors and functionality challenge the current model of hierarchical T cell exhaustion. Our report opens new avenues in the investigation of T cell responses during human chronic viral infection and may have many implications in the understanding of virus-specific immune response and the development of T cell based therapeutics.

7. REFERENCES

1. Maini, M. K., and A. Bertoletti. 2017. HBV in 2016: Global and immunotherapeutic insights into hepatitis B. *Nat Rev Gastroenterol Hepatol* 14: 71-72.
2. Bertoletti, A., and C. Ferrari. 2012. Innate and adaptive immune responses in chronic hepatitis B virus infections: towards restoration of immune control of viral infection. *Gut* 61: 1754-1764.
3. Rehermann, B., and M. Nascimbeni. 2005. Immunology of hepatitis B virus and hepatitis C virus infection. *Nature reviews. Immunology* 5: 215-229.
4. Shin, E. C., P. S. Sung, and S. H. Park. 2016. Immune responses and immunopathology in acute and chronic viral hepatitis. *Nat Rev Immunol* 16: 509-523.
5. Diepolder, H. M., R. Zachoval, R. M. Hoffmann, E. A. Wierenga, T. Santantonio, M. C. Jung, D. Eichenlaub, and G. R. Pape. 1995. Possible mechanism involving T-lymphocyte response to non-structural protein 3 in viral clearance in acute hepatitis C virus infection. *Lancet* 346: 1006-1007.
6. Ferrari, C., A. Penna, A. Bertoletti, A. Valli, A. D. Antoni, T. Giuberti, A. Cavalli, M. A. Petit, and F. Fiaccadori. 1990. Cellular immune response to hepatitis B virus-encoded antigens in acute and chronic hepatitis B virus infection. *Journal of immunology* 145: 3442-3449.
7. Lechner, F., D. K. Wong, P. R. Dunbar, R. Chapman, R. T. Chung, P. Dohrenwend, G. Robbins, R. Phillips, P. Klenerman, and B. D. Walker. 2000. Analysis of successful immune responses in persons infected with hepatitis C virus. *The Journal of experimental medicine* 191: 1499-1512.
8. Rehermann, B., P. Fowler, J. Sidney, J. Person, A. Redeker, M. Brown, B. Moss, A. Sette, and F. V. Chisari. 1995. The cytotoxic T lymphocyte response to multiple hepatitis B virus polymerase epitopes during and after acute viral hepatitis. *The Journal of experimental medicine* 181: 1047-1058.
9. Thimme, R., D. Oldach, K. M. Chang, C. Steiger, S. C. Ray, and F. V. Chisari. 2001. Determinants of viral clearance and persistence during acute hepatitis C virus infection. *The Journal of experimental medicine* 194: 1395-1406.
10. Wedemeyer, H., X. S. He, M. Nascimbeni, A. R. Davis, H. B. Greenberg, J. H. Hoofnagle, T. J. Liang, H. Alter, and B. Rehermann. 2002. Impaired effector function of hepatitis C virus-specific CD8+ T cells in chronic hepatitis C virus infection. *Journal of immunology* 169: 3447-3458.
11. Chang, M. L., and Y. F. Liaw. 2014. Hepatitis B flares in chronic hepatitis B: pathogenesis, natural course, and management. *J Hepatol* 61: 1407-1417.
12. Lim, S. G., C. T. Wai, A. Rajnakova, T. Kajiji, and R. Guan. 2002. Fatal hepatitis B reactivation following discontinuation of nucleoside analogues for chronic hepatitis B. *Gut* 51: 597-599.

13. Bauer, T., M. Sprinzl, and U. Protzer. 2011. Immune control of hepatitis B virus. *Dig Dis* 29: 423-433.
14. Liaw, Y. F., and C. M. Chu. 2009. Hepatitis B virus infection. *Lancet* 373: 582-592.
15. European Association for the Study of the Liver. Electronic address, e. e. e., and L. European Association for the Study of the. 2017. EASL 2017 Clinical Practice Guidelines on the management of hepatitis B virus infection. *J Hepatol*.
16. Liaw, Y. F., N. Leung, J. H. Kao, T. Piratvisuth, E. Gane, K. H. Han, R. Guan, G. K. Lau, and S. Locarnini. 2008. Asian-Pacific consensus statement on the management of chronic hepatitis B: a 2008 update. *Hepatol Int* 2: 263-283.
17. Bertoletti, A., and M. Hong. 2014. Age-Dependent Immune Events during HBV Infection from Birth to Adulthood: An Alternative Interpretation. *Front Immunol* 5: 441.
18. Kennedy, P. T., E. Sandalova, J. Jo, U. Gill, I. Ushiro-Lumb, A. T. Tan, S. Naik, G. R. Foster, and A. Bertoletti. 2012. Preserved T-cell function in children and young adults with immune-tolerant chronic hepatitis B. *Gastroenterology* 143: 637-645.
19. Thimme, R., S. Wieland, C. Steiger, J. Ghrayeb, K. A. Reimann, R. H. Purcell, and F. V. Chisari. 2003. CD8(+) T cells mediate viral clearance and disease pathogenesis during acute hepatitis B virus infection. *Journal of virology* 77: 68-76.
20. Bertoletti, A., A. Sette, F. V. Chisari, A. Penna, M. Levrero, M. De Carli, F. Fiaccadori, and C. Ferrari. 1994. Natural variants of cytotoxic epitopes are T-cell receptor antagonists for antiviral cytotoxic T cells. *Nature* 369: 407-410.
21. Isogawa, M., Y. Furuichi, and F. V. Chisari. 2005. Oscillating CD8(+) T cell effector functions after antigen recognition in the liver. *Immunity* 23: 53-63.
22. Maini, M. K., C. Boni, C. K. Lee, J. R. Larrubia, S. Reignat, G. S. Ogg, A. S. King, J. Herberg, R. Gilson, A. Alisa, R. Williams, D. Vergani, N. V. Naoumov, C. Ferrari, and A. Bertoletti. 2000. The role of virus-specific CD8(+) cells in liver damage and viral control during persistent hepatitis B virus infection. *The Journal of experimental medicine* 191: 1269-1280.
23. Maini, M. K., C. Boni, G. S. Ogg, A. S. King, S. Reignat, C. K. Lee, J. R. Larrubia, G. J. Webster, A. J. McMichael, C. Ferrari, R. Williams, D. Vergani, and A. Bertoletti. 1999. Direct ex vivo analysis of hepatitis B virus-specific CD8(+) T cells associated with the control of infection. *Gastroenterology* 117: 1386-1396.
24. Webster, G. J., S. Reignat, D. Brown, G. S. Ogg, L. Jones, S. L. Seneviratne, R. Williams, G. Dusheiko, and A. Bertoletti. 2004. Longitudinal analysis of CD8+ T cells specific for structural and nonstructural hepatitis B virus proteins in patients with chronic hepatitis B: implications for immunotherapy. *Journal of virology* 78: 5707-5719.

25. Guidotti, L. G., R. Rochford, J. Chung, M. Shapiro, R. Purcell, and F. V. Chisari. 1999. Viral clearance without destruction of infected cells during acute HBV infection. *Science* 284: 825-829.
26. Boni, C., P. Fisicaro, C. Valdatta, B. Amadei, P. Di Vincenzo, T. Giuberti, D. Laccabue, A. Zerbini, A. Cavalli, G. Missale, A. Bertoletti, and C. Ferrari. 2007. Characterization of hepatitis B virus (HBV)-specific T-cell dysfunction in chronic HBV infection. *J Virol* 81: 4215-4225.
27. Schurich, A., P. Khanna, A. R. Lopes, K. J. Han, D. Peppa, L. Micco, G. Nebbia, P. T. Kennedy, A. M. Geretti, G. Dusheiko, and M. K. Maini. 2011. Role of the coinhibitory receptor cytotoxic T lymphocyte antigen-4 on apoptosis-Prone CD8 T cells in persistent hepatitis B virus infection. *Hepatology* 53: 1494-1503.
28. Das, A., M. Hoare, N. Davies, A. R. Lopes, C. Dunn, P. T. Kennedy, G. Alexander, H. Finney, A. Lawson, F. J. Plunkett, A. Bertoletti, A. N. Akbar, and M. K. Maini. 2008. Functional skewing of the global CD8 T cell population in chronic hepatitis B virus infection. *The Journal of experimental medicine* 205: 2111-2124.
29. Nebbia, G., D. Peppa, A. Schurich, P. Khanna, H. D. Singh, Y. Cheng, W. Rosenberg, G. Dusheiko, R. Gilson, J. ChinAleong, P. Kennedy, and M. K. Maini. 2012. Upregulation of the Tim-3/galectin-9 pathway of T cell exhaustion in chronic hepatitis B virus infection. *PloS one* 7: e47648.
30. Bengsch, B., B. Martin, and R. Thimme. 2014. Restoration of HBV-specific CD8+ T-cell function by PD-1 blockade in inactive carrier patients is linked to T-cell differentiation. *Journal of hepatology*.
31. Lopes, A. R., P. Kellam, A. Das, C. Dunn, A. Kwan, J. Turner, D. Peppa, R. J. Gilson, A. Gehring, A. Bertoletti, and M. K. Maini. 2008. Bim-mediated deletion of antigen-specific CD8 T cells in patients unable to control HBV infection. *The Journal of clinical investigation* 118: 1835-1845.
32. Schurich, A., L. J. Pallett, D. Jajbhay, J. Wijngaarden, I. Otano, U. S. Gill, N. Hansi, P. T. Kennedy, E. Nastouli, R. Gilson, C. Frezza, S. M. Henson, and M. K. Maini. 2016. Distinct Metabolic Requirements of Exhausted and Functional Virus-Specific CD8 T Cells in the Same Host. *Cell Rep* 16: 1243-1252.
33. Reignat, S., G. J. Webster, D. Brown, G. S. Ogg, A. King, S. L. Seneviratne, G. Dusheiko, R. Williams, M. K. Maini, and A. Bertoletti. 2002. Escaping high viral load exhaustion: CD8 cells with altered tetramer binding in chronic hepatitis B virus infection. *The Journal of experimental medicine* 195: 1089-1101.
34. Boettler, T., E. Panther, B. Bengsch, N. Nazarova, H. C. Spangenberg, H. E. Blum, and R. Thimme. 2006. Expression of the interleukin-7 receptor alpha chain (CD127) on virus-specific CD8+ T cells identifies functionally and phenotypically defined memory T cells during acute resolving hepatitis B virus infection. *Journal of virology* 80: 3532-3540.

35. Altman, J. D., P. A. Moss, P. J. Goulder, D. H. Barouch, M. G. McHeyzer-Williams, J. I. Bell, A. J. McMichael, and M. M. Davis. 1996. Phenotypic analysis of antigen-specific T lymphocytes. *Science* 274: 94-96.
36. Doherty, P. C., and J. P. Christensen. 2000. Accessing complexity: the dynamics of virus-specific T cell responses. *Annu Rev Immunol* 18: 561-592.
37. Bertoni, R., J. Sidney, P. Fowler, R. W. Chesnut, F. V. Chisari, and A. Sette. 1997. Human histocompatibility leukocyte antigen-binding supermotifs predict broadly cross-reactive cytotoxic T lymphocyte responses in patients with acute hepatitis. *J Clin Invest* 100: 503-513.
38. Evans, A., A. Riva, H. Cooksley, S. Phillips, S. Puranik, A. Nathwani, S. Brett, S. Chokshi, and N. V. Naoumov. 2008. Programmed death 1 expression during antiviral treatment of chronic hepatitis B: Impact of hepatitis B e-antigen seroconversion. *Hepatology* 48: 759-769.
39. Bertoletti, A., A. Costanzo, F. V. Chisari, M. Levrero, M. Artini, A. Sette, A. Penna, T. Giuberti, F. Fiaccadori, and C. Ferrari. 1994. Cytotoxic T lymphocyte response to a wild type hepatitis B virus epitope in patients chronically infected by variant viruses carrying substitutions within the epitope. *J Exp Med* 180: 933-943.
40. Gehring, A. J., S. A. Xue, Z. Z. Ho, D. Teoh, C. Ruedl, A. Chia, S. Koh, S. G. Lim, M. K. Maini, H. Stauss, and A. Bertoletti. 2011. Engineering virus-specific T cells that target HBV infected hepatocytes and hepatocellular carcinoma cell lines. *J Hepatol* 55: 103-110.
41. Ji, C., K. S. Sastry, G. Tiefenthaler, J. Cano, T. Tang, Z. Z. Ho, D. Teoh, S. Bohini, A. Chen, S. Sankuratri, P. A. Macary, P. Kennedy, H. Ma, S. Ries, K. Klumpp, E. Kopetzki, and A. Bertoletti. 2012. Targeted delivery of interferon-alpha to hepatitis B virus-infected cells using T-cell receptor-like antibodies. *Hepatology* 56: 2027-2038.
42. Toebes, M., M. Coccoris, A. Bins, B. Rodenko, R. Gomez, N. J. Nieuwkoop, W. van de Kasteele, G. F. Rimmelzwaan, J. B. Haanen, H. Ovaa, and T. N. Schumacher. 2006. Design and use of conditional MHC class I ligands. *Nat Med* 12: 246-251.
43. Newell, E. W., L. O. Klein, W. Yu, and M. M. Davis. 2009. Simultaneous detection of many T-cell specificities using combinatorial tetramer staining. *Nat Methods* 6: 497-499.
44. Newell, E. W., N. Sigal, N. Nair, B. A. Kidd, H. B. Greenberg, and M. M. Davis. 2013. Combinatorial tetramer staining and mass cytometry analysis facilitate T-cell epitope mapping and characterization. *Nature biotechnology* 31: 623-629.
45. Davis, M. M., J. D. Altman, and E. W. Newell. 2011. Interrogating the repertoire: broadening the scope of peptide-MHC multimer analysis. *Nature reviews. Immunology* 11: 551-558.
46. Nitschke, K., T. Flecken, J. Schmidt, E. Gostick, M. Marget, C. Neumann-Haefelin, H. E. Blum, D. A. Price, and R. Thimme. 2014. Tetramer-enrichment reveals presence of phenotypically diverse hepatitis C virus specific CD8+ T cells in chronic infection. *J Virol*.
47. Gallimore, A., A. Glithero, A. Godkin, A. C. Tissot, A. Pluckthun, T. Elliott, H. Hengartner, and R. Zinkernagel. 1998. Induction and

exhaustion of lymphocytic choriomeningitis virus-specific cytotoxic T lymphocytes visualized using soluble tetrameric major histocompatibility complex class I-peptide complexes. *The Journal of experimental medicine* 187: 1383-1393.
48. Zajac, A. J., J. N. Blattman, K. Murali-Krishna, D. J. Sourdive, M. Suresh, J. D. Altman, and R. Ahmed. 1998. Viral immune evasion due to persistence of activated T cells without effector function. *The Journal of experimental medicine* 188: 2205-2213.
49. Virgin, H. W., E. J. Wherry, and R. Ahmed. 2009. Redefining chronic viral infection. *Cell* 138: 30-50.
50. Wherry, E. J. 2011. T cell exhaustion. *Nat Immunol* 12: 492-499.
51. Moskophidis, D., F. Lechner, H. Pircher, and R. M. Zinkernagel. 1993. Virus persistence in acutely infected immunocompetent mice by exhaustion of antiviral cytotoxic effector T cells. *Nature* 362: 758-761.
52. Wherry, E. J., S. J. Ha, S. M. Kaech, W. N. Haining, S. Sarkar, V. Kalia, S. Subramaniam, J. N. Blattman, D. L. Barber, and R. Ahmed. 2007. Molecular signature of CD8+ T cell exhaustion during chronic viral infection. *Immunity* 27: 670-684.
53. Masopust, D., V. Vezys, E. J. Wherry, and R. Ahmed. 2007. A brief history of CD8 T cells. *European journal of immunology* 37 Suppl 1: S103-110.
54. Bengsch, B., B. Seigel, M. Ruhl, J. Timm, M. Kuntz, H. E. Blum, H. Pircher, and R. Thimme. 2010. Coexpression of PD-1, 2B4, CD160 and KLRG1 on exhausted HCV-specific CD8+ T cells is linked to antigen recognition and T cell differentiation. *PLoS Pathog* 6: e1000947.
55. Fuller, M. J., B. Callendret, B. Zhu, G. J. Freeman, D. L. Hasselschwert, W. Satterfield, A. H. Sharpe, L. B. Dustin, C. M. Rice, A. Grakoui, R. Ahmed, and C. M. Walker. 2013. Immunotherapy of chronic hepatitis C virus infection with antibodies against programmed cell death-1 (PD-1). *Proceedings of the National Academy of Sciences of the United States of America* 110: 15001-15006.
56. McMahan, R. H., L. Golden-Mason, M. I. Nishimura, B. J. McMahon, M. Kemper, T. M. Allen, D. R. Gretch, and H. R. Rosen. 2010. Tim-3 expression on PD-1+ HCV-specific human CTLs is associated with viral persistence, and its blockade restores hepatocyte-directed in vitro cytotoxicity. *The Journal of clinical investigation* 120: 4546-4557.
57. Paley, M. A., D. C. Kroy, P. M. Odorizzi, J. B. Johnnidis, D. V. Dolfi, B. E. Barnett, E. K. Bikoff, E. J. Robertson, G. M. Lauer, S. L. Reiner, and E. J. Wherry. 2012. Progenitor and terminal subsets of CD8+ T cells cooperate to contain chronic viral infection. *Science* 338: 1220-1225.
58. Day, C. L., D. E. Kaufmann, P. Kiepiela, J. A. Brown, E. S. Moodley, S. Reddy, E. W. Mackey, J. D. Miller, A. J. Leslie, C. DePierres, Z. Mncube, J. Duraiswamy, B. Zhu, Q. Eichbaum, M. Altfeld, E. J. Wherry, H. M. Coovadia, P. J. Goulder, P. Klenerman, R. Ahmed, G. J. Freeman, and B. D. Walker. 2006. PD-1 expression on HIV-specific T cells is

associated with T-cell exhaustion and disease progression. *Nature* 443: 350-354.
59. Angelosanto, J. M., S. D. Blackburn, A. Crawford, and E. J. Wherry. 2012. Progressive loss of memory T cell potential and commitment to exhaustion during chronic viral infection. *J Virol* 86: 8161-8170.
60. Barber, D. L., E. J. Wherry, D. Masopust, B. Zhu, J. P. Allison, A. H. Sharpe, G. J. Freeman, and R. Ahmed. 2006. Restoring function in exhausted CD8 T cells during chronic viral infection. *Nature* 439: 682-687.
61. Pauken, K. E., M. A. Sammons, P. M. Odorizzi, S. Manne, J. Godec, O. Khan, A. M. Drake, Z. Chen, D. R. Sen, M. Kurachi, R. A. Barnitz, C. Bartman, B. Bengsch, A. C. Huang, J. M. Schenkel, G. Vahedi, W. N. Haining, S. L. Berger, and E. J. Wherry. 2016. Epigenetic stability of exhausted T cells limits durability of reinvigoration by PD-1 blockade. *Science* 354: 1160-1165.
62. Kao, C., K. J. Oestreich, M. A. Paley, A. Crawford, J. M. Angelosanto, M. A. Ali, A. M. Intlekofer, J. M. Boss, S. L. Reiner, A. S. Weinmann, and E. J. Wherry. 2011. Transcription factor T-bet represses expression of the inhibitory receptor PD-1 and sustains virus-specific CD8+ T cell responses during chronic infection. *Nat Immunol* 12: 663-671.
63. Wherry, E. J., and M. Kurachi. 2015. Molecular and cellular insights into T cell exhaustion. *Nat Rev Immunol* 15: 486-499.
64. Angelosanto, J. M., and E. J. Wherry. 2010. Transcription factor regulation of CD8+ T-cell memory and exhaustion. *Immunol Rev* 236: 167-175.
65. Kaech, S. M., and E. J. Wherry. 2007. Heterogeneity and cell-fate decisions in effector and memory CD8+ T cell differentiation during viral infection. *Immunity* 27: 393-405.
66. Shin, H., S. D. Blackburn, A. M. Intlekofer, C. Kao, J. M. Angelosanto, S. L. Reiner, and E. J. Wherry. 2009. A role for the transcriptional repressor Blimp-1 in CD8(+) T cell exhaustion during chronic viral infection. *Immunity* 31: 309-320.
67. Freeman, G. J., A. J. Long, Y. Iwai, K. Bourque, T. Chernova, H. Nishimura, L. J. Fitz, N. Malenkovich, T. Okazaki, M. C. Byrne, H. F. Horton, L. Fouser, L. Carter, V. Ling, M. R. Bowman, B. M. Carreno, M. Collins, C. R. Wood, and T. Honjo. 2000. Engagement of the PD-1 immunoinhibitory receptor by a novel B7 family member leads to negative regulation of lymphocyte activation. *The Journal of experimental medicine* 192: 1027-1034.
68. Nishimura, H., T. Okazaki, Y. Tanaka, K. Nakatani, M. Hara, A. Matsumori, S. Sasayama, A. Mizoguchi, H. Hiai, N. Minato, and T. Honjo. 2001. Autoimmune dilated cardiomyopathy in PD-1 receptor-deficient mice. *Science* 291: 319-322.
69. Kroy, D. C., D. Ciuffreda, J. H. Cooperrider, M. Tomlinson, G. D. Hauck, J. Aneja, C. Berger, D. Wolski, M. Carrington, E. J. Wherry, R. T. Chung, K. K. Tanabe, N. Elias, G. J. Freeman, R. H. de Kruyff, J. Misdraji, A. Y. Kim, and G. M. Lauer. 2014. Liver environment and HCV replication affect human T-cell phenotype and expression of inhibitory receptors. *Gastroenterology* 146: 550-561.

70. Zhu, C., A. C. Anderson, A. Schubart, H. Xiong, J. Imitola, S. J. Khoury, X. X. Zheng, T. B. Strom, and V. K. Kuchroo. 2005. The Tim-3 ligand galectin-9 negatively regulates T helper type 1 immunity. *Nature immunology* 6: 1245-1252.
71. Osuna, C. E., A. M. Gonzalez, H. H. Chang, A. S. Hung, E. Ehlinger, K. Anasti, S. M. Alam, and N. L. Letvin. 2014. TCR affinity associated with functional differences between dominant and subdominant SIV epitope-specific CD8+ T cells in Mamu-A*01+ rhesus monkeys. *PLoS Pathog* 10: e1004069.
72. Richter, K., P. Agnellini, and A. Oxenius. 2010. On the role of the inhibitory receptor LAG-3 in acute and chronic LCMV infection. *Int Immunol* 22: 13-23.
73. Vigano, S., R. Banga, F. Bellanger, C. Pellaton, A. Farina, D. Comte, A. Harari, and M. Perreau. 2014. CD160-associated CD8 T-cell functional impairment is independent of PD-1 expression. *PLoS Pathog* 10: e1004380.
74. Cai, G., X. Nie, L. Li, L. Hu, B. Wu, J. Lin, C. Jiang, H. Wang, X. Wang, and Q. Shen. 2013. B and T lymphocyte attenuator is highly expressed on intrahepatic T cells during chronic HBV infection and regulates their function. *J Gastroenterol* 48: 1362-1372.
75. Chew, G. M., T. Fujita, G. M. Webb, B. J. Burwitz, H. L. Wu, J. S. Reed, K. B. Hammond, K. L. Clayton, N. Ishii, M. Abdel-Mohsen, T. Liegler, B. I. Mitchell, F. M. Hecht, M. Ostrowski, C. M. Shikuma, S. G. Hansen, M. Maurer, A. J. Korman, S. G. Deeks, J. B. Sacha, and L. C. Ndhlovu. 2016. TIGIT Marks Exhausted T Cells, Correlates with Disease Progression, and Serves as a Target for Immune Restoration in HIV and SIV Infection. *PLoS Pathog* 12: e1005349.
76. Tauriainen, J., L. Scharf, J. Frederiksen, A. Naji, H. G. Ljunggren, A. Sonnerborg, O. Lund, G. Reyes-Teran, F. M. Hecht, S. G. Deeks, M. R. Betts, M. Buggert, and A. C. Karlsson. 2017. Perturbed CD8+ T cell TIGIT/CD226/PVR axis despite early initiation of antiretroviral treatment in HIV infected individuals. *Sci Rep* 7: 40354.
77. Blackburn, S. D., H. Shin, W. N. Haining, T. Zou, C. J. Workman, A. Polley, M. R. Betts, G. J. Freeman, D. A. Vignali, and E. J. Wherry. 2009. Coregulation of CD8+ T cell exhaustion by multiple inhibitory receptors during chronic viral infection. *Nat Immunol* 10: 29-37.
78. Jin, H. T., A. C. Anderson, W. G. Tan, E. E. West, S. J. Ha, K. Araki, G. J. Freeman, V. K. Kuchroo, and R. Ahmed. 2010. Cooperation of Tim-3 and PD-1 in CD8 T-cell exhaustion during chronic viral infection. *Proceedings of the National Academy of Sciences of the United States of America* 107: 14733-14738.
79. Nakamoto, N., H. Cho, A. Shaked, K. Olthoff, M. E. Valiga, M. Kaminski, E. Gostick, D. A. Price, G. J. Freeman, E. J. Wherry, and K. M. Chang. 2009. Synergistic reversal of intrahepatic HCV-specific CD8 T cell exhaustion by combined PD-1/CTLA-4 blockade. *PLoS Pathog* 5: e1000313.
80. Peretz, Y., Z. He, Y. Shi, B. Yassine-Diab, J. P. Goulet, R. Bordi, A. Filali-Mouhim, J. B. Loubert, M. El-Far, F. P. Dupuy, M. R. Boulassel, C. Tremblay, J. P. Routy, N. Bernard, R. Balderas, E. K. Haddad, and R. P.

Sekaly. 2012. CD160 and PD-1 co-expression on HIV-specific CD8 T cells defines a subset with advanced dysfunction. *PLoS Pathog* 8: e1002840.
81. Grosso, J. F., M. V. Goldberg, D. Getnet, T. C. Bruno, H. R. Yen, K. J. Pyle, E. Hipkiss, D. A. Vignali, D. M. Pardoll, and C. G. Drake. 2009. Functionally distinct LAG-3 and PD-1 subsets on activated and chronically stimulated CD8 T cells. *Journal of immunology* 182: 6659-6669.
82. Leitner, J., A. Rieger, W. F. Pickl, G. Zlabinger, K. Grabmeier-Pfistershammer, and P. Steinberger. 2013. TIM-3 does not act as a receptor for galectin-9. *PLoS Pathog* 9: e1003253.
83. Li, H., K. Wu, K. Tao, L. Chen, Q. Zheng, X. Lu, J. Liu, L. Shi, C. Liu, G. Wang, and W. Zou. 2012. Tim-3/galectin-9 signaling pathway mediates T-cell dysfunction and predicts poor prognosis in patients with hepatitis B virus-associated hepatocellular carcinoma. *Hepatology* 56: 1342-1351.
84. Schlaphoff, V., S. Lunemann, P. V. Suneetha, J. Jaroszewicz, J. Grabowski, J. Dietz, F. Helfritz, H. Bektas, C. Sarrazin, M. P. Manns, M. Cornberg, and H. Wedemeyer. 2011. Dual function of the NK cell receptor 2B4 (CD244) in the regulation of HCV-specific CD8+ T cells. *PLoS Pathog* 7: e1002045.
85. Jones, R. B., L. C. Ndhlovu, J. D. Barbour, P. M. Sheth, A. R. Jha, B. R. Long, J. C. Wong, M. Satkunarajah, M. Schweneker, J. M. Chapman, G. Gyenes, B. Vali, M. D. Hyrcza, F. Y. Yue, C. Kovacs, A. Sassi, M. Loutfy, R. Halpenny, D. Persad, G. Spotts, F. M. Hecht, T. W. Chun, J. M. McCune, R. Kaul, J. M. Rini, D. F. Nixon, and M. A. Ostrowski. 2008. Tim-3 expression defines a novel population of dysfunctional T cells with highly elevated frequencies in progressive HIV-1 infection. *The Journal of experimental medicine* 205: 2763-2779.
86. Anderson, A. C., D. E. Anderson, L. Bregoli, W. D. Hastings, N. Kassam, C. Lei, R. Chandwaskar, J. Karman, E. W. Su, M. Hirashima, J. N. Bruce, L. P. Kane, V. K. Kuchroo, and D. A. Hafler. 2007. Promotion of tissue inflammation by the immune receptor Tim-3 expressed on innate immune cells. *Science* 318: 1141-1143.
87. Gorman, J. V., G. Starbeck-Miller, N. L. Pham, G. L. Traver, P. B. Rothman, J. T. Harty, and J. D. Colgan. 2014. Tim-3 directly enhances CD8 T cell responses to acute Listeria monocytogenes infection. *Journal of immunology* 192: 3133-3142.
88. Flynn, R., T. Hutchinson, K. M. Murphy, C. F. Ware, M. Croft, and S. Salek-Ardakani. 2013. CD8 T cell memory to a viral pathogen requires trans cosignaling between HVEM and BTLA. *PLoS One* 8: e77991.
89. Okazaki, T., S. Chikuma, Y. Iwai, S. Fagarasan, and T. Honjo. 2013. A rheostat for immune responses: the unique properties of PD-1 and their advantages for clinical application. *Nature immunology* 14: 1212-1218.
90. Blattman, J. N., E. J. Wherry, S. J. Ha, R. G. van der Most, and R. Ahmed. 2009. Impact of epitope escape on PD-1 expression and CD8

T-cell exhaustion during chronic infection. *Journal of virology* 83: 4386-4394.
91. Boettler, T., F. Moeckel, Y. Cheng, M. Heeg, S. Salek-Ardakani, S. Crotty, M. Croft, and M. G. von Herrath. 2012. OX40 facilitates control of a persistent virus infection. *PLoS Pathog* 8: e1002913.
92. Lanier, L. L., E. G. Engleman, P. Gatenby, G. F. Babcock, N. L. Warner, and L. A. Herzenberg. 1983. Correlation of functional properties of human lymphoid cell subsets and surface marker phenotypes using multiparameter analysis and flow cytometry. *Immunol Rev* 74: 143-160.
93. Bendall, S. C., G. P. Nolan, M. Roederer, and P. K. Chattopadhyay. 2012. A deep profiler's guide to cytometry. *Trends in immunology* 33: 323-332.
94. Chattopadhyay, P. K., T. M. Gierahn, M. Roederer, and J. C. Love. 2014. Single-cell technologies for monitoring immune systems. *Nat Immunol* 15: 128-135.
95. Bandura, D. R., V. I. Baranov, O. I. Ornatsky, A. Antonov, R. Kinach, X. Lou, S. Pavlov, S. Vorobiev, J. E. Dick, and S. D. Tanner. 2009. Mass cytometry: technique for real time single cell multitarget immunoassay based on inductively coupled plasma time-of-flight mass spectrometry. *Anal Chem* 81: 6813-6822.
96. Bendall, S. C., E. F. Simonds, P. Qiu, A. D. Amir el, P. O. Krutzik, R. Finck, R. V. Bruggner, R. Melamed, A. Trejo, O. I. Ornatsky, R. S. Balderas, S. K. Plevritis, K. Sachs, D. Pe'er, S. D. Tanner, and G. P. Nolan. 2011. Single-cell mass cytometry of differential immune and drug responses across a human hematopoietic continuum. *Science* 332: 687-696.
97. Newell, E. W., N. Sigal, S. C. Bendall, G. P. Nolan, and M. M. Davis. 2012. Cytometry by time-of-flight shows combinatorial cytokine expression and virus-specific cell niches within a continuum of CD8+ T cell phenotypes. *Immunity* 36: 142-152.
98. Ornatsky, O., D. Bandura, V. Baranov, M. Nitz, M. A. Winnik, and S. Tanner. 2010. Highly multiparametric analysis by mass cytometry. *J Immunol Methods* 361: 1-20.
99. Tanner, S. D., V. I. Baranov, O. I. Ornatsky, D. R. Bandura, and T. C. George. 2013. An introduction to mass cytometry: fundamentals and applications. *Cancer Immunol Immunother* 62: 955-965.
100. Houk, R. S., V. A. Fassel, G. D. Flesch, H. J. Svec, A. L. Gray, and C. E. Taylor. 1980. Inductively coupled argon plasma as an ion source for mass spectrometric determination of trace elements. *Anal Chem* 52: 2283-2289.
101. Bjornson, Z. B., G. P. Nolan, and W. J. Fantl. 2013. Single-cell mass cytometry for analysis of immune system functional states. *Curr Opin Immunol* 25: 484-494.
102. Cheng, Y., and E. W. Newell. 2016. Deep Profiling Human T Cell Heterogeneity by Mass Cytometry. *Adv Immunol* 131: 101-134.
103. Aghaeepour, N., G. Finak, C. A. P. C. Flow, D. Consortium, H. Hoos, T. R. Mosmann, R. Brinkman, R. Gottardo, and R. H. Scheuermann.

2013. Critical assessment of automated flow cytometry data analysis techniques. *Nat Methods* 10: 228-238.
104. Newell, E. W., and M. M. Davis. 2014. Beyond model antigens: high-dimensional methods for the analysis of antigen-specific T cells. *Nat Biotechnol* 32: 149-157.
105. Newell, E. W., and Y. Cheng. 2016. Mass cytometry: blessed with the curse of dimensionality. *Nat Immunol* 17: 890-895.
106. Hotelling, H. 1933. Analysis of a complex of statistical variables into principal components. *Journal of Educational Psychology* 24: 417-441, 498-520.
107. Fergusson, J. R., K. E. Smith, V. M. Fleming, N. Rajoriya, E. W. Newell, R. Simmons, E. Marchi, S. Bjorkander, Y. H. Kang, L. Swadling, A. Kurioka, N. Sahgal, H. Lockstone, D. Baban, G. J. Freeman, E. Sverremark-Ekstrom, M. M. Davis, M. P. Davenport, V. Venturi, J. E. Ussher, C. B. Willberg, and P. Klenerman. 2014. CD161 defines a transcriptional and functional phenotype across distinct human T cell lineages. *Cell Rep* 9: 1075-1088.
108. Sen, N., G. Mukherjee, A. Sen, S. C. Bendall, P. Sung, G. P. Nolan, and A. M. Arvin. 2014. Single-cell mass cytometry analysis of human tonsil T cell remodeling by varicella zoster virus. *Cell Rep* 8: 633-645.
109. Swadling, L., S. Capone, R. D. Antrobus, A. Brown, R. Richardson, E. W. Newell, J. Halliday, C. Kelly, D. Bowen, J. Fergusson, A. Kurioka, V. Ammendola, M. Del Sorbo, F. Grazioli, M. L. Esposito, L. Siani, C. Traboni, A. Hill, S. Colloca, M. Davis, A. Nicosia, R. Cortese, A. Folgori, P. Klenerman, and E. Barnes. 2014. A human vaccine strategy based on chimpanzee adenoviral and MVA vectors that primes, boosts, and sustains functional HCV-specific T cell memory. *Sci Transl Med* 6: 261ra153.
110. van der Maaten, L. H., G. 2008. Visualizing data using t-SNE. *Journal of Machine Learning Research* 9: 85.
111. Amir el, A. D., K. L. Davis, M. D. Tadmor, E. F. Simonds, J. H. Levine, S. C. Bendall, D. K. Shenfeld, S. Krishnaswamy, G. P. Nolan, and D. Pe'er. 2013. viSNE enables visualization of high dimensional single-cell data and reveals phenotypic heterogeneity of leukemia. *Nat Biotechnol* 31: 545-552.
112. Becher, B., A. Schlitzer, J. Chen, F. Mair, H. R. Sumatoh, K. W. Teng, D. Low, C. Ruedl, P. Riccardi-Castagnoli, M. Poidinger, M. Greter, F. Ginhoux, and E. W. Newell. 2014. High-dimensional analysis of the murine myeloid cell system. *Nat Immunol* 15: 1181-1189.
113. Wong, M. T., J. Chen, S. Narayanan, W. Lin, R. Anicete, H. T. Kiaang, M. A. De Lafaille, M. Poidinger, and E. W. Newell. 2015. Mapping the Diversity of Follicular Helper T Cells in Human Blood and Tonsils Using High-Dimensional Mass Cytometry Analysis. *Cell Rep* 11: 1822-1833.
114. Mason, G. M., K. Lowe, R. Melchiotti, R. Ellis, E. de Rinaldis, M. Peakman, S. Heck, G. Lombardi, and T. I. Tree. 2015. Phenotypic Complexity of the Human Regulatory T Cell Compartment Revealed by Mass Cytometry. *J Immunol* 195: 2030-2037.

115. Shekhar, K., P. Brodin, M. M. Davis, and A. K. Chakraborty. 2014. Automatic Classification of Cellular Expression by Nonlinear Stochastic Embedding (ACCENSE). *Proc Natl Acad Sci U S A* 111: 202-207.
116. Cheng, Y., M. T. Wong, L. van der Maaten, and E. W. Newell. 2016. Categorical Analysis of Human T Cell Heterogeneity with One-Dimensional Soli-Expression by Nonlinear Stochastic Embedding. *J Immunol* 196: 924-932.
117. Wong, M. T., D. E. Ong, F. S. Lim, K. W. Teng, N. McGovern, S. Narayanan, W. Q. Ho, D. Cerny, H. K. Tan, R. Anicete, B. K. Tan, T. K. Lim, C. Y. Chan, P. C. Cheow, S. Y. Lee, A. Takano, E. H. Tan, J. K. Tam, E. Y. Tan, J. K. Chan, K. Fink, A. Bertoletti, F. Ginhoux, M. A. Curotto de Lafaille, and E. W. Newell. 2016. A High-Dimensional Atlas of Human T Cell Diversity Reveals Tissue-Specific Trafficking and Cytokine Signatures. *Immunity* 45: 442-456.
118. Coifman, R. R., S. Lafon, A. B. Lee, M. Maggioni, B. Nadler, F. Warner, and S. W. Zucker. 2005. Geometric diffusions as a tool for harmonic analysis and structure definition of data: diffusion maps. *Proc Natl Acad Sci U S A* 102: 7426-7431.
119. Haghverdi, L., F. Buettner, and F. J. Theis. 2015. Diffusion maps for high-dimensional single-cell analysis of differentiation data. *Bioinformatics* 31: 2989-2998.
120. See, P., C. A. Dutertre, J. Chen, P. Gunther, N. McGovern, S. E. Irac, M. Gunawan, M. Beyer, K. Handler, K. Duan, H. R. B. Sumatoh, N. Ruffin, M. Jouve, E. Gea-Mallorqui, R. C. M. Hennekam, T. Lim, C. C. Yip, M. Wen, B. Malleret, I. Low, N. B. Shadan, C. F. S. Fen, A. Tay, J. Lum, F. Zolezzi, A. Larbi, M. Poidinger, J. K. Y. Chan, Q. Chen, L. Renia, M. Haniffa, P. Benaroch, A. Schlitzer, J. L. Schultze, E. W. Newell, and F. Ginhoux. 2017. Mapping the human DC lineage through the integration of high-dimensional techniques. *Science*.
121. Ramachandiran, V., V. Grigoriev, L. Lan, E. Ravkov, S. A. Mertens, and J. D. Altman. 2007. A robust method for production of MHC tetramers with small molecule fluorophores. *J Immunol Methods* 319: 13-20.
122. Bakker, A. H., R. Hoppes, C. Linnemann, M. Toebes, B. Rodenko, C. R. Berkers, S. R. Hadrup, W. J. van Esch, M. H. Heemskerk, H. Ovaa, and T. N. Schumacher. 2008. Conditional MHC class I ligands and peptide exchange technology for the human MHC gene products HLA-A1, -A3, -A11, and -B7. *Proceedings of the National Academy of Sciences of the United States of America* 105: 3825-3830.
123. Wooldridge, L., A. Lissina, D. K. Cole, H. A. van den Berg, D. A. Price, and A. K. Sewell. 2009. Tricks with tetramers: how to get the most from multimeric peptide-MHC. *Immunology* 126: 147-164.
124. Finck, R., E. F. Simonds, A. Jager, S. Krishnaswamy, K. Sachs, W. Fantl, D. Pe'er, G. P. Nolan, and S. C. Bendall. 2013. Normalization of mass cytometry data with bead standards. *Cytometry A* 83: 483-494.
125. Carlson, C. S., R. O. Emerson, A. M. Sherwood, C. Desmarais, M. W. Chung, J. M. Parsons, M. S. Steen, M. A. LaMadrid-Herrmannsfeldt, D. W. Williamson, R. J. Livingston, D. Wu, B. L. Wood, M. J. Rieder, and

H. Robins. 2013. Using synthetic templates to design an unbiased multiplex PCR assay. *Nat Commun* 4: 2680.
126. Robins, H. S., P. V. Campregher, S. K. Srivastava, A. Wacher, C. J. Turtle, O. Kahsai, S. R. Riddell, E. H. Warren, and C. S. Carlson. 2009. Comprehensive assessment of T-cell receptor beta-chain diversity in alphabeta T cells. *Blood* 114: 4099-4107.
127. Li, S., M. P. Lefranc, J. J. Miles, E. Alamyar, V. Giudicelli, P. Duroux, J. D. Freeman, V. D. Corbin, J. P. Scheerlinck, M. A. Frohman, P. U. Cameron, M. Plebanski, B. Loveland, S. R. Burrows, A. T. Papenfuss, and E. J. Gowans. 2013. IMGT/HighV QUEST paradigm for T cell receptor IMGT clonotype diversity and next generation repertoire immunoprofiling. *Nat Commun* 4: 2333.
128. Okonechnikov, K., O. Golosova, M. Fursov, and U. team. 2012. Unipro UGENE: a unified bioinformatics toolkit. *Bioinformatics* 28: 1166-1167.
129. Edgar, R. C. 2004. MUSCLE: multiple sequence alignment with high accuracy and high throughput. *Nucleic Acids Res* 32: 1792-1797.
130. Bailey, T. L., M. Boden, F. A. Buske, M. Frith, C. E. Grant, L. Clementi, J. Ren, W. W. Li, and W. S. Noble. 2009. MEME SUITE: tools for motif discovery and searching. *Nucleic Acids Res* 37: W202-208.
131. Frith, M. C., N. F. Saunders, B. Kobe, and T. L. Bailey. 2008. Discovering sequence motifs with arbitrary insertions and deletions. *PLoS Comput Biol* 4: e1000071.
132. Huson, D. H., D. C. Richter, C. Rausch, T. Dezulian, M. Franz, and R. Rupp. 2007. Dendroscope: An interactive viewer for large phylogenetic trees. *BMC Bioinformatics* 8: 460.
133. Waterhouse, A. M., J. B. Procter, D. M. Martin, M. Clamp, and G. J. Barton. 2009. Jalview Version 2--a multiple sequence alignment editor and analysis workbench. *Bioinformatics* 25: 1189-1191.
134. Alexander, J., C. Oseroff, J. Sidney, P. Wentworth, E. Keogh, G. Hermanson, F. V. Chisari, R. T. Kubo, H. M. Grey, and A. Sette. 1997. Derivation of HLA-A11/Kb transgenic mice: functional CTL repertoire and recognition of human A11-restricted CTL epitopes. *J Immunol* 159: 4753-4761.
135. Rybczynska, J., K. Campbell, S. Kamili, S. Locarnini, K. Krawczynski, and C. M. Walker. 2016. CD4+ T Cells Are Not Required for Suppression of Hepatitis B Virus Replication in the Liver of Vaccinated Chimpanzees. *The Journal of infectious diseases* 213: 49-56.
136. Werner, J. M., A. Abdalla, N. Gara, M. G. Ghany, and B. Rehermann. 2013. The hepatitis B vaccine protects re-exposed health care workers, but does not provide sterilizing immunity. *Gastroenterology* 145: 1026-1034.
137. Amir el, A. D., K. L. Davis, M. D. Tadmor, E. F. Simonds, J. H. Levine, S. C. Bendall, D. K. Shenfeld, S. Krishnaswamy, G. P. Nolan, and D. Pe'er. 2013. viSNE enables visualization of high dimensional single-cell data and reveals phenotypic heterogeneity of leukemia. *Nature biotechnology* 31: 545-552.

138. van der Maaten, L. 2009. Learning a parametric embedding by preserving local structure. *Proceedings of AI-STATS*.
139. Croft, M. 2003. Co-stimulatory members of the TNFR family: keys to effective T-cell immunity? *Nat Rev Immunol* 3: 609-620.
140. Gupta, P. K., J. Godec, D. Wolski, E. Adland, K. Yates, K. E. Pauken, C. Cosgrove, C. Ledderose, W. G. Junger, S. C. Robson, E. J. Wherry, G. Alter, P. J. Goulder, P. Klenerman, A. H. Sharpe, G. M. Lauer, and W. N. Haining. 2015. CD39 Expression Identifies Terminally Exhausted CD8+ T Cells. *PLoS Pathog* 11: e1005177.
141. Fang, F., M. Yu, M. M. Cavanagh, J. Hutter Saunders, Q. Qi, Z. Ye, S. Le Saux, W. Sultan, E. Turgano, C. L. Dekker, L. Tian, C. M. Weyand, and J. J. Goronzy. 2016. Expression of CD39 on Activated T Cells Impairs their Survival in Older Individuals. *Cell Rep* 14: 1218-1231.
142. Ishioka, G. Y., J. Fikes, G. Hermanson, B. Livingston, C. Crimi, M. Qin, M. F. del Guercio, C. Oseroff, C. Dahlberg, J. Alexander, R. W. Chesnut, and A. Sette. 1999. Utilization of MHC class I transgenic mice for development of minigene DNA vaccines encoding multiple HLA-restricted CTL epitopes. *J Immunol* 162: 3915-3925.
143. Kefalakes, H., B. Budeus, A. Walker, C. Jochum, G. Hilgard, A. Heinold, F. M. Heinemann, G. Gerken, D. Hoffmann, and J. Timm. 2015. Adaptation of the hepatitis B virus core protein to CD8(+) T-cell selection pressure. *Hepatology* 62: 47-56.
144. Blattman, J. N., R. Antia, D. J. Sourdive, X. Wang, S. M. Kaech, K. Murali-Krishna, J. D. Altman, and R. Ahmed. 2002. Estimating the precursor frequency of naive antigen-specific CD8 T cells. *J Exp Med* 195: 657-664.
145. Neller, M. A., K. Ladell, J. E. McLaren, K. K. Matthews, E. Gostick, J. M. Pentier, G. Dolton, A. J. Schauenburg, D. Koning, A. I. Fontaine Costa, T. S. Watkins, V. Venturi, C. Smith, R. Khanna, K. Miners, M. Clement, L. Wooldridge, D. K. Cole, D. van Baarle, A. K. Sewell, S. R. Burrows, D. A. Price, and J. J. Miles. 2015. Naive CD8(+) T-cell precursors display structured TCR repertoires and composite antigen-driven selection dynamics. *Immunol Cell Biol* 93: 625-633.
146. Alanio, C., F. Lemaitre, H. K. Law, M. Hasan, and M. L. Albert. 2010. Enumeration of human antigen-specific naive CD8+ T cells reveals conserved precursor frequencies. *Blood* 115: 3718-3725.
147. Zhang, S., R. K. Bakshi, P. V. Suneetha, P. Fytili, D. A. Antunes, G. F. Vieira, R. Jacobs, C. S. Klade, M. P. Manns, A. R. Kraft, H. Wedemeyer, V. Schlaphoff, and M. Cornberg. 2015. Frequency, Private Specificity, and Cross-Reactivity of Preexisting Hepatitis C Virus (HCV)-Specific CD8+ T Cells in HCV-Seronegative Individuals: Implications for Vaccine Responses. *J Virol* 89: 8304-8317.
148. Pulko, V., J. S. Davies, C. Martinez, M. C. Lanteri, M. P. Busch, M. S. Diamond, K. Knox, E. C. Bush, P. A. Sims, S. Sinari, D. Billheimer, E. K. Haddad, K. O. Murray, A. M. Wertheimer, and J. Nikolich-Zugich. 2016. Human memory T cells with a naive phenotype accumulate with aging and respond to persistent viruses. *Nat Immunol* 17: 966-975.

149. Hong, M., E. Sandalova, D. Low, A. J. Gehring, S. Fieni, B. Amadei, S. Urbani, Y. S. Chong, E. Guccione, and A. Bertoletti. 2015. Trained immunity in newborn infants of HBV-infected mothers. *Nat Commun* 6: 6588.
150. Jamieson, B. D., and R. Ahmed. 1988. T-cell tolerance: exposure to virus in utero does not cause a permanent deletion of specific T cells. *Proc Natl Acad Sci U S A* 85: 2265-2268.
151. McGovern, N., A. Shin, G. Low, D. Low, K. Duan, L. J. Yao, R. Msallam, I. Low, N. B. Shadan, H. R. Sumatoh, E. Soon, J. Lum, E. Mok, S. Hubert, P. See, E. H. Kunxiang, Y. H. Lee, B. Janela, M. Choolani, C. N. Z. Mattar, Y. Fan, T. K. H. Lim, D. K. H. Chan, K. K. Tan, J. K. C. Tam, C. Schuster, A. Elbe-Burger, X. N. Wang, V. Bigley, M. Collin, M. Haniffa, A. Schlitzer, M. Poidinger, S. Albani, A. Larbi, E. W. Newell, J. K. Y. Chan, and F. Ginhoux. 2017. Human fetal dendritic cells promote prenatal T-cell immune suppression through arginase-2. *Nature* 546: 662-666.
152. Cheung, T. C., L. M. Oborne, M. W. Steinberg, M. G. Macauley, S. Fukuyama, H. Sanjo, C. D'Souza, P. S. Norris, K. Pfeffer, K. M. Murphy, M. Kronenberg, P. G. Spear, and C. F. Ware. 2009. T cell intrinsic heterodimeric complexes between HVEM and BTLA determine receptivity to the surrounding microenvironment. *J Immunol* 183: 7286-7296.
153. Murphy, K. M., C. A. Nelson, and J. R. Sedy. 2006. Balancing co-stimulation and inhibition with BTLA and HVEM. *Nat Rev Immunol* 6: 671-681.
154. Croft, M. 2009. The role of TNF superfamily members in T-cell function and diseases. *Nat Rev Immunol* 9: 271-285.
155. Huang, M., W. Zhang, J. Guo, X. Wei, K. Phiwpan, J. Zhang, and X. Zhou. 2016. Improved Transgenic Mouse Model for Studying HLA Class I Antigen Presentation. *Sci Rep* 6: 33612.
156. Turner, S. J., N. L. La Gruta, K. Kedzierska, P. G. Thomas, and P. C. Doherty. 2009. Functional implications of T cell receptor diversity. *Curr Opin Immunol* 21: 286-290.
157. Turner, S. J., P. C. Doherty, J. McCluskey, and J. Rossjohn. 2006. Structural determinants of T-cell receptor bias in immunity. *Nat Rev Immunol* 6: 883-894.
158. Chen, G., X. Yang, A. Ko, X. Sun, M. Gao, Y. Zhang, A. Shi, R. A. Mariuzza, and N. P. Weng. 2017. Sequence and Structural Analyses Reveal Distinct and Highly Diverse Human CD8+ TCR Repertoires to Immunodominant Viral Antigens. *Cell Rep* 19: 569-583.
159. Peggs, K., S. Verfuerth, A. Pizzey, J. Ainsworth, P. Moss, and S. Mackinnon. 2002. Characterization of human cytomegalovirus peptide-specific CD8(+) T-cell repertoire diversity following in vitro restimulation by antigen-pulsed dendritic cells. *Blood* 99: 213-223.
160. Koning, D., A. I. Costa, R. Hasrat, B. P. Grady, S. Spijkers, N. Nanlohy, C. Kesmir, and D. van Baarle. 2014. In vitro expansion of antigen-specific CD8(+) T cells distorts the T-cell repertoire. *J Immunol Methods* 405: 199-203.

161. Day, E. K., A. J. Carmichael, I. J. ten Berge, E. C. Waller, J. G. Sissons, and M. R. Wills. 2007. Rapid CD8+ T cell repertoire focusing and selection of high-affinity clones into memory following primary infection with a persistent human virus: human cytomegalovirus. *J Immunol* 179: 3203-3213.
162. Trautmann, L., M. Rimbert, K. Echasserieau, X. Saulquin, B. Neveu, J. Dechanet, V. Cerundolo, and M. Bonneville. 2005. Selection of T cell clones expressing high-affinity public TCRs within Human cytomegalovirus-specific CD8 T cell responses. *J Immunol* 175: 6123-6132.
163. Gil, A., M. B. Yassai, Y. N. Naumov, and L. K. Selin. 2015. Narrowing of human influenza A virus-specific T cell receptor alpha and beta repertoires with increasing age. *J Virol* 89: 4102-4116.
164. Schneider, T. D., and R. M. Stephens. 1990. Sequence logos: a new way to display consensus sequences. *Nucleic Acids Res* 18: 6097-6100.
165. Venturi, V., D. A. Price, D. C. Douek, and M. P. Davenport. 2008. The molecular basis for public T-cell responses? *Nat Rev Immunol* 8: 231-238.
166. Abdel-Hakeem, M. S., M. Boisvert, J. Bruneau, H. Soudeyns, and N. H. Shoukry. 2017. Selective expansion of high functional avidity memory CD8 T cell clonotypes during hepatitis C virus reinfection and clearance. *PLoS Pathog* 13: e1006191.
167. Dong, T., G. Stewart-Jones, N. Chen, P. Easterbrook, X. Xu, L. Papagno, V. Appay, M. Weekes, C. Conlon, C. Spina, S. Little, G. Screaton, A. van der Merwe, D. D. Richman, A. J. McMichael, E. Y. Jones, and S. L. Rowland-Jones. 2004. HIV-specific cytotoxic T cells from long-term survivors select a unique T cell receptor. *J Exp Med* 200: 1547-1557.
168. Price, D. A., T. E. Asher, N. A. Wilson, M. C. Nason, J. M. Brenchley, I. S. Metzler, V. Venturi, E. Gostick, P. K. Chattopadhyay, M. Roederer, M. P. Davenport, D. I. Watkins, and D. C. Douek. 2009. Public clonotype usage identifies protective Gag-specific CD8+ T cell responses in SIV infection. *J Exp Med* 206: 923-936.
169. Campos-Lima, P. O., V. Levitsky, M. P. Imreh, R. Gavioli, and M. G. Masucci. 1997. Epitope-dependent selection of highly restricted or diverse T cell receptor repertoires in response to persistent infection by Epstein-Barr virus. *J Exp Med* 186: 83-89.
170. Afik, S., K. B. Yates, K. Bi, S. Darko, J. Godec, U. Gerdemann, L. Swadling, D. C. Douek, P. Klenerman, E. J. Barnes, A. H. Sharpe, W. N. Haining, and N. Yosef. 2017. Targeted reconstruction of T cell receptor sequence from single cell RNA-seq links CDR3 length to T cell differentiation state. *Nucleic Acids Res*.
171. Milich, D. R. 2016. The Concept of Immune Tolerance in Chronic Hepatitis B Virus Infection Is Alive and Well. *Gastroenterology* 151: 801-804.
172. Mason, W. S., U. S. Gill, S. Litwin, Y. Zhou, S. Peri, O. Pop, M. L. Hong, S. Naik, A. Quaglia, A. Bertoletti, and P. T. Kennedy. 2016. HBV DNA Integration and Clonal Hepatocyte Expansion in Chronic Hepatitis B

Patients Considered Immune Tolerant. *Gastroenterology* 151: 986-998 e984.
173. Protzer, U., and P. Knolle. 2016. "To Be or Not to Be": Immune Tolerance in Chronic Hepatitis B. *Gastroenterology* 151: 805-806.
174. Farci, P., G. Diaz, Z. Chen, S. Govindarajan, A. Tice, L. Agulto, S. Pittaluga, D. Boon, C. Yu, R. E. Engle, M. Haas, R. Simon, R. H. Purcell, and F. Zamboni. 2010. B cell gene signature with massive intrahepatic production of antibodies to hepatitis B core antigen in hepatitis B virus-associated acute liver failure. *Proc Natl Acad Sci U S A* 107: 8766-8771.
175. Bertoletti, A., and C. Ferrari. 2016. Adaptive immunity in HBV infection. *J Hepatol* 64: S71-83.
176. Yan, H., G. Zhong, G. Xu, W. He, Z. Jing, Z. Gao, Y. Huang, Y. Qi, B. Peng, H. Wang, L. Fu, M. Song, P. Chen, W. Gao, B. Ren, Y. Sun, T. Cai, X. Feng, J. Sui, and W. Li. 2012. Sodium taurocholate cotransporting polypeptide is a functional receptor for human hepatitis B and D virus. *Elife* 1: e00049.
177. Chen, C. L., J. Y. Yang, S. F. Lin, C. A. Sun, C. H. Bai, S. L. You, C. J. Chen, J. H. Kao, P. J. Chen, and D. S. Chen. 2015. Slow decline of hepatitis B burden in general population: Results from a population-based survey and longitudinal follow-up study in Taiwan. *J Hepatol* 63: 354-363.
178. Bertoletti, A., and P. T. Kennedy. 2014. The immune tolerant phase of chronic HBV infection: new perspectives on an old concept. *Cellular & molecular immunology*.
179. Protzer, U., M. K. Maini, and P. A. Knolle. 2012. Living in the liver: hepatic infections. *Nat Rev Immunol* 12: 201-213.
180. Crespo, J., H. Sun, T. H. Welling, Z. Tian, and W. Zou. 2013. T cell anergy, exhaustion, senescence, and stemness in the tumor microenvironment. *Curr Opin Immunol* 25: 214-221.
181. Schwartz, R. H. 2003. T cell anergy. *Annual review of immunology* 21: 305-334.
182. Wherry, E. J., D. L. Barber, S. M. Kaech, J. N. Blattman, and R. Ahmed. 2004. Antigen-independent memory CD8 T cells do not develop during chronic viral infection. *Proc Natl Acad Sci U S A* 101: 16004-16009.
183. Akbar, A. N., S. M. Henson, and A. Lanna. 2016. Senescence of T Lymphocytes: Implications for Enhancing Human Immunity. *Trends in immunology* 37: 866-876.
184. Klenerman, P., and A. Oxenius. 2016. T cell responses to cytomegalovirus. *Nat Rev Immunol* 16: 367-377.
185. Kared, H., S. Martelli, T. P. Ng, S. L. Pender, and A. Larbi. 2016. CD57 in human natural killer cells and T-lymphocytes. *Cancer Immunol Immunother* 65: 441-452.
186. Ahmed, R., A. Salmi, L. D. Butler, J. M. Chiller, and M. B. Oldstone. 1984. Selection of genetic variants of lymphocytic choriomeningitis virus in spleens of persistently infected mice. Role in suppression of cytotoxic T lymphocyte response and viral persistence. *J Exp Med* 160: 521-540.

187. Oldstone, M. B. 2007. A suspenseful game of 'hide and seek' between virus and host. *Nat Immunol* 8: 325-327.
188. Ahmed, R., and M. B. Oldstone. 1988. Organ-specific selection of viral variants during chronic infection. *J Exp Med* 167: 1719-1724.
189. Gairin, J. E., H. Mazarguil, D. Hudrisier, and M. B. Oldstone. 1995. Optimal lymphocytic choriomeningitis virus sequences restricted by H-2Db major histocompatibility complex class I molecules and presented to cytotoxic T lymphocytes. *J Virol* 69: 2297-2305.
190. Buggert, M., J. Tauriainen, T. Yamamoto, J. Frederiksen, M. A. Ivarsson, J. Michaelsson, O. Lund, B. Hejdeman, M. Jansson, A. Sonnerborg, R. A. Koup, M. R. Betts, and A. C. Karlsson. 2014. T-bet and Eomes are differentially linked to the exhausted phenotype of CD8+ T cells in HIV infection. *PLoS Pathog* 10: e1004251.
191. Kurktschiev, P. D., B. Raziorrouh, W. Schraut, M. Backmund, M. Wachtler, C. M. Wendtner, B. Bengsch, R. Thimme, G. Denk, R. Zachoval, A. Dick, M. Spannagl, J. Haas, H. M. Diepolder, M. C. Jung, and N. H. Gruener. 2014. Dysfunctional CD8+ T cells in hepatitis B and C are characterized by a lack of antigen-specific T-bet induction. *J Exp Med* 211: 2047-2059.
192. Kamphorst, A. O., A. Wieland, T. Nasti, S. Yang, R. Zhang, D. L. Barber, B. T. Konieczny, C. Z. Daugherty, L. Koenig, K. Yu, G. L. Sica, A. H. Sharpe, G. J. Freeman, B. R. Blazar, L. A. Turka, T. K. Owonikoko, R. N. Pillai, S. S. Ramalingam, K. Araki, and R. Ahmed. 2017. Rescue of exhausted CD8 T cells by PD-1-targeted therapies is CD28-dependent. *Science* 355: 1423-1427.
193. Hui, E., J. Cheung, J. Zhu, X. Su, M. J. Taylor, H. A. Wallweber, D. K. Sasmal, J. Huang, J. M. Kim, I. Mellman, and R. D. Vale. 2017. T cell costimulatory receptor CD28 is a primary target for PD-1-mediated inhibition. *Science* 355: 1428-1433.
194. Im, S. J., M. Hashimoto, M. Y. Gerner, J. Lee, H. T. Kissick, M. C. Burger, Q. Shan, J. S. Hale, J. Lee, T. H. Nasti, A. H. Sharpe, G. J. Freeman, R. N. Germain, H. I. Nakaya, H. H. Xue, and R. Ahmed. 2016. Defining CD8+ T cells that provide the proliferative burst after PD-1 therapy. *Nature* 537: 417-421.
195. Utzschneider, D. T., M. Charmoy, V. Chennupati, L. Pousse, D. P. Ferreira, S. Calderon-Copete, M. Danilo, F. Alfei, M. Hofmann, D. Wieland, S. Pradervand, R. Thimme, D. Zehn, and W. Held. 2016. T Cell Factor 1-Expressing Memory-like CD8(+) T Cells Sustain the Immune Response to Chronic Viral Infections. *Immunity* 45: 415-427.
196. Speiser, D. E., D. T. Utzschneider, S. G. Oberle, C. Munz, P. Romero, and D. Zehn. 2014. T cell differentiation in chronic infection and cancer: functional adaptation or exhaustion? *Nat Rev Immunol* 14: 768-774.
197. Fuller, M. J., A. Khanolkar, A. E. Tebo, and A. J. Zajac. 2004. Maintenance, loss, and resurgence of T cell responses during acute, protracted, and chronic viral infections. *J Immunol* 172: 4204-4214.

198. Richer, M. J., J. C. Nolz, and J. T. Harty. 2013. Pathogen-specific inflammatory milieux tune the antigen sensitivity of CD8(+) T cells by enhancing T cell receptor signaling. *Immunity* 38: 140-152.
199. Wei, F., S. Zhong, Z. Ma, H. Kong, A. Medvec, R. Ahmed, G. J. Freeman, M. Krogsgaard, and J. L. Riley. 2013. Strength of PD-1 signaling differentially affects T-cell effector functions. *Proc Natl Acad Sci U S A* 110: E2480-2489.
200. Schmidt, J., C. Neumann-Haefelin, T. Altay, E. Gostick, D. A. Price, V. Lohmann, H. E. Blum, and R. Thimme. 2011. Immunodominance of HLA-A2-restricted hepatitis C virus-specific CD8+ T cell responses is linked to naive-precursor frequency. *J Virol* 85: 5232-5236.
201. Nitschke, K., T. Flecken, J. Schmidt, E. Gostick, M. Marget, C. Neumann-Haefelin, H. E. Blum, D. A. Price, and R. Thimme. 2015. Tetramer enrichment reveals the presence of phenotypically diverse hepatitis C virus-specific CD8+ T cells in chronic infection. *J Virol* 89: 25-34.
202. Middleton, D., L. Menchaca, H. Rood, and R. Komerofsky. 2003. New allele frequency database: http://www.allelefrequencies.net. *Tissue Antigens* 61: 403-407.
203. Messaoudi, I., J. A. Guevara Patino, R. Dyall, J. LeMaoult, and J. Nikolich-Zugich. 2002. Direct link between mhc polymorphism, T cell avidity, and diversity in immune defense. *Science* 298: 1797-1800.
204. Dyall, R., I. Messaoudi, S. Janetzki, and J. Nikolic-Zugic. 2000. MHC polymorphism can enrich the T cell repertoire of the species by shifts in intrathymic selection. *J Immunol* 164: 1695-1698.
205. Miles, J. J., S. L. Silins, A. G. Brooks, J. E. Davis, I. Misko, and S. R. Burrows. 2005. T-cell grit: large clonal expansions of virus-specific CD8+ T cells can dominate in the peripheral circulation for at least 18 years. *Blood* 106: 4412-4413.
206. Kaech, S. M., and W. Cui. 2012. Transcriptional control of effector and memory CD8+ T cell differentiation. *Nat Rev Immunol* 12: 749-761.
207. van Leeuwen, E. M., G. J. de Bree, E. B. Remmerswaal, S. L. Yong, K. Tesselaar, I. J. ten Berge, and R. A. van Lier. 2005. IL-7 receptor alpha chain expression distinguishes functional subsets of virus-specific human CD8+ T cells. *Blood* 106: 2091-2098.
208. Meyer-Olson, D., N. H. Shoukry, K. W. Brady, H. Kim, D. P. Olson, K. Hartman, A. K. Shintani, C. M. Walker, and S. A. Kalams. 2004. Limited T cell receptor diversity of HCV-specific T cell responses is associated with CTL escape. *J Exp Med* 200: 307-319.
209. Tickotsky, N., T. Sagiv, J. Prilusky, E. Shifrut, and N. Friedman. 2017. McPAS-TCR: A manually-curated catalogue of pathology-associated T cell receptor sequences. *Bioinformatics*.